UNIVERSIDADE ESTADUAL DE CAMPINAS

Faculdade de Engenharia Química

MARIA FERNANDA OLIVEIRA

DESENVOLVIMENTO DE UMA NOVA METODOLOGIA PARA ESTIMATIVA RÁPIDA DO TEMPO DE ASCENSÃO DE GÁS EM MEIO AQUOSO

DEVELOPMENT OF A NEW METHODOLOGY FOR QUICK ESTIMATE OF GAS RISING TIME IN WATER MEDIUM

CAMPINAS - SP

2023

MARIA FERNANDA OLIVEIRA

DEVELOPMENT OF A NEW METHODOLOGY FOR QUICK ESTIMATE OF GAS RISING TIME IN WATER MEDIUM

DESENVOLVIMENTO DE UMA NOVA METODOLOGIA PARA ESTIMATIVA RÁPIDA DO TEMPO DE ASCENSÃO DE GÁS EM MEIO AQUOSO

Tese apresentada à Faculdade de Engenharia Química da Universidade Estadual de Campinas como parte dos requisitos exigidos para a obtenção do título de Doutora em Engenharia Química

Thesis presented to the School of Chemical Engineering of the University of Campinas in partial fulfillment of the requirements for the degree of Doctor in Chemical Engineering

Supervisor: Prof. Dr. Sávio Souza Venâncio Vianna
Co-Supervisor: Prof. Dr. Ana Maria Frattini Fileti

ESTE TRABALHO CORRESPONDE À VERSÃO FINAL DA TESE DEFENDIDA PELA ALUNA MARIA FERNANDA OLIVEIRA, ORIENTADA PELO PROF. DR. SÁVIO SOUZA VENÂNCIO VIANNA E CO-ORIENTADA PELA PROFA. DRA. ANA MARIA FRATTINI FILETI

CAMPINAS - SP
2023

Ficha catalográfica
Universidade Estadual de Campinas
Biblioteca da Área de Engenharia e Arquitetura
Rose Meire da Silva - CRB 8/5974

OL4d

Oliveira, Maria Fernanda, 1992-
Development of a new methodogy for quick estimate of gas rising time in water medium / Maria Fernanda Oliveira. – Campinas, SP : [s.n.], 2023.

Orientador: Sávio Souza Venâncio Vianna.
Coorientador: Ana Maria Frattini Fileti.
Tese (doutorado) – Universidade Estadual de Campinas, Faculdade de Engenharia Química.

1. Fluidodinâmica computacional. 2. Escoamento bifásico. 3. Gás - Vazamento. I. Vianna, Sávio Souza Venâncio, 1975-. II. Fileti, Ana Maria Frattini, 1965-. III. Universidade Estadual de Campinas. Faculdade de Engenharia Química. IV. Título.

Informações Complementares

Título em outro idioma: Desenvolvimento de uma nova metodologia para estimativa rápida do tempo de ascensão de gás em meio aquoso
Palavras-chave em inglês:
Computational fluid dynamics
Two-phase flow
Gas leakage
Área de concentração: Engenharia Química
Titulação: Doutora em Engenharia Química
Banca examinadora:
Sávio Souza Venâncio Vianna [Orientador]
Tânia Suaiden Klein
Nicolas Spogis
Raphael Soeiro Suppino
Leonardo Vasconcelos Fregolente
Data de defesa: 15-05-2023
Programa de Pós-Graduação: Engenharia Química

Identificação e informações acadêmicas do(a) aluno(a)
- ORCID do autor: https://orcid.org/0000-0002-2802-1984
- Currículo Lattes do autor: https://lattes.cnpq.br/4335216874273384

Tese de Doutorado defendida por **Maria Fernanda Oliveira** e aprovada em 15 de maio de 2023 pela Comissão Examinadora constituída pelos doutores:

Prof. Dr. Sávio Souza Venâncio Vianna (Orientador)
FEQ/UNICAMP

Profa. Dra. Tânia Suaiden Klein
UFRJ - Escola de Química
Videoconferência

Prof. Dr. Nicolas Spogis
PUC-Campinas

Prof. Dr. Raphael Soeiro Suppino
FEQ/UNICAMP

Prof. Dr. Leonardo Vasconcelos Fregolente
FEQ/UNICAMP

A Ata da defesa com as respectivas assinaturas dos membros encontra-se no SIGA/Sistema de Fluxo de Dissertação/Tese e na Secretaria do Programa da Unidade

To my family and to my pack

Acknowledgments

To God, for always giving me the strength to continue facing my challenges.

To Professor Sávio Souza Venâncio Vianna, for giving me this opportunity, trusting me, guiding me, and helping me during my path.

To Professor Ana Maria Frattini Fileti for being the first person to welcome me and encourage me to pursue this journey.

To Thiago, who has been my greatest support throughout this challenge.

To my family, especially my parents, Lurdinha and Roberto, with whom I share all my achievements, and to Vitória and Roseli, who have always cheered me.

To all my co-workers at L4R1S4, who made my days happier, especially Angela, André, Guilherme, João, Karen, Pamella, Nicolás, Tatiele, and Tássia.

To my dear friends Daniel, Guilherme, Nadia, and Natália. Once again, I say: the years go by, and you are still the best thing that Unicamp has given me!

To all the many professors and employees of the School of Chemical Engineering at Unicamp who contributed to my professional development over these long years.

To those who contributed financially to this endeavor. This work was carried out with the support of CNPq, National Council for Scientific and Technological Development – Brazil (processes 164925/2018-0 and 140909/2019-2), and of Univesp, the Virtual University of the State of São Paulo.

And to all those many who, although not mentioned, contributed to the realization of this work.

"Love of learning is the most necessary passion... in it lies our happiness. It's a sure remedy for what ails us, an unending source of pleasure."

Émilie du Châtelet

Resumo

Liberações acidentais de gases em ambientes marinhos são um assunto que tem recebido cada vez mais atenção da comunidade científica. Estima-se que os pequenos vazamentos acontecem em praticamente todas os sistemas de transporte de gás, enquanto os vazamentos maiores são mais raros, porém associados a acidentes catastróficos. Dessa forma, desenvolver medidas que minimizem as consequências deste fenômeno significa reduzir danos ao meio ambiente, evitar prejuízos financeiros e, principalmente, preservar vidas humanas. No entanto, por mais atenção que o assunto tenha recebido da comunidade científica nos últimos anos, o conhecimento acerca do fenômeno de liberação de gás em ambiente submarino ainda é muito escasso. Inspirado pelo cenário descrito, o presente estudo tenta fornecer uma contribuição a esse campo de pesquisa. Uma nova metodologia para obtenção de uma expressão capaz de estimar o tempo de ascensão de um gás em meio submerso foi proposta. Essa metodologia utilizou Fluidodinâmica Computacional, mais especificamente uma configuração de custo computacional relativamente baixo usando o método multifásico de Volume de Fluidos, para obtenção de dados da pluma resultante da liberação ascendente de ar em água. A metodologia resultou em equações que descrevem satisfatoriamente o comportamento do gás. No entanto, essas equações estão limitadas a sistemas com pequenas colunas de água, em que efeitos de troca térmica e compressibilidade são praticamente desprezíveis. Além disso, no redimensionamento do domínio de análise, outros efeitos, como presença de correntes marinhas, devem ser considerados. Ainda durante o desenvolvimento do modelo, um fator de forma que relaciona o tamanho característico dos grupos de bolha com a velocidade de subida do gás foi obtido para cada altura de coluna de água avaliada. Esse fator de forma, calculado por meio de uma análise dimensional, é semelhante ao fator de forma descrito na literatura para uma única bolha em ascensão, mas acredita-se que que a proposta de um fator de forma para grupo de bolhas ainda não tenha sido feita anteriormente. Foi verificado que esse novo fator variou de acordo com as dimensões do sistema gás-líquido estudado, embora outras variáveis potencialmente estejam envolvidas nessas mudanças de valor. Além disso, a combinação de análise dimensional e Fluidodinâmica Computacional para desenvolver modelos que estimam parâmetros de plumas em escoamentos multifásicos ainda é limitada. Espera-se que estudos subsequentes a este poderão auxiliar na formulação de planos de resposta em casos de emergência envolvendo vazamentos submarinos de gases. Mesmo assim, as contribuições deste trabalho já podem ser consideradas significativas ao campo de estudo de liberação de gases em água.

Palavras-chave: Fluidodinâmica Computacional, Liberação de gases em água, Escoamento bifásico

Abstract

Accidental subsea gas releases are a subject that has received increasing attention from the scientific community. It is estimated that small leaks happen in practically all gas transport systems, while larger leaks are rarer, but associated with catastrophic accidents. Thus, developing measures that minimize the consequences of this phenomenon means reducing damage to the environment, avoiding financial losses, and above all, preserving human lives. However, as much attention as the subject has received from the scientific community in recent years, knowledge about the phenomenon of subsea gas release is still very scarce. Inspired by the described scenario, the present study tries to provide a contribution to this field of research. A new methodology for obtaining an expression capable of estimating the rising time of a gas in a submerged medium was proposed. This methodology used Computational Fluid Dynamics, more specifically a relatively low computational cost configuration using the multiphase Volume of Fluid method, to obtain plume data resulting from the upward release of air into water. The methodology resulted in equations that satisfactorily describe the behavior of the gas. However, these equations are limited to systems with small water depths, where heat exchange and compressibility effects are practically negligible. In addition, when rescaling the analysis domain, other effects, such as the presence of marine currents, must be considered. During the development of the model, a shape factor that relates the characteristic size of the bubble groups with the ascending velocity of the gas was obtained for each evaluated water column height. This shape factor, calculated through dimensional analysis, is similar to the shape factor described in the literature for a single rising bubble. However, it is believed that the proposal of a bubble group shape factor has not been made before. This new shape factor varied according to the dimensions of the studied gas-liquid system, although other variables are potentially involved in these value changes. Furthermore, the combination of dimensional analysis and Computational Fluid Dynamics to develop models that estimate plume parameters in multiphase flows is still limited. It is expected that studies subsequent to this one will be able to help in the formulation of response plans in cases of emergencies involving the accidental underwater release of gases. Even so, the contributions of this work can already be considered significant to the field of study of gas release into water.

Keywords: Computational Fluid Dynamics, Underwater gas release, Two-phase flow

List of Figures

List of Tables

Nomenclature

List of abbreviations

CFD Computational Fluid Dynamics

DNS Direct Numerical Simulation

DPM Discrete Phase Model

FVM Finite Volume Method

LES Large Eddy Simulation

RANS Reynolds-Averaged Navier-Stokes

RSM Reynolds Stress Model

URANS Unsteady Reynolds-Averaged Navier-Stokes

VLES Very Large Eddy Scale

VOF Volume of Fluid

Conservation equations in multiphase flows

α_N Volume fraction of a component or phase N [-]

δ_{ki} Kronecker delta

ρ Density of the mixture [ML^{-3}]

σ_{Cki} Stress tensor [$\mathrm{ML}^{-2}\mathrm{T}^{-2}$]

σ^D_{Cki} Deviatoric stress tensor component [$\mathrm{ML}^{-2}\mathrm{T}^{-2}$]

F^T_{Nk} Net force in the k direction acting on the component or phase N [$\mathrm{ML}^{-2}\mathrm{T}^{-2}$]

G_i Total mass flux [$\mathrm{ML}^{-2}\mathrm{T}^{-1}$]

G_{Ni} Mass flux of a component or phase N [$\mathrm{ML}^{-2}\mathrm{T}^{-1}$]

i Notation for dimension

I_N Mass interaction term [$\mathrm{ML^{-3}T^{-1}}$]

j_i Total volumetric flux [$\mathrm{LT^{-1}}$]

j_{Ni} Volumetric flux of a component or phase N [$\mathrm{LT^{-1}}$]

N Phase or component ($N = p, q...$)

u_{Ni} Velocity of a component or phase N [$\mathrm{LT^{-1}}$]

The dynamic of a gas bubble ascending through liquid

α Shape factor [-]

θ Spherical coordinate [-]

g Gravity acceleration [$\mathrm{LT^{-2}}$]

O Origin of the spherical coordinates

q_s Water velocity at the bubble [$\mathrm{LT^{-1}}$]

R Radius of curvature on the stagnation point [L]

r Spherical coordinate [L]

S Stagnation point

U Bubble ascending speed [$\mathrm{LT^{-1}}$]

The Volume of Fluid method

α VOF scalar, with $\sum_{p=1}^{n} \alpha_p = 1$ [-]

$\dot{m}_{pq}$ Mass transfer from phase p to phase q [$\mathrm{ML^{-3}T^{-1}}$]

ρ Fluid density [$\mathrm{ML^{-3}}$]

ρ_q Phase density [$\mathrm{ML^{-3}}$]

τ_{ij} Viscous stress tensor [$\mathrm{ML^{-1}T^{-2}}$]

g_i Gravity acceleration [$\mathrm{LT^{-2}}$]

P Pressure [$\mathrm{ML^{-1}T^{-2}}$]

p Fluid phase

S_i Source term [$\mathrm{ML^{-2}T^{-2}}$]

$S_{\alpha q}$ Source term [$\mathrm{ML^{-3}T^{-1}}$]

u_i Fluid velocity [$\mathrm{LT^{-1}}$]

u_q Phase velocity [$\mathrm{LT^{-1}}$]

RANS turbulence modeling in CFD

δ_{ki} Kronecker delta

Γ Diffusion coefficient [$\mathrm{ML^{-1}T^{-1}}$]

μ_t Turbulent (or eddy) viscosity [$\mathrm{ML^{-1}T^{-1}}$]

Φ Generic scalar mean value [variable]

ϕ Generic scalar [variable]

ϕ' Fluctuating component of the generic scalar [variable]

ρ Density [$\mathrm{ML^{-3}}$]

τ_{ij} Reynolds' stress equals to $-\rho\overline{u_i' u_j'}$ [$\mathrm{ML^{-1}T^{-2}}$]

k Turbulent kinetic energy per unit mass [$\mathrm{L^2T^{-2}}$]

S Source term [variable]

U Velocity mean value [$\mathrm{LT^{-1}}$]

u_i' Fluctuating component of the velocity [$\mathrm{LT^{-1}}$]

u_i Velocity [$\mathrm{LT^{-1}}$]

The standard k-ε model

ℓ Characteristic length of eddies on large scales [L]

γ Isentropic expansion factor [-]

μ Viscosity [$\mathrm{ML^{-1}T^{-1}}$]

μ_t Turbulent (or eddy) viscosity [$\mathrm{ML^{-1}T^{-1}}$]

ρ Density [$\mathrm{ML^{-3}}$]

σ_ε Turbulent Prandtl number for ε [-]

σ_k Turbulent Prandtl number for k [-]

ε Dissipation rate of the turbulent kinetic energy [L^2T^{-3}]

a Speed of the sound [LT^{-1}]

C_μ Dimensionless constant [-]

$C_{1\varepsilon}$ Constant of the k-ε model [-]

$C_{2\varepsilon}$ Constant of the k-ε model [-]

$C_{3\varepsilon}$ Constant of the k-ε model [-]

G_b Generation of turbulence kinetic energy due to buoyancy [$ML^{-1}T^{-3}$]

g_i Component of the gravitational vector in the i^{th} direction [LT^{-2}]

G_k Generation of turbulence kinetic energy due to the mean velocity gradients [$ML^{-1}T^{-3}$]

k Turbulent kinetic energy [L^2T^{-2}]

Pr_t Turbulent Prandtl number for energy [-]

R Molar gas constant [$L^2T^{-2}\theta^{-1}$]

S_ε User-defined source terms of the k-ε model [$ML^{-1}T^{-4}$]

S_k User-defined source terms of the k-ε model [$ML^{-1}T^{-3}$]

T Temperature [θ]

u Component of the flow velocity perpendicular to the gravitational vector [LT^{-1}]

u_i Component of the flow velocity [LT^{-1}]

u_i' Fluctuating component of the velocity u_i [LT^{-1}]

u_j' Fluctuating component of the velocity u_j [LT^{-1}]

V Characteristic velocity of eddies on large scales [LT^{-1}]

v Component of the flow velocity parallel to the gravitational vector [LT^{-1}]

Y_M Contribution of the fluctuating dilatation in compressible turbulence to the overall dissipation rate [$ML^{-1}T^{-3}$]

The realizable k-ε model

μ Viscosity [$ML^{-1}T^{-1}$]

μ_t Turbulent (or eddy) viscosity [$\mathrm{ML^{-1}T^{-1}}$]

ν Molecular kinematic viscosity [$\mathrm{L^2T^{-1}}$]

ρ Density [$\mathrm{ML^{-3}}$]

σ_ε Turbulent Prandtl number for ε [-]

σ_k Turbulent Prandtl number for k [-]

ε Dissipation rate of the turbulent kinetic energy[$\mathrm{L^2T^{-3}}$]

C_1 Realizable k-ε model parameter [-]

C_2 Realizable k-ε model constant [-]

$C_{1\varepsilon}$ Realizable k-ε model constant [-]

$C_{3\varepsilon}$ Realizable k-ε model parameter [-]

G_b Generation of turbulence kinetic energy due to buoyancy [$\mathrm{ML^{-1}T^{-3}}$]

G_k Generation of turbulence kinetic energy due to the mean velocity gradients [$\mathrm{ML^{-1}T^{-3}}$]

k Turbulent kinetic energy [$\mathrm{L^2T^{-2}}$]

S_ε User-defined source terms of the realizable k-ε model [$\mathrm{ML^{-1}T^{-4}}$]

S_k User-defined source terms of the realizable k-ε model [$\mathrm{ML^{-1}T^{-3}}$]

u_j Component of the flow velocity [$\mathrm{LT^{-1}}$]

Y_M Contribution of the fluctuating dilatation in compressible turbulence to the overall dissipation rate [$\mathrm{ML^{-1}T^{-3}}$]

Dimensional analysis

α Parameter which relates the variable $V_{bubbles}$ with $r_{bubbles}$ [-]

g Gravitational acceleration [$\mathrm{LT^{-2}}$]

$r_{bubbles}$ Characteristic size of the bubble clusters [L]

$V_{bubbles}$ Average ascending velocity of the bubble clusters [$\mathrm{LT^{-1}}$]

Contents

Chapter 1

Introduction

Accidental subsea gas releases are a matter of concern in the process industry. Considering the complexity of the physics involved in this phenomenon, since it usually occurs below great water depths, it is sufficient to state that additional challenges are posed to any research regarding this theme. This research involved the investigation of the phenomenon of the underwater release of gases through controlled numerical experiments. Inspired by the scenario of subsea gas releases, the current chapter addresses some challenges related to the study of this theme, especially when using computational tools. The chapter also presents the objectives and the organizational structure of this thesis.

1.1 Purpose of this study

Natural gas exploitation is essential to human activities. It is responsible for moving billions of dollars, generating thousands of jobs, providing raw materials for the manufacturing of various products, and supplying fuel used to generate electricity and thermal energy. Despite its advantages, it is a non-renewable material of limited occurrence, and its production chain is not only expensive but also generates a series of environmental impacts, the best known being the contribution to the increase in the emission of gases related to the greenhouse effect and, consequently, to global warming. Currently, significant efforts are being made to discover new technologies and materials with the aim of replacing fossil fuels and reducing dependence on oil and gas as energy sources and raw materials for various processes. These researches are, in fact, necessary due to the non-renewable of these fuels. However, it is impossible to deny the dependency that society still has on fossil fuels. Thus, in addition to searching for alternatives to replacing fossil fuels, it is also important to find new ways to make their processing more efficient, making the same process produce more fuel with fewer negative impacts.

It is estimated that all subsea gas transport lines experience some form of leakage, resulting in a significant loss of natural gas. This not only has a financial impact on gas companies but also poses an environmental risk to marine fauna. When the gas

reaches the surface, it is toxic to people, may hinder platform buoyancy, and may cause severe explosions. Even so, gas companies do not report statistics of small gas leaks. It often happens because it is too difficult to detect a leak until some severe damage has already happened. The study of gas behavior underwater may be essential to the development and improvement of technologies that aim to detect leaks at an early stage.

The gas leak and plume formation underwater are physically described as a two-phase flow, in which a gas phase is dispersed within the liquid phase. Two-phase flows are a physical phenomenon widely present in industrial and non-industrial activities, moreover, knowing its physics is necessary to comprehend how several different processes occur, and how they can be improved. However, even though the study of the single-phase flow of fluids has been a subject of attention of scientists and engineers for many years, there is still a lack of knowledge on the development, understanding, and application of modeling governing equations about the flow of multiphase systems.

In Fluid Mechanics studies, sometimes running experimental tests can be too expensive or impractical, especially when dealing with a scenario of large dimensions or a risky situation. Therefore, Computational Fluid Dynamics (CFD) has become a very popular tool for flow investigation in academia and also in the industry. It might well serve as an alternative to the experimental approach. By means of CFD modeling, it is possible to obtain numerical solutions of the governing equations for fluid flows, including multiphase flows. The utilization of computer simulation for studying the fluid dynamics of gases is interesting because it allows faster and cheaper achievement of results if compared to the use of a pilot plant, for example. However, computer simulation is also a study approach that presents some difficulties.

Despite the efficiency, the use of CFD, especially for multiphase flows, is computationally expensive, even when resources are available. Therefore, it is necessary to develop CFD methodologies capable of accurately simulating the desired flows and with a viable computational cost. Furthermore, it is also necessary to develop ways to reduce the dependence on this tool aiming at developing faster action plans and mitigation in case of accidents. Understanding the physics which governs a phenomenon allows the development of mathematical models able to provide rapid information about it. Therefore, it is necessary to increase the knowledge about underwater gas plumes and their behavior under different flow conditions. In this case, CFD works as an auxiliary tool for the study of subsea gas releases, but the physical analysis becomes the focus of the research.

This thesis presents the steps of the development of a new methodology capable of estimating the air rising time in small columns of water. It is inspired by the scenario of accidental underwater gas releases and guided by the idea that the use of a CFD tool associated with a physical analysis of the phenomena is a promising way for the analysis of gas releases in liquid media. The results of this study will serve as a basis for future studies on the theme, as well as assist on the elaboration of emergency response in case

of an accidental subsea gas release.

1.2 Objectives of this work

1.2.1 General goal

The objective of this work was to develop a methodology that leads to a physics-based mathematical expression able to estimate the rising time of the underwater gas ascending by associating data obtained through computer simulation and models obtained through dimensional analysis.

1.2.2 Specific goals

The specific goals of this work were:

- Understanding the phenomenon of subsea gas releases and making simplifications for its study using CFD;
- Proposing and validating a CFD setup with a reduced computational cost;
- Using the CFD setup to obtain data about underwater gas releases;
- Using dimensional analysis to develop a mathematical model relating flow parameters;
- Verifying the applicability of the model and understanding its limitations.

1.3 Organization of this thesis

The next chapters of this thesis are organized as follows:

- Chapter 2 comprises the literature review, with the summarized information necessary to understand the discussions presented in this work;
- Chapter 3 covers the development of the proposed methodology used in each stage of this study;
- Chapter 4 brings the results obtained in each stage of this work, along with their corresponding discussion and partial conclusions;
- Chapter 5 presents the general conclusions of this work, the suggestions for future work, and the scientific production associated with this study.

The figures included in this thesis were created independently. Any figures that have been previously presented in works authored by the researcher have been reproduced here with permission from the respective publishers.

Chapter 2

Literature review

This work aims to study the modeling of a challenging multiphase problem related to subsea gas releases. The understanding of the underwater gas plume formation, and the physics regarding gas-liquid two-phase flow is essential to accomplish the objectives of this research. For solving the modeling equations, it is also substantial to comprehend the numerical approaches that can be applied to do so, and the turbulence phenomenon, which is proved to be a major aspect of the studied problem.

Thus, this chapter presents a succinct literature review about the main themes that will be discussed in this work. Evidently, each section contains only a small part of the vast content available in the literature for each subject. However, it is expected that with this chapter the reader will gradually understand the relevance of the study, how the work proposal has been developed, and the results presented in this thesis.

2.1 Subsea gas release

This section attempts to introduce the reader to some aspects of the subsea gas release, explaining why the theme of the present work is relevant and shortly presenting the phenomenon.

2.1.1 The importance of the industry of natural gas

Natural gas production is of utmost importance to human society. Until the 19th Century it was used almost only for lighting. Nowadays, this product is used mostly as a fuel, and as a raw material in manufacturing. It is less harmful to the environment than other fossil fuels because its emissions of nitrous oxide and carbon dioxide are lower, and of sulfur dioxide are negligible, which reduces problems related to acid rain, ozone layer depletion, or greenhouse gas emissions (Mokhatab and Poe, 2012). As a consequence of these advantages, in 2019, 22% of all primary energy supply by fuel was attributed to natural gas (IEA, 2020).

Although its significance to society is clear, it is important to highlight that natural gas is a limited non-renewable source of energy. Furthermore, the environmental impacts resulting from its extraction and the risk involved in its entire production chain are widely known, which drives the search for new, preferably renewable, sources of energy and raw material. However, because of the heavy dependence, already described, that exists between human activities and the use of natural gas, current studies should not only be restricted to finding ways to replace it, but also to develop new approaches to its processing. New technologies should make natural gas production safer, more environmentally and socially responsible, and still keep it economically viable. Thus, improving natural gas processing is a safety, environmental, and economical issue.

2.1.2 Risks in subsea gas production

Since the exploitation of natural gas has become an essential business for human life, it is important to assess the environmental and safety aspects and impacts that occur as a result of this activity. In this context, a problem related to the natural gas industry is definitely the submarine release of gases involved in these processes. A gas release can receive different classifications, according to its extension and ease of detection. Ruptures and blowouts are characterized by the release of significant amounts of gases, making them readily detectable, and requiring immediate action to mitigate and halt the release. On the other hand, leaks happen due to faulty equipment or infrastructure, and due to their low flow rate, they are usually not detected until greater consequences are perceived. Leaks can be subclassified as minor leaks (0.1-1 kg/s), medium leaks (1-10 kg/s), or major leaks (greater than 10 kg/s). The smaller the leak, the longer it usually occurs (Olsen and Skjetne, 2016a).

A recent study showed that more than a thousand super-emitter sites were responsible for releasing huge amounts of methane gas into the atmosphere, a factor responsible for 25% of the global heating. The exact contribution of methane released due to accidental underwater leaks was not specified, but it was proved that the majority of the methane that contributes to global warming comes from the activities of the oil and gas industries (The Guardian, 2023). Besides the environmental damages due to its release into the atmosphere, when released underwater, a gas can dissolve, or react, and potentially damage different species of sea mammals, turtles, fish, and other animals (Cordes et al., 2016). In addition to the toxicity it poses to marine fauna, when the released gas disperses in the atmosphere, there is a risk of dispersing and causing toxic effects to other living beings or of encountering an ignition source, leading to explosions. Moreover, it can also affect the stability of surface vessels or platforms (Li, Chen, and Khan, 2019). Since risk can be defined as the potential that a negative consequence of an event has to occur (Y. Bai and Q. Bai, 2010), any gas release from a subsea oil or gas production

facility means a potential safety and environmental risk. In addition to the likely damage to animals, people, and the environment, any accidental gas release can also result in the loss of process reliability and, consequently, to loss of reputation and money to any company involved in the incident.

A study from 2019 observed eight oil and gas platforms in the North Sea and concluded that all of them leak methane (CH_4) while operating. They also suggest a potentially large missing source of methane emissions in the national UK methane emission inventory. The study also estimates that there are approximately 0.19% of methane loss during offshore production in the world, which corresponds to an overall emission of 0.8 Tg (881849 tons) of methane per year (Riddick et al., 2019). Despite this information, most of the gas leak incidents statistics are unknown, but it is estimated that about 40% of methane emissions caused by humans are due to leaks in the fossil fuel production chain (The Guardian, 2023). Details of minor incidents involving gas spills are available in companies and local petroleum safety reports, but the data is not always public and easy to obtain. Usually, in the most notable accidents, a gas blowout is cited as a cause, and not as the accident itself (Olsen and Skjetne, 2016a).

It is undeniable the necessity of adopting measures to minimize the chances of accidental gas releases. However, if it occurs, the early detection of the leak's location and the previous knowledge of how the gas plume will behave underwater are extremely important for proper measures to be taken in time, in order to prevent further damage. In essence, a continuous assessment process is required to prevent major incidents involving gas release. This methodology of identifying, analyzing, and responding to risks, is known as risk management (Y. Bai and Q. Bai, 2010).

2.1.3 Subsea pipeline incidents

The majority of the incidents involving gas leaks remain unknown, and the information regarding the known releases is usually not available. However, some accidents related to gas releases were so disastrous that they became widely known. Some of these incidents are presented below.

On August 27, 1981, in the South China Sea, the drilling ship Petromar V capsized after a gas blowout. No fatalities were registered, but the ship sank and was lost (Ismail et al., 2014; Li, Han, et al., 2020; Olsen and Skjetne, 2016a).

On October 7, 1985, the facility West Vanguard, located in Norway hit shallow gas. The escaped gas caused a very violent explosion, followed by a fireball. The blowout rate remained constant for six days and then controlled gradually over the next couple of months. One person died due to the blowout and major repairs on the rig were necessary, but it eventually returned to work (Bjerketvedt, Bakke, and Van Wingerden, 1997; Energy Global News, 2021; Olsen and Skjetne, 2016a).

On September 22, 1988, the Ocean Odyssey Rig, in the UK, was operating in the North Sea in a high-pressure formation when a blowout happened. Large quantities of gas were released and fire hit the rig and the surface of the sea. One fatality was registered due to smoke inhalation and, like in the West Vanguard accident, major repairs on the rig were necessary to reestablish the operations (Energy Voice, 2021; Ismail et al., 2014; Olsen and Skjetne, 2016a).

The Santa Fe Al Baz drilling rig, in Nigeria, suffered a blowout on April 28, 1989. The gas liberated ignited and killed 5 crew members due to the flame or drowning after jumping to escape the fire. The intense heat melted and destroyed important parts of the barge causing a crater on the rig and making it sink after the accident. Further investigation concluded that rocks and sand caused the ignition (Ismail et al., 2014; Olsen and Skjetne, 2016a; ONGC, 2014).

Besides no fatalities were registered, the accident ocurred in 1993 in Actinia facility (South China Sea off the coast of Vietnam) deserves to be mentioned because of the magnitude of its environmental consequences. The blowout caused the ejection of liquids up to 2 km wide on the surface, and the release of gas was estimated to 60000 m^3/s (37000 kg/s) (Ismail et al., 2014; Olsen and Skjetne, 2016a).

On August 20, 2004, a rupture, probably caused by fishing gear, in a pipeline from Jotun A was detected due to a pressure drop. Later, another leakage was noticed. Although the incident had the potential for significant safety consequences, it was controlled and the gas volume released to the atmosphere was 1.3 million Sm^3 (Olsen and Skjetne, 2016a; Vinnem, 2007).

Another incident in the North Sea, also in 2004, occurred on the Norwegian Continental Shelf at Snorre A. The estimated release rate ranged between 20 to 30 kg/s. Fortunately, no one died and the actions of the crew prevented the accident to take large proportions (Ismail et al., 2014; Olsen and Skjetne, 2016a).

In 2009, in Nigeria, a blowout with an unknown gas release rate occurred at the Sedco 700. More information about this incident is scarce (Olsen and Skjetne, 2016a).

The most famous accident involving gas release is the Deepwater Horizon (Macondo Blowout) in the Gulf of Mexico, in 2010. It was responsible for 11 fatalities, and the largest marine oil spill in history. The accident is attributed to an expansion of high-pressure methane, which ignited and exploded. For 87 days approximately 86.7 L/s of oil and 16.5 kg/s of methane gas were released from a depth of 1600 m (CSB, 2016; Olsen and Skjetne, 2016a).

On July 2, 2021, an incident happened with the Ku Maloob Zap rig, in the Gulf of Mexico. Gas from a subsea gas leak reached the surface, and due to a lightning storm, the surface gas ignited and a subaquatic fireball was formed. The fire was controlled and there were no injuries (Fobes Mexico, 2021; Folha de São Paulo, 2021; Offshore, 2021).

More recently, in the second half of 2022, seismologists have detected underwa-

ter explosions allegedly linked to leaks near Russian oil pipelines in northern Europe, close to Sweden and Denmark. There is a possibility of sabotage, as the incident is directly linked to the war in Ukraine. Although the information is that the pipelines were not in operation due to the war, it is known that they were full of gas for technical reasons. There is a possibility of an unprecedented environmental impact (CNN Brasil, 2022; G1 - France Presse, 2022).

2.1.4 Subsea gas bubble plumes

The physics of a subsea gas release is governed by the interaction between the gas and the liquid phases. The main mechanism governing the bubble plume is buoyancy, mostly influenced by the density of the gas along the flow. Other mechanisms governing the plume are the drag, turbulence, and gas dissolution, for example. The closer the gas gets to the surface, the more the momentum generated by the buoyancy becomes the dominant driving force of the flow. Considering the changes in the governing mechanisms along a gas plume, it can be divided into different zones, as shown in Figure 1, designed based on the illustration of Olsen and Skjetne (2016).

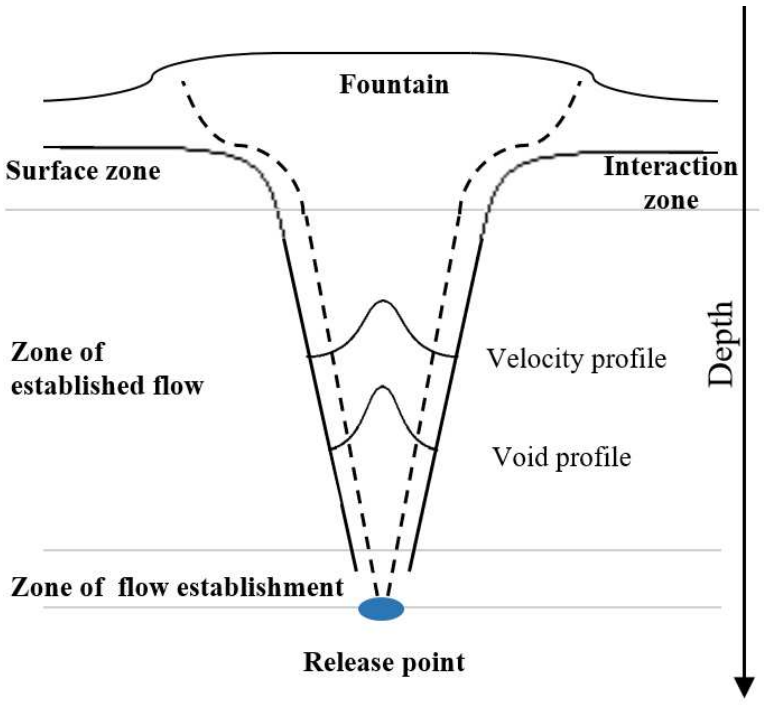

Figure 1: Different zones of a subsea bubble plume.

The virtual origin, or release point, is the point where the width of the plume can be considered equal to zero, and can be determined by extrapolating the plume width from the source of the pure plume. Besides its depth, this point is described by its area,

the reservoir volume and pressure, gas flow rate, temperature, and gas composition (Friedl and Fanneløp, 2000; Olsen and Skjetne, 2016a).

The zone of flow establishment, also known as the gas release zone, is characterized by the flow close to the source. This zone is relatively small if compared to the size of the pure plume, and it is not very important at large scales. The penetration distance of the jet will depend on the initial momentum of the gas, the gas expansion, and the break up of the gas into bubbles. The gas enters the liquid zone as a bubbling jet if the flow is not choked, or a gaseous jet if the flow is choked (Friedl and Fanneløp, 2000; Olsen and Skjetne, 2016a). A choked flow occurs when a fluid passes through a constriction and reaches the maximum velocity at which flow can no longer increase. The Mach number of a choked flow is equal to 1 (sonic condition), while the value for an unchoked flow is lower than 1 (subsonic condition) (Robert H. Perry, 1999).

The zone of established flow is the dominant zone of the pure plume, and it is located above the zone of flow establishment. The difference between the density of the gas and the water increases the buoyancy force, which becomes much greater than the momentum carried by the jet and becomes the main driving force of the flow (Olsen and Skjetne, 2016a).

Finally, the surface zone is the region where the gas is released into the atmosphere. This zone does not appear if the gas is completely dissolved in water, but if the amount of gas in the flow is high enough, it is possible to detect a spout of water and gas. The gas solubilities depend on the salinity and temperature of the water. The water depth also has a great influence on the values, since higher depths result in higher solubilities. Each molecule will be differently influenced by these and other parameters. A gas such as CO_2 is much more soluble than CH_4, for example, and will have a resultant plume much less visible (Olsen and Skjene, 2020). The consequent elevation of water generates a region denominated fountain. However, while the gas will continue to flow upward and disperse in the atmosphere, the water will divert into a radial flow. This points to another important region, the interaction zone, which shows the interaction between the plume and the water surface when the first reaches water depths smaller than its radius (Friedl and Fanneløp, 2000; Olsen and Skjetne, 2016a).

Besides the characteristics of the release point, the cross-currents in the water can also affect the bubble plume behavior. Depending on the current, the gas dissolution may become even more significant due to its mixing with water, or due to changes in the residence time of the gas bubbles. In this case, the surface zone may not be formed (Olsen and Skjetne, 2016a).

2.2 Main aspects of two-phase flows

This work studies the behavior of a phenomenon that involves two different phases. This section introduces the concept of a two-phase flow.

2.2.1 What is two-phase flow?

A multiphase flow is defined as a fluid movement with the simultaneous flow of two or more phases having a level of separation above the molecular level (Yeoh and Tu, 2010). It is important to note that a flow can be classified as single or multiphase and, irrespective of being a single-phase flow, may also be categorized as single or multicomponent because while a phase is the state of the matter, a component is a chemical specie (element or substance) (Crowe et al., 2011). A two-phase flow is the simplest case of multiphase flow and, when the two phases are not consisted of the same chemical substance, although the mathematical description remains the same, it is also called two-component flow (Wallis, 1969).

Two-phase flows can occur in a wide range of contexts, such as in nature, as rain, snow, or fog; in everyday processes, such as baking a cake or pouring a beer; and in biological systems, such as the presence of bubbles, particles, and droplets in suspension in blood, and other body fluids. Technical examples of two-phase are fire extinguisher techniques; production and transportation of oil and gas in the petroleum industry; and accidental and deliberate fires, such as automobile engines. In the industrial field, two-phase or multiphase flows are present in processes such as power generation, refrigeration, distillation, desalination, paper manufacturing, and others. It is estimated that multiphase flows appear in over half of Chemical Engineering procedures, and two-phase flow is encountered in a great part of them. As it can be noted, two-phase flow is a topic that encompasses a wide variety of applications and includes a great range of engineering disciplines (Brennen, 2005; Shoham, 2006; Wallis, 1969).

Two-phase flows can be classified as gas-liquid, gas-solid, liquid-liquid, or liquid-solid (Crowe et al., 2011). Despite the multiple classifications, and although the two-phase flow phenomenon is understood in different technological contexts, and can be observed in different scales of processes, the central purpose of this section is to understand the behavior of a gas ascending through a liquid phase, which is the focus of this work.

2.2.2 Conservation equations in multiphase flows

Consider now a fluid flowing in an arbitrary direction and passing through an infinitesimally small element of fluid, with the axes in Cartesian coordinates, and edges parallel to x_1, x_2, and x_3 directions (or i, j and k directions), such as in Figure 2. In order

to apply the conservation laws of physics, the continuum hypothesis is adopted, the flow is assumed compressible, and the rate of mass increase in the fluid element is considered equal to the net rate of mass flow into the fluid element.

Due to the high complexity of the mass, momentum, and energy conservation equations, they appear in the literature in different notations, depending on their application. The notation used in this work is based on the one described by Brennen (2005), also where the equations presented below can be found in more details. Here, it is assumed that the bounding surfaces of the volume element never cut through disperse phase particles.

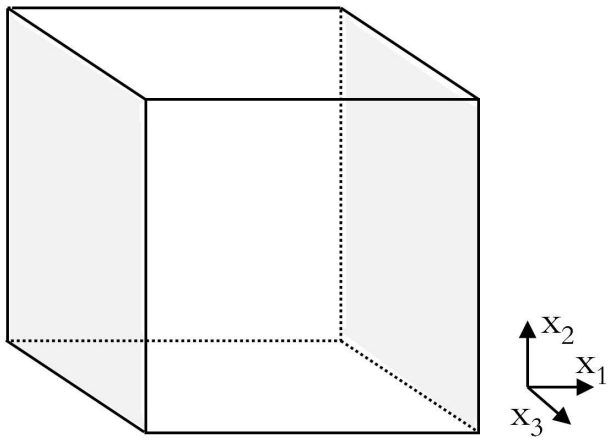

Figure 2: Arbitrary volume element.

To facilitate comprehension of the subsequent equations, please take into account the constraint expressions below:

- The volume fraction of a component or phase N is denoted by α_N, and $\sum_N \alpha_N = 1$;
- For a two-phase flow of components or phases $N = p$ and $N = q$, $\alpha_p + \alpha_q = 1$;
- The volumetric flux of a component or phase N is given by: $j_{Ni} = \alpha_N u_{Ni}$, where u_{Ni} is the velocity of N;
- The mass flux of a component or phase N is given by $G_{Ni} = \rho_N j_{Ni} = \rho_N \alpha_N u_{Ni}$;
- The total volumetric flux is $j_i = j_{pi} + j_{qi} + ... = \sum_N \alpha_N u_{Ni}$;
- The total mass flux is $G_i = G_{pi} + G_{qi} + ... = \sum_N \rho_N \alpha_N u_{Ni}$;
- In a mixture, the density ρ is given by $\sum_N \alpha_N \rho_N$;
- In a three dimensional flow, i is equal to 1, 2, or 3.

To model the conservation of mass, we define the increase rate of the mass of a component or of a phase N stored in an elemental volume such as that described in Figure 2 as described in Equation 1.

$$\frac{\partial}{\partial t}(\rho_N \alpha_N) + \frac{\partial}{\partial x_i}(\rho_N \alpha_N u_{Ni}) = I_N \tag{1}$$

Where I_N denotes the mass interaction terms, which are the transfer of mass rate to N per unit total volume. This transfer of mass is a result of a phase change or chemical reaction. Since mass as a whole must be conserved, $\sum_N I_N = 0$. Then Equation 2 and Equation 3 are derived.

$$\frac{\partial}{\partial t}\left(\sum_N \rho_N \alpha_N\right) + \frac{\partial}{\partial x_i}\left(\sum_N \rho_N \alpha_N u_{Ni}\right) = 0 \tag{2}$$

Or simply:

$$\frac{\partial \rho}{\partial t} + \frac{\partial}{\partial x_i}\left(\sum_N \rho_N \alpha_N u_{Ni}\right) = 0 \tag{3}$$

Note that if the relative velocity between phases is zero, $u_{Ni} = u_i$, and Equation 3 can be reduced to the Mixture Continuity Equation, which is equal to that for a single phase flow of density ρ and is shown in Equation 4.

$$\frac{\partial \rho}{\partial t} + \frac{\partial}{\partial x_i}(\rho u_i) = 0 \tag{4}$$

Now, if the conservation of momentum is considered, still according to Figure 2, the flux of momentum of the component N in the k direction (x_i where $i = 3$) through a side perpendicular to the i direction (x_i where $i = 1$) is $\rho_N \alpha_N u_{Ni} u_{Nk}$. The net force in the k direction acting on the component N per unit of volume F_{Nk}^T is given by Equation 5.

$$F_{Nk}^T = \frac{\partial}{\partial t}(\rho_N \alpha_N u_{Nk}) + \frac{\partial}{\partial x_i}(\rho_N \alpha_N u_{Ni} u_{Nk}) \tag{5}$$

To account F_{Nk}^T, besides the force due to the pressure and viscous stresses on the exterior of a unit of volume, we must also consider the force that each component N imposes on the other components.

First, we define that there is a contribution due to an external force field. In the case of gravitational forces, we have $\alpha_N \rho_N g_k$. Then, we have a contribution to F_{Nk}^T due to traction on the control volume, given by Equation 6, which is considered only for the continuous phase.

$$\frac{\partial \sigma_{Cki}}{\partial x_i} \tag{6}$$

We can decompose the stress tensor σ_{Cki} from Equation 6 into a pressure and a deviatoric stress components, as shown in Equation 7.

$$\sigma_{Cki} = -p\delta_{ki} + \sigma_{Cki}^D \tag{7}$$

Where δ_{ki} is the Kronecker delta ($\delta_{ki} = 1$ for $k = i$ and $\delta_{ki} = 0$ for $k \neq i$).

The third contribution to the net force in the k direction is the force imposed on N by other components within the element of volume, here defined as F_{Nk}. Then, we can rewrite Equation 5 as Equation 8.

$$\frac{\partial}{\partial t}(\rho_N \alpha_N u_{Nk}) + \frac{\partial}{\partial x_i}(\rho_N \alpha_N u_{Ni} u_{Nk}) = \alpha_N \rho_N g_k + F_{Nk} - \delta_N \left\{ \frac{\partial p}{\partial x_k} - \frac{\sigma^D_{Cki}}{\partial x_i} \right\} \tag{8}$$

Where $\delta_N = 0$ for the dispersed phase, and $\delta_N = 1$ for the continuous phase. Note that, alike the case of mass interaction, $\sum_N F_{Nk} = 0$, and the equation for momentum conservation for a combined phase is written as Equation 9.

$$\frac{\partial}{\partial t}\left(\sum_N \rho_N \alpha_N u_{Nk}\right) + \frac{\partial}{\partial x_i}\left(\sum_N \rho_N \alpha_N u_{Ni} u_{Nk}\right) = \rho g_k - \frac{\partial p}{\partial x_k} + \frac{\partial \sigma^D_{Cki}}{\partial x_i} \tag{9}$$

2.2.3 The dynamic of a gas bubble ascending through liquid

The knowledge of how some variables of the flow of a single bubble are related to each other can help to better understand the behavior of multiple bubbles ascending in an underwater gas release. The analysis exhibited below is presented by Batchelor (2000) for a single bubble rising in a liquid medium.

A considered bubble has a finite volume and a free surface (shape). The volume of small bubbles is usually under 6×10^{-4} cm^3, and the surface tension keeps the bubble spherical. When the bubble grows, the mass of the gas becomes large enough for the gas pressure to control its volume. Then, when the volume of the bubble increases, the liquid phase will have a larger Reynolds number and the bubble becomes oblate and oscillates while ascending, due to the changes in the pressure in the water over its surface. If the bubble size is greater than 5 cm^3, the surface tension effects get smaller and the gas is flattened and acquires the shape of an umbrella (Batchelor, 2000). Figure 3 is based on the figure provided by Batchelor (2000) and gives a schematic representation of the bubble shape under the described conditions. The above-given description proves that when flowing up across a liquid with constant density under the action of gravitational forces, the volume and shape of the gas bubbles are of great importance to the study. In Figure 3 the bubble has two different contour profiles. The top part is smooth and almost spherical, and the bottom is irregularly rounded and saw-shaped.

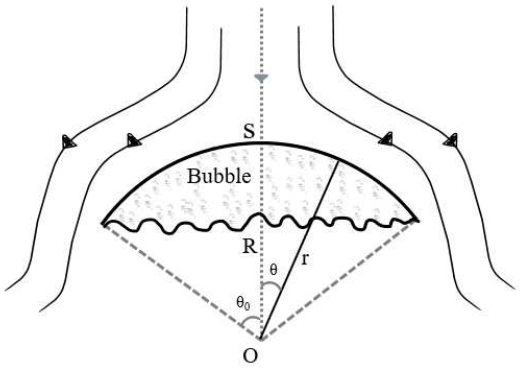

Figure 3: Representation of a spherical-cap large bubble ascending through a liquid.

The analysis found below models the behavior of the bubble and is valid for the following considerations (Batchelor, 2000):

- The vertical motion of the bubble is approximately steady;
- The applicability of the Bernoulli Equation to a streamline at the bubble surface is valid;
- The liquid phase is infinite and the pressure on the bubble surface is uniform.

If all three conditions are satisfied, it is possible to write Equation 10 (Batchelor, 2000). Note that the mathematical expression is obtained through a physical analysis.

$$\frac{1}{2}q_s^2 = g(R - r\cos\theta) \tag{10}$$

Where q_s is the water velocity at the bubble surface, g is the gravity acceleration, R is the radius of curvature of the bubble on the stagnation point S, r and θ are spherical coordinates with origin in O. All these variables can be identified in Figure 3. At a high Reynolds number, the velocity of the water at the gas bubble surface depends on the bubble size and the bubble ascending speed U. If a very small region around S is considered, q_s varies linearly with the distance, as shown in Equation 11 (Batchelor, 2000). This mathematical relationship depends on the geometry features of a single bubble in ascension.

$$q_s = \alpha U\theta \tag{11}$$

In Equation 11, α is a constant which depends only on the bubble shape.

The third step presented by Batchelor (2000) is the expansion of the right-hand side of the Equation 10 in powers of θ. The author mentions that the terms of order θ and θ^2 are equal to zero by the definition of R, and Equation 12 can be obtained.

$$r = R + O(\theta^3) \tag{12}$$

Substituting the left side of Equation 10 by Equation 11 and its right side by the value of r given by Equation 12, it is possible to obtain an expression. The value obtained when the angle θ assumes very small values leads to Equation 13.

$$\alpha^2 U^2 = gR \tag{13}$$

Equation 13 is exact and represents a physical analysis applicable to the system geometry, but it requires a value for the shape factor α.

To find a proper value for α in Equation 13, Batchelor (2000) relied to the fact that the inner boundary of the irrotational flow is approximately spherical, which allows estimating q_s as part of a sphere of radius R moving in an inviscid fluid and obtaining Equation 14.

$$q_s = \frac{3}{2} U \sin\theta \tag{14}$$

For small values of θ, Equation 14 can be compared with Equation 11 and a value of $\alpha = 3/2$ can be inferred. Substituting it in Equation 13, Equation 15 is obtained.

$$U = \frac{2}{3}(gR)^{1/2} \tag{15}$$

For a single bubble with a volume greater than 2 cm^3 ascending in water, the applicability of Equation 15, with the shape factor equal to 3/2, has already been proved valid (Batchelor, 2000). However, the applicability of this equation for multiphase systems with multiple bubbles lacks investigation.

2.3 CFD multiphase modeling

In the engineering field, when analyzing two-phase flows involving accidental subsea gas release, different approaches can be used. This section explains why Computational Fluid Dynamics was a highly recommended tool for obtaining data for this study.

2.3.1 What is CFD and why use it?

In Fluid Mechanics, Computational Fluid Dynamics (CFD) is the set of methodologies that enable a computer to perform a numerical simulation of fluid flows, allowing the analysis of the phenomena related to the movement of fluids and, consequently, to momentum, mass, and energy conservation. During a simulation, a virtual representation of a system is created on a computer, and billions of calculations are performed in order to provide a complete description of several characteristics of this system. This approach

is made possible due to the development of computer technology since it requires high computational resources (Hirsch, 2007; Versteeg and Malalasekera, 2007).

Within the scope of considering CFD to solve engineering problems, there are other fundamental procedures that can also be used instead of or combined with CFD. In the empirical approach, correlations are created using data collected from previous experiments. It can lead to universal solutions if developed under dimensional analysis, but usually, the applicability range of the model is restricted to the range under which experimental data was taken. The most accurate approach used to solve conservation equations is the rigorous one, but its applicability is very restrained since it requires the solution of the conservation equations with their boundary conditions, and this is not always possible. Lastly, the modeling approach consists of using a simplified physical model expressed mathematically in order to describe a phenomenon as closely as possible. It is a combination of the empirical and rigorous approach since it can use experimental measurements to refine the model, but it still requires an analytic tool to be solved (Shoham, 2006). Choosing the right approach is essential for obtaining a precise and fast solution to a given problem.

Multiphase flows occur according to all basic laws of fluid mechanics, but the equations are more numerous and complicated. This often makes it difficult, or even impossible, to use experimental approaches or rigorous solutions to describe these systems. Using CFD as a tool to solve problems is often a favorable choice when other techniques are compared. The possibility of using CFD depends on having high-performance hardware. Also, if one chooses to use commercial software, a license fee may be required. This usually results in a high investment cost, making CFD an expensive tool. However the cost of an experiment depends on the number of data points obtained and the configurations tested, and this number is often high enough to make the use of the CFD tool less expensive than the experimental approach. In addition to the lower cost, CFD is also capable to simulate situations where the experiments are difficult to perform or are too dangerous.

Another aspect to consider when choosing CFD is the difficulty in obtaining data for posterior mathematical analysis. The number of experiments in the literature involving gas release into the water, even in small-dimensioned experimental setups, is already limited. If true ocean conditions are considered, the data is even scarcer. In addition, it has already been proved that the scale-up of current integral models is not sufficiently accurate to predict the bubble plume behavior of large plumes (Cloete, Olsen, and Skjetne, 2009). In this context, CFD stands out for offering the possibility to carry out numerical experiments safely and at a relatively low cost, compared to most experimental studies.

Thanks to the continuous development of various turbulence and physical models over the years, CFD has emerged as a highly useful and efficient tool for solving conservation equations and analyzing risk scenarios through a numerical approach. There

are many software packages for multiphase flow analysis. They provide different detailed levels of physical approximation and numerical solutions. Among several aspects, the choice of appropriate software must take into consideration the desired precision to be acquired, the ability of the hardware to support it, and its cost (Flowe, Kumar, and Ojha, 2001).

2.3.2 Elements of a CFD code

All CFD codes contain three main elements: a pre-processor, a solver, and a post-processor (Versteeg and Malalasekera, 2007). Each one can be divided into several activities, which are essential to perform a simulation and obtain the correct desired results.

The pre-processor phase is characterized by the actions which define the flow problem that one is trying to solve. According to Versteeg and Malalasekera (2007), the main steps of this element are:

- Definition of the computational domain, which consists in creating a model geometry;
- Sub-division of the domain into a number of smaller sub-domains, also known as defining and creating the mesh;
- Selection of the physical and chemical phenomena that will be evaluated;
- Definition of fluid properties;
- Specification of boundary conditions.

The accuracy of a solution is directly linked to the number of cells in the grid: the larger the number of cells, the higher the accuracy. In addition, best meshes are usually non-uniform, due to the complexity of the geometries. The CFD user is responsible for designing a grid that strikes a balance between achieving a sufficiently accurate solution and maintaining a feasible computational cost. Over half of the time spent on CFD in an industry is estimated to go to geometry design and meshing. For this reason, many CFD codes include their own CAD-style interface and mesh generators. Other features that may be available in a CFD code are preprogrammed physical and chemical process models and fluid flow equations, and libraries of material properties (Versteeg and Malalasekera, 2007).

In order to correctly simulate a fluid flow, a CFD code can use numerical solution techniques such as finite difference, finite element and spectral methods. This work uses the Finite Volume Method. The solver element consists of three main steps (Versteeg and Malalasekera, 2007):

- Integration of the governing equations of fluid flow over the control volumes of the domain;
- Conversion of the integral equations into a system of algebraic equations, also known as discretization;
- Calculation of the solution of these algebraic equations using an iterative method.

The Finite Volume Method expresses a clear relationship between the numerical algorithm and the physical conservation principles. Therefore, the control volume integration results in the exact conservation of a variable for each cell. The CFD also has different discretization techniques for treating the different transport phenomena (convection, diffusion, and source terms) which may occur to a variable ϕ in a certain amount of time. Finally, the iterative solution approach can use different solution procedures and algorithms in order to correctly calculate complex and non-linear equations obtained in the previous step (Versteeg and Malalasekera, 2007).

After the calculations, it is necessary to interpret the obtained results. Since a lot of data is available, powerful visualization software is necessary to generate graphics that correctly summarize the results. This step of the simulation is post-processing. Some of the tools included in one software with CFD code are geometry and grid displays, with view manipulation; 2D and 3D vector, contour, and surface plots; particle tracking; animation for dynamic result display; and data export facilities for further manipulation external to the code (Versteeg and Malalasekera, 2007).

2.3.3 The Finite Volume Method

CFD codes are structured around the idea of using numerical methods to calculate fluid flow parameters. Numerical methods are widely employed to solve engineering problems when we are not able to obtain a rigorous (exact) solution, sometimes due to the complexity of the governing differential equations, or sometimes due to difficulties related to the boundary and initial conditions. When using a numerical method, one needs a discretization process, because differently from the rigorous solution, which gives the information at any point within the system, the numerical methods are able to show the approximate solutions only at discrete points, called nodes (Moaveni, 2008).

All discretization methods work by replacing the continuous exact solution of the partial differential conservation equation with discrete values. Besides the domain discretization in structured grids, there must be an equation discretization, which positions the results within the cells of the discretized physical domain. The main discretization methods are the Finite Difference Method, the Finite Element Method, and the Finite Volume Method, also known as FVM (Moukalled, Mangani, and Darwish, 2016).

The FVM consists in discretize the integral or differential equations of the conservation laws directly in the physical space, in discrete algebraic equations over finite volumes. Then, the divergence theorem is used to transform volume integrals into surface integrals. The terms are computed as fluxes at the surface of each small finite volume (Hirsch, 2007; Moukalled, Mangani, and Darwish, 2016).

According to Moukalled, Mangani, and Darwish (2016), there are two different variable arrangements in the FVM, which are the approach used to define the shape and position of the control volumes in a grid. The cell-centered uses the centroid of grid cells to store quantities, while the grid lines demarcate the finite volumes. The vertex-centered arrangement stores variables at the vertices and the cell can be created around the grid point in several ways. The cell-centered is preferred by the FVM and is used in software like ANSYS Fluent, and OpenFOAM.

The FVM is the most commonly used method in CFD, and due to the many advantages of the method, in the near future, is likely to remain so. First, the method is considered strictly conservative, since it turns conservation equations into fluxes that flows through finite volume faces, and considers the flux entering a volume equal to the flux leaving the adjacent volume. Secondly, the method can easily be implemented for arbitrary grids, working effectively on structured or unstructured polygon meshes. And lastly, as the unknown variables are evaluated at the centroids of the volume elements, instead of their boundary faces, the boundary conditions are not invasive, and easier to implement (Hirsch, 2007; Moukalled, Mangani, and Darwish, 2016).

2.3.4 CFD two-phase modeling approach

There are several types of flows that can be studied using CFD tools and, for a two-phase flow, there are basically two distinct ways to describe the motion of a fluid: the Eulerian description, and the Lagrangian description. In the Eulerian description, also known as Euler-Euler or Eulerian-Eulerian, the fluid flows in and out of a finite volume called control volume and, instead of keeping track of the position and velocity of a mass of fluid particles, we track field variables within the control volume. In the Lagrangian approach, also known as Euler-Lagrange or Eulerian-Lagrangian representation, the continuous phase is treated in an Eulerian representation, and the fluid elements of the disperse phase are individually tracked and studied according to Newton's laws (Çengel and Cimbala, 2006; Michaelides, Crowe, and Schwarzkopf, 2016; Sokolichin et al., 1997; Versteeg and Malalasekera, 2007).

The Lagrangian approach assumes that the dispersed phase, which can exchange momentum, mass, and energy with the fluid phase, has no volume. This makes it useful to model situations where the second phase has a very low volume fraction, such as spray dryers. However, it is inappropriate for modeling situations in which the vol-

ume fraction of the second phase can not be neglected, such as in fluidized beds. In the Eulerian approach, the different phases have significant volumes and are mathematically treated as interpenetrating continua. For this reason, it is introduced the concept of volume fraction, in which the sum is always equal to 1. In ANSYS Fluent, there are three different Eulerian multiphase models available: the Volume of Fluid (VOF) model, the Mixture Model, and the Eulerian Model (ANSYS Fluent, 2019).

The VOF model is advised to be used when there is a desire to track the position of the interface between two or more immiscible fluids. In this model, a single set of equations is shared between the phases and the concept of volume fraction is introduced. The Mixture Model solves the momentum equation for the mixture and assigns it to the relative velocities of the dispersed phases. If the model is chosen for the simulations, additional information regarding the dispersed phase may be needed for proper case setup. Lastly, the Eulerian Model, the most complex multiphase model in ANSYS Fluent, is capable of solving n momentum and continuity equations for each phase, which makes it the most computationally expensive model (ANSYS Fluent, 2019).

In underwater gas release studies, both Lagrangian and Eulerian coordinates have been successfully used to simulate flows. Each coordinate representation has its advantages and disadvantages. However, only an Eulerian coordinate approach is able to properly track the interface between two fluids. In this context, since this work chooses to focus on the study of the interfaces between gas and liquid, an Eulerian approach was chosen for this purpose despite its higher computational cost.

The gas rising in a water medium is a relatively complex multiphase flow, which makes it very hard to be correctly modeled. The choice of the proper Eulerian model must consider the most relevant aspect of the flow. A detailed representation of the interface formed by water and air at the surface is of great importance in the area of process safety, since it is the region where the leaked gas starts to interact with offshore structures. Furthermore, it is the region of interest for calculating the gas rising time. Finally, the choice of a mixture model would depend on information about the bubbles formed during the flow, something that was not available and could be determined only through the study, and not for it. These characteristics contributed to the VOF model, described below, being selected for this work.

2.3.5 The Volume of Fluid method

The VOF was proposed by Hirt and Nichols (1981) to provide information about how a mesh cell is occupied by one fluid in multiphase flows using a simple data structure. To define the occupation of the domain by the phases, in VOF, a scalar between 0 and 1 is used to indicate which fluid, or fluids, occupies each cell of a mesh. Suppose that we define α as the VOF scalar. When the value α is 1, any point of the cell is occupied

by a certain fluid. When α is 0, the cell does not contains such fluid. In a two-phase CFD study, by constraint, it is possible to affirm that when α is equal to 0, the cell is fully occupied by a second fluid. Lastly, when α is a value between 0 and 1, the cell must contain a free surface, because it will contain both fluids (Yeoh and Tu, 2010).

In short, in a two-phase simulation, three scenarios are possible for the variable α:

- $\alpha = 1$, which means that the cell is fully filled with fluid q;
- $\alpha = 0$, which means that the cell does not have any region filled with fluid q and is fully filled with fluid p;
- $0 < \alpha < 1$, which means that the cell has an interface between fluid q and fluid p.

For the qth phase, the material balance is described by Equation 16 (ANSYS Fluent, 2019).

$$\frac{1}{\rho_q}\left[\frac{\partial}{\partial t}\left(\alpha_q \rho_q\right) + \frac{\partial}{\partial x_i}\left(\alpha_q \rho_q u_q\right) = S_{\alpha_q} + \sum_{p=1}^{n}\left(\dot{m}_{pq} - \dot{m}_{qp}\right)\right] \tag{16}$$

Where ρ_q is the phase density, $\dot{m}_{pq}$ is the mass transfer from phase p to phase q, $\dot{m}_{qp}$ is the mass transfer from phase q to phase p, S_{α_q} is a source term equal to 0 by default, but changeable. It is important to remind that $\sum_{p=1}^{n} \alpha_q = 1$.

In the VOF method, the momentum balance is derived from the Navier-Stokes equations and can be expressed as Equation 17 (ANSYS Fluent, 2019).

$$\frac{\partial}{\partial t}(\rho u_i) + \frac{\partial}{\partial x_j}(\rho u_i u_j) = -\frac{\partial P}{\partial x_i} + \frac{\partial}{\partial x_j}(\tau_{ij}) + \rho g_i + S_i \tag{17}$$

Where ρ is the fluid density, u_i the velocity, P is the pressure, τ_{ij} is the viscous stress tensor, g_i is the gravity acceleration and S_i is the source term.

It is important to emphasize that the presence of multiple phases in the domain is considered since the fluid properties are expressed as a function of α. For a two-phase flow, a property such as the fluid density can be expressed as Equation 18.

$$\rho = \alpha_p \rho_p + (1 - \alpha_p)\rho_q \tag{18}$$

Other properties (e.g., viscosity) follow the same mathematical relationship to be computed.

In the study of multiphase flows, it is important to consider the effects of interaction and information exchange between the phases or interfaces of the system. This effect is called "coupling" and occurs when the conservation equations are solved for each phase and the solutions are updated iteratively considering all phases. Coupling

methods vary depending on the problem studied. Common examples are the implicit coupling method, and the explicit coupling method (ANSYS Fluent, 2019).

In the implicit scheme, equations are solved simultaneously for all phases because the value of the volume fraction at the current time step is used to calculate the other variables. This method tends to be more stable and accurate, especially for simulations with significant differences in density, viscosity, or other parameters between phases. In transient studies, for each time step, a scalar transport equation needs to be solved iteratively for each of the secondary-phase volume fractions. As a consequence, standard finite-difference interpolation schemes need to be used to calculate the face fluxes for all cells. In ANSYS Fluent, the implicit scheme is suitable for both transient and steady-state simulations. In the explicit coupling, each phase is solved sequentially, considering updated information from previous phases. For transient studies, it computes the variables using the values of their previous time step. The advantage is that, for each time step, this formulation does not need to solve the transport equations during each time step using iterative solution schemes, as is required for the implicit scheme. Therefore, the choice of formulation depends on the nature of the problem, the characteristics of the phases involved, and the objectives of the simulation. Each method has its advantages and disadvantages and they are applicable in different scenarios (ANSYS Fluent, 2019).

Finally, although a value of α different from 0 or 1 indicates the existence of an interface, it does not indicate where that interface is located in the cell, requiring an algorithm to do so. The tracking of the interface begins with the solution of a continuity equation for the volume fraction of one or more phases.

The two available techniques to interpolate the face fluxes are the interface reconstruction and the finite volume discretization scheme. Examples of reconstruction-based schemes in ANSYS Fluent are the Geo-Reconstruct and Donor-Acceptor, while examples of discretization schemes are First Order Upwind, Second Order Upwind, CICSAM, Modified HRIC, and QUICK. The choice of the interpolation technique will depend on the coupling method (implicit or explicit), the solution being time-dependent, and the type of cells in the mesh, among other criteria. As an example, the schemes available for a transient simulation with VOF model, implicit formulation and sharp interface modeling type are the Compressive and the Modified HRIC. The Compressive scheme seeks to deal with abrupt changes in the interface. It uses techniques to smooth variations and minimize numerical oscillations, while the Modified HRIC is designed to provide high-resolution interface capture using high-order interpolation and techniques to preserve mass and minimize oscillations (ANSYS Fluent, 2019).

2.4 Turbulence modeling

A very important aspect of CFD two-phase flow modeling is the choice of a suitable turbulence model. This section presents a brief review of what is the turbulence phenomenon and explains which group of turbulence models will be investigated in this work.

2.4.1 What is turbulence?

When a flow is characterized by its smooth layers of fluid with highly ordered motion, it is called laminar flow. Regardless of its complexity, every flow becomes unstable above a certain critical Reynolds number value. This inconstancy is characterized by a fluid flowing with highly disordered motion and with irregular fluctuations around the average values of its properties. In some cases, these fluctuations can reach values around 10%, in other cases, even higher, such as 20% in free turbulent flows. This stochastic motion of each little element of a fluid particle is named turbulence and characterizes the turbulent flow. If the flow alternates between laminar and turbulent, it is called transitional (Çengel and Cimbala, 2006; Hirsch, 2007; Versteeg and Malalasekera, 2007).

Near the boundaries of a control volume, the turbulence creates a mixing with random currents of recirculating fluid called eddy motions. Through these boundaries, the eddies carry mass, momentum, and energy into and out of the control volume. This indicates that the traditional equations for mass, momentum and energy balances should be affected by the turbulence caused by the fluctuations (Versteeg and Malalasekera, 2007).

In engineering, most flows are turbulent, and, for some processes being able to occur properly, it is mandatory to promote or avoid turbulence in many cases. This makes interesting studying the turbulence phenomenon not restricted only to a theoretical level but also aiming for practical applications (Hirsch, 2007; Versteeg and Malalasekera, 2007).

The analytic or numerical solution for turbulent flows can be obtained in different levels of precision, depending on the description of the flow characteristics. When turbulence modeling is necessary for the study of a multiphase flow, obtaining analytical solutions become impossible. However, the numerical description of the turbulent fluctuations requires a combination of advanced mathematical modeling and high computational power but is already possible. Furthermore, the increase computing power and memory of computers in the last decades allowed the simulation of turbulent fluctuations on the computer using the time-dependent Navier–Stokes equations, and it is expected that in the coming years the computational capacity to perform such calculations will keep increasing (Versteeg and Malalasekera, 2007).

Turbulence models and multiphase flows are two of the most challenging topics in fluid mechanics. When the two are combined, the difficulty in their study becomes even higher, because of the stochastic nature of the carrier phase, turbulence has to be modeled along with the random distribution of the dispersed phase (Balachandar and Eaton, 2010). In the study of bubble plumes in water, the breakup of bubbles in a turbulent environment is considered a very complex physical process, because they are formed in different sizes and shapes (Friedl and Fanneløp, 2000).

2.4.2 RANS turbulence modeling in CFD

Currently, there are three main categories of methods used to model turbulent effects. The Reynolds-Averaged Navier–Stokes (RANS) focus on computing the mean flow and its properties, using supplementary models to calculate the effects of interactions between turbulent fluctuations. The Large Eddy Simulation (LES) simulates turbulent fluctuations of larger eddies scales and models the smaller scales. The Direct Numerical Simulation (DNS) computes the mean flow along with the turbulent velocity fluctuations and the time-dependent Navier–Stokes equations are solved in grids fine enough to resolve the Kolmogorov length scales (Hirsch, 2007; Versteeg and Malalasekera, 2007).

While choosing a method to model turbulence effects, it is important to consider the feasibility in terms of time and computing capacity when choosing a method. Most engineering flow calculations stand on RANS since the method requires modest computing resources if compared to LES and DNS. Currently, LES is already reaching the industrial stage, but it is still too costly for most of the engineering applications. Nonetheless, as a consequence of simulating all turbulent velocity fluctuations, the computer requirements for DNS simulation are still extremely high, making it unfeasible to be used in industrial flow computations (Chaouat, 2017). Considering the complexity of multiphase flows, the RANS models are the most feasible approach for computing turbulent flow quantities, especially for multiphase flows.

When using RANS, the turbulence effects are modeled and the quantities are calculated based on their average values. As an example, Figure 4 illustrates the behavior of the velocity component (u_i) over time. The inconstancy of turbulence can be related to the convective term of equations of motion. The fluctuating term is nonlinear, even when the fluid is incompressible, and it is three-dimensional even when the quantity varies in one or two space dimensions. As a consequence, all quantities related to this variable will assume a statistical behavior, and the conservation equations are solved along with the turbulent transport equations (Hirsch, 2007; Versteeg and Malalasekera, 2007).

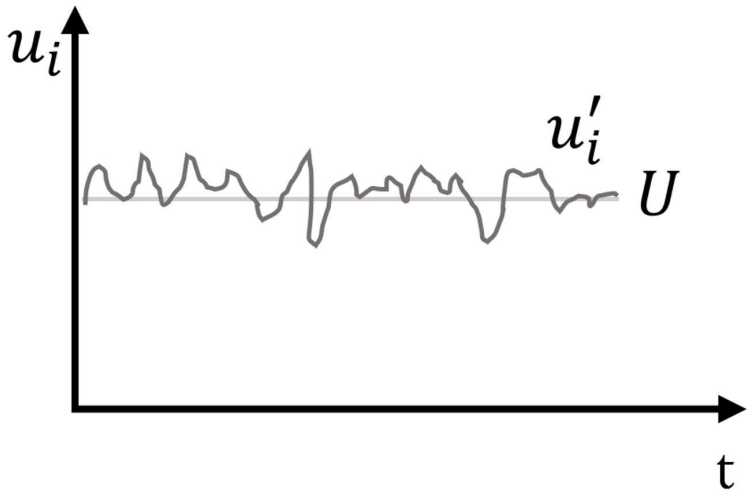

Figure 4: Value of u_i over time.

In Figure 4, the velocity is decomposed into a steady mean value U and a fluctuating component u_i', and can be written as $u_i = U + u_i'$. This notation is called Reynolds decomposition. Similarly, any scalar quantity can be written as $\phi = \Phi + \phi'$. Since all variables follow a generalized conservation principle, for the variable ϕ, the differential balance equation is given by Equation 19 (Patankar, 1980):

$$\frac{\partial(\rho\phi)}{\partial t} + \frac{\partial}{\partial x_i}\left(\rho u_i \phi - \Gamma_\phi \frac{\partial \phi}{\partial x_i}\right) = S_\phi \tag{19}$$

Where ρ is the density, Γ is diffusion coefficient, and S is the source term. If the value of ϕ in Equation 19 is replaced by its mean value Φ added to its fluctuation ϕ', we have Equation 20, where the overbar refres to a time-averaged variable and the tilde to a Favre-averaged variable (Versteeg and Malalasekera, 2007).

$$\frac{\partial}{\partial t}(\bar{\rho}\tilde{\Phi}) + \frac{\partial}{\partial x_i}\left(\bar{\rho}\tilde{\Phi}\tilde{U} - \Gamma_\Phi \frac{\partial \tilde{\Phi}}{\partial x_i}\right) = \left[-\frac{\partial \overline{\bar{\rho}u_i'\phi'}}{\partial x_i} - \frac{\partial \overline{\bar{\rho}u_j'\phi'}}{\partial x_j} - \frac{\partial \overline{\bar{\rho}u_k'\phi'}}{\partial x_k}\right] + S_\Phi \tag{20}$$

The effects of turbulence appear in the sum of the three first terms on the right hand side of Equation 20.

In cases where the variable ϕ represents the velocity, this sum acquires tension units and become known as as Reynolds stresses. Considering the balance equations and the Reynolds stresses, there are more variable unknowns than there are equations. The turbulence models were developed to describe these Reynolds stress terms and close the equations (Versteeg and Malalasekera, 2007).

In order to solve the conservation equations, predicting the Reynolds stresses and the scalar transport terms correctly, it is necessary to develop turbulence models, which must be accurate, simple, economical to run, and have wide applicability. A turbulence model can add new equations that need to be solved along with the usual transport

equations. Some common turbulence models are the Spalart-Allmaras, which is a one-equation model, k-ε and k–ω, which are two-equation models, and Reynolds Stress Model (RSM), which is a more comprehensive turbulence model that includes seven additional transport equations in 3D problems or five equations in 2D problems. These and other models can suffer small modifications in order to better describe a specific flow. The choice of an appropriate model may define the success of a CFD simulation (Versteeg and Malalasekera, 2007).

In 1877, Boussinesq proposed a relationship between the turbulent stresses and the mean flow's velocity gradients, in analogy with Newton's law of viscosity (Souza et al., 2011). Equation 21 summarizes the Boussinesq hypothesis.

$$\tau_{ij} = -\rho\overline{u_i' u_j'} = \mu_t \left(\frac{\partial U_i}{\partial x_j} + \frac{\partial U_j}{\partial x_i} \right) - \frac{2}{3}\rho k \delta_{ij} \tag{21}$$

Where τ_{ij} represents the Reynolds' stress which can also be expressed as $-\rho\overline{u_i' u_j'}$, μ_t means the turbulent (or eddy) viscosity, which is a property of the flow, not of the fluid, k means the turbulent kinetic energy per unit mass and is equal to $\frac{1}{2}(\overline{u_i'^2})$, and δ_{ki} is the Kronecker delta (Versteeg and Malalasekera, 2007). When assuming the Boussinesq hypothesis, the necessity of developing expressions for the turbulent viscosity calculation comes up. To fill that need, different RANS models had been proposed. Next, please find a brief description of the two turbulence models used in the simulations of this work.

2.4.3 The standard k-ε model

The standard k-ε model is a semi-empirical model which combines two separate transport equations, one related to the turbulent kinetic energy (k), and the other to its dissipation rate (ε) (Launder and Spalding, 1974). When dealing with k, the model transport equation is derived from the exact equation. On the other hand, the derivation of ε comes from physical reasoning. The model assumes that the flow is fully turbulent (ANSYS Fluent, 2019).

The velocity and length scales representative of the large-scale turbulence can be defined as $V = k^{1/2}$ and $\ell = \frac{k^{3/2}}{\varepsilon}$. Then, the turbulent viscosity is computed using k and ε according to Equation 22.

$$\mu_t = \rho C_\mu V \ell = \rho C_\mu \frac{k^2}{\varepsilon} \tag{22}$$

Where C_μ is a dimensionless constant.

The transport equations for k and ε are given by Equations 23 and 24.

$$\frac{\partial}{\partial t}(\rho k) + \frac{\partial}{\partial x_i}(\rho k u_i) = \frac{\partial}{\partial x_j}\left[\left(\mu + \frac{\mu_t}{\sigma_k}\right)\frac{\partial k}{\partial x_j}\right] + G_k + G_b - \rho\varepsilon - Y_M + S_k \tag{23}$$

$$\frac{\partial}{\partial t}(\rho \varepsilon) + \frac{\partial}{\partial x_i}(\rho \varepsilon u_i) = \frac{\partial}{\partial x_j}\left[\left(\mu + \frac{\mu_t}{\sigma_\varepsilon}\right)\frac{\partial \varepsilon}{\partial x_j}\right] + C_{1\varepsilon}\frac{\varepsilon}{k}(G_k + C_{3\varepsilon}G_b) - C_{2\varepsilon}\rho\frac{\varepsilon^2}{k} + S_\varepsilon \tag{24}$$

Where $C_{1\varepsilon}$, $C_{2\varepsilon}$ and $C_{3\varepsilon}$ are constants. In ANSYS Fluent, $C_{1\varepsilon} = 1.44$, $C_{2\varepsilon} = 1.92$ and $C_{3\varepsilon}$ is calculated by Equation 25. Furthermore, σ_k and σ_ε are, respectively, the turbulent Prandtl numbers for k and ε equal to 1.0 and 1.3 respectively, and S_k and S_ε are user-defined additional source terms.

$$C_{3\varepsilon} = tanh\left|\frac{v}{u}\right| \tag{25}$$

Where v is the component of the flow velocity parallel to the gravitational vector and u is the component of the flow velocity perpendicular to the gravitational vector.

In Equations 23 and 24, G_k is the generation of turbulent kinetic energy due to the mean velocity gradients, given by Equation 26, and G_b is the generation of turbulent kinetic energy due to buoyancy, given by Equation 27.

$$G_k = -\rho\overline{u_i' u_j'}\frac{\partial u_j}{\partial x_i} = \mu_t S^2 \tag{26}$$

$$G_b = -\frac{1}{\rho}\left(\frac{\partial \rho}{\partial T}\right)_p g_i \frac{\mu_t}{Pr_t}\frac{\partial T}{\partial x_i} \tag{27}$$

Where $S = \sqrt{2S_{ij}S_{ij}}$ and S_{ij} is given by Equation 28.

$$S_{ij} = \frac{1}{2}\left[\frac{\partial u_i}{\partial x_j} + \frac{\partial u_j}{\partial x_i}\right] \tag{28}$$

In Equation 27, Pr_t is the turbulent Prandtl number for energy and T is the temperature. For ideal gases, Equation 27 is summarized in Equation 29.

$$G_b = -g_i \frac{\mu_t}{\rho Pr_t}\frac{\partial \rho}{\partial x_i} \tag{29}$$

Still regarding Equation 23, Y_M represents the contribution of the fluctuating dilatation in compressible turbulence to the overall dissipation rate and is given by Equation 30.

$$Y_M = 2\rho\varepsilon M_t^2 \tag{30}$$

Where $M_t = \sqrt{\frac{k}{a^2}}$ and $a = \sqrt{\gamma RT}$. With a being the speed of the sound, calculated using the temperature T, the molar gas constant R, and the isentropic expansion factor γ.

2.4.4 The realizable k-ε model

The realizable k-ε model is a modified form of the standard k-ε which receives its name from the fact that it satisfies some mathematical limitations verified in the original model when describing the Reynolds stresses. These limitations are related to the physics of turbulent flows and are also not satisfied by other models, such as k-ω. The standard equations differ from the realizable in two ways: it has a different formulation for the turbulence viscosity; and the dissipation rate is modeled by a different equation, derived from an exact equation for the transport of the mean-square vorticity fluctuation (ANSYS Fluent, 2019).

Compared to the standard k-ε, the realizable k-ε model improved features related to the streamlined curvature, vortices, and rotation. As a consequence, the model provides the best performance describing separated flows, for example. Additionally, this model is effective in predicting the dispersion of gases in submersed jets, while traditional models fail in predicting the dispersion of jets due to the modeled dissipation equation (ANSYS Fluent, 2019; Sun et al., 2020).

Equations 31 and 32 present, respectively, the modeled transport equations for k and ε in the realizable k-ε model.

$$\frac{\partial}{\partial t}(\rho k) + \frac{\partial}{\partial x_j}(\rho k u_j) = \frac{\partial}{\partial x_j}\left[\left(\mu + \frac{\mu_t}{\sigma_k}\right)\frac{\partial k}{\partial x_j}\right] + G_k + G_b - \rho\varepsilon - Y_M + S_k \tag{31}$$

$$\frac{\partial}{\partial t}(\rho\varepsilon) + \frac{\partial}{\partial x_j}(\rho\varepsilon u_j) = \frac{\partial}{\partial x_j}\left[\left(\mu + \frac{\mu_t}{\sigma_\varepsilon}\right)\frac{\partial \varepsilon}{\partial x_j}\right] + \rho C_1 S\varepsilon - \rho C_2 \frac{\varepsilon^2}{k + \sqrt{\nu\varepsilon}} + C_{1\varepsilon}\frac{\varepsilon}{k}C_{3\varepsilon}G_b + S_\varepsilon \tag{32}$$

Where $C_1 = \max\left[0.43, \frac{\eta}{\eta+5}\right]$, $\eta = S\frac{k}{\varepsilon}$, and $S = \sqrt{2S_{ij}S_{ij}}$.

In Equations 31 and 32, G_k represents the generation of turbulence kinetic energy due to the mean velocity gradients; G_b accounts for the generation of turbulence kinetic energy due to buoyancy; Y_M represents the contribution of the fluctuating dilatation in compressible turbulence to the overall dissipation rate. These three variables follow Equations 26, 27 and 30, just like for the standard k-ε model. Also, C_2 and $C_{1\varepsilon}$ are constants; C_1 and $C_{3\varepsilon}$ are parameters of the model; σ_k and σ_ε are the turbulent Prandtl numbers for k and ε, respectively; S_k and S_ε are additional user-defined source terms; and ν is the molecular kinematic viscosity (ANSYS Fluent, 2019).

While Equation 31 differs from 23 only in the model constants, Equation 32 shows more differences from Equation 24. As an example, the production of ε does not consider the production of k. In ANSYS Fluent, $C_{1\varepsilon}$=1.44, C_2=1.9, σ_k=1.0, and σ_ε=1.2 (ANSYS Fluent, 2019).

Similar to the standard k-ε model, the realizable k-ε model computes the eddy viscosity according to Equation 22. However, the great difference between the two models comes from the fact that realizable k-ε does not consider C_μ a constant but computes its value from Equation 33 (ANSYS Fluent, 2019).

$$C_\mu = \frac{1}{A_0 + A_S \frac{kU^*}{\epsilon}} \tag{33}$$

Where $U^* \equiv \sqrt{S_{ij}S_{ij} + \tilde{\Omega}_{ij}\tilde{\Omega}_{ij}}$, $\tilde{\Omega}_{ij} = \Omega_{ij} - 2\varepsilon_{ijk}\omega_k$, and $\Omega_{ij} = \overline{\Omega_{ij}} - \varepsilon_{ijk}\omega_k$. Note that $\overline{\Omega_{ij}}$ represents the mean rate-of-rotation tensor viewed in a moving reference frame with the angular velocity ω_k. The constant A_0 is equal to 4.04 and A_S is calculated according to Equation 34 (ANSYS Fluent, 2019).

$$A_S = \sqrt{6}cos\phi \tag{34}$$

Where $\phi = \frac{1}{3}cos^{-1}(\sqrt{6}W)$, $W = \frac{S_{ij}S_{jk}S_{ki}}{\tilde{S}^3}$, $\tilde{S} = \sqrt{S_{ij}S_{ij}}$, and $S_{ij} = \frac{1}{2}\left(\frac{\partial u_j}{\partial x_i} + \frac{\partial u_i}{\partial x_j}\right)$.

2.5 Literature supporting work

This section introduces the main works available in the literature that were used in the development of the methodology and in the interpretation of the results presented in this thesis. The selected works bring information from either realistic experiments or numerical experiments.

2.5.1 Fanneløp experiments

Fanneløp and Sjøen (1980) did some experiments to analyze air liberation in a water tank with two distinct water column heights: 5.5 m and 10.0 m. The tank was 260 m × 10.5 m. There was a nozzle of 0.1 m with 150 holes of 1 mm at the center of the bottom face of the tank, from where the air was released at 0.022 Nm^3/s. The authors collect data about the geometric parameters that characterized the resulting stationary plumes, especially the ascending velocity of the gas at different horizontal positions and at three distances below the surface: 7.75, 6.15, and 2.95 m. The authors also monitored the continuous plume volatility profile and the volumetric air fraction at three different heights.

2.5.2 Engebretsen experiments

Another relevant experimental work was developed by Engebretsen et al. (1997). The authors evaluated the air liberation in a 7 m deep tank with a base of 9 m× 6 m, with an orifice of 0.34 m at the center of its bottom face. The air flow rates were 0.050, 0.100, and 0.450 m^3/s. Information regarding the gas rising time and fountain heights at the rising time and after 15 s of flow was collected. The authors also monitored the continuous plume velocity profile and the volumetric air fraction at three different heights.

2.5.3 Cloete numerical experiments

One of the first attempts to simulate underwater gas release was made by Cloete, Olsen, and Skjetne (2009). The authors tried to reproduce the experiments of Engebretsen et al. (1997) using FLUENT 6.3.26. To model the air and water interaction, a combination of the Eulerian-Eulerian VOF method with the Eulerian-Lagrangian Discrete Phase Model (DPM) was applied. This method consists in tracking the bubble plume with the DPM method, which means treating the bubbles as point sources of momentum to save computational resources in the simulations, and at the same time, using the VOF method to track the sharp interface between water and air at the surface of the tank. The computational schemes used were PRESTO! for pressure discretization, PISO for pressure-velocity coupling, Geo-Reconstruct for interface tracking, and a second-order upwind scheme for the other options. The results obtained were very satisfactory for the rising times, with absolute errors of 0.1, 0.28, and 0.06 s for the flow rates of 0.050, 0.100, and 0.450 m^3/s, respectively. Regarding the fountain heights, the values were calculated at the rising times and the results obtained were discrepant 0.02 and 0.36 m from the experimental results for 0.100 and 0.450 m^3/s, respectively. The fountain for 0.050 m^3/s was not obtained. The continuous plume velocity profile and the volumetric air fraction at three different heights were also monitored, but the comparison with the experimental data did not show great agreement due to the averaged representation of the plume given by a RANS turbulent model.

2.5.4 Wu numerical experiments

Wu et al. (2017) studied in ANSYS CFX software four different numerical approaches for modeling the turbulence of air liberation into a water tank: two RANS (standard k-ε and modified k-ε), an Unsteady Reynolds-Averaged Navier-Stokes (URANS), and LES. An Eulerian-Eulerian model was used, which simplified the implementation of physics models and turbulence effects. To validate the simulated data, the authors used the experimental work from Fanneløp and Sjøen (1980) for validation: velocity profiles at depths of 7.75, 6.15, and 2.95 m from the surface were obtained. Following the directions

from the original experimental work, the water depth considered was 10 m, the air release rate was 0.022 Nm^3/s, and the computational domain was 260 m in length, 10.5 m in width, and 10 m in depth. A total time of 40 s was simulated. The work concluded that the k-ε models (RANS) are not effectively capable of capturing the fluctuating velocity components in the plume and, as a consequence, the central velocities of the plume were overestimated and the plume widths were underestimated due to the lack of mechanisms to distribute and dissipate the momentum related to the release of the plume. On the other hand, the LES approach was able to distribute and dissipate correctly the momentum, however, the computational cost of LES simulations was significantly higher than it was for RANS models.

2.5.5 Other relevant CFD works

Although there are several knowledge gaps regarding the use of CFD to correctly predict underwater gas releases, the tool is already capable of computing some details and reproducing realistic features of the phenomenon. Some relevant contributions to this research field are chronologically listed below.

The work of Pan et al. (2014) is based on the the work of Cloete, Olsen, and Skjetne (2009). The Eulerian-Lagrangian VOF+DPM approach was used in FLUENT to try to reproduce the experimental results of Engebretsen et al. (1997). The authors chose to try improving the turbulence modeling by modifying the k-ε model. A new model was proposed to predict the behavior of bubble plumes resulting from a subsea gas release.

Once again, the Eulerian-Lagrangian approach proposed by Cloete, Olsen, and Skjetne (2009) was used to try to numerically reproduce the results of Engebretsen et al. (1997). Olsen and Skjetne (2016) used the software ANSYS Fluent with several user-defined functions to simulate the phenomenon. The choice of the k-ε turbulence model was pointed out as the main cause of the divergence between experimental and simulated results. The authors also highlighted the importance of including an appropriate correlation for the mass transfer coefficient when gas and liquid phases have strong interactions.

Olsen, Skjetne, and Johansen (2017) used a Very Large Eddy Scale (VLES) model, which is a filtered modification of the URANS model, to simulate air release at flow rates of 0.03, 0.14, 0.34 and 0.71 kg/s in a domain filled with a column of 50 m of water. The authors compared the VLES model and the k-ε model (RANS) with experimental data and affirmed that the k-ε model, besides being the most used turbulence model in two-phase flow simulation, fails to predict transient behavior. Although hardware information and values of the simulations times have not been specified, the VLES simulations are said to provide more details about flow turbulence compared to the k-ε model "at little extra computational cost".

Another relevant work was developed by Xinhong et al. (2018). They used the VOF+DPM approach to simulate in Fluent the air release from a pipeline with a hole of 0.005 m. The simulated data was compared to the experimental data of Engebretsen et al. (1997) for validation. Similar to what occurred in the previously cited works, the inherently RANS nature of the k-ε model was mentioned as responsible for retaining the momentum to the core of the gas plume instead of distributing it. As a consequence, higher plume centerline velocities were identified.

Li, Chen, and Khan (2019) used an Eulerian-Lagrangian CFD model in the simulation of air release into the water. They analyzed three leak directions, three leak sizes, and three leak pressures. The simulated data were compared to their own experimental results. Their small-scale experiment differs from the one from Engebretsen et al. (1997) due to the boundary conditions. Through the realizable k-ε turbulence model, the simulations resulted in close experimental and simulated parameters, but with an underestimated width of the plume and an overestimated height of the fountain. Despite that, using the deviation statistics analysis method, the authors considered the level of the results acceptable and the simulation setup validated.

Olsen and Skjene (2020) used the VOF+DPM to compare the release of CH_4 and CO_2. They also compared the VLES with the k-ε turbulence model on the prediction of the plume parameters. One of the experiments used for data validation was the data from Engebretsen et al. (1997). An important observation was that a greater discrepancy between the model and the observed results was verified in releases with high jet momentum. The study also showed the importance of understanding the effects of interaction between liquid and gas phases, since different gases interact in different ways with the water.

Sun et al. (2020) studied a 3D model based on coupled Eulerian-Lagrangian approach on the evaluation of air leaking into water under the effects of water currents. The realizable k-ε model was suggested for modeling the turbulence of the underwater gas jet due to its high accuracy in predicting the gas dispersion under these conditions, if compared to other RANS turbulence models. The authors verified the non-linearity between the variables of gas flow rate and the rising time of the plume.

Li, Han, et al. (2020) compared the Eulerian-Eulerian and Eulerian-Lagrangian methods on the simulation of air release into the water. Both methods were consistent with the experimental data, but the Eulerian-Eulerian had higher computational costs in all evaluated cases. The authors, therefore, showed a preference for the Eulerian-Lagrangian model.

Geng et al. (2021) compared experimental and simulated data from air released from underwater soil. Effects of the leak pressures, water depths, and buried depths were evaluated. The deviation statistical analysis method was used to validate the simulation setup, although the simulated plume width and fountain height values were

slightly overestimated by the simulations, while the gas rising time was overestimated. The Eulerian-Eulerian VOF approach and realizable k-ε model were used in Fluent 17.0.

Li and Wang (2023) included the effects of waves and currents in the simulation of gas releases using the VOF and the SST k-ω turbulence model. The study was carried out considering large gas flows and small leak sizes (high pressures) and validated by comparing the simulated plumes with images from an experimental study. The porosity of the soil through which the leakage occurs was also taken into account. Parameters related to the release and the characteristics of the resulting plumes were analyzed.

Cassano et al. (2023) used a hybrid Eulerian-Eulerian model (Euler-Euler and VOF) along with the k-ε turbulence model to study the time evolution of natural gas releases from high-pressure pipelines. The setup was validated by comparing the diameter of the plumes and the gas outlet velocities with experimental data, which showed satisfactory agreement. The release depths of 15 m and 55 m were evaluated. The study was performed in OpenFOAM®. The authors focused on trying to find a relationship between the flow parameters and the diameter of the resulting plum at the surface.

2.6 Chapter conclusion

In this chapter, the main theoretical concepts necessary to understand the methodology developed, the results and final conclusions of this work were introduced. The importance of studying accidental subsea gas releases and related phenomena was presented and justified with information on occurrences of this problem. The main theoretical aspects of two-phase flows, including their modeling equations, were briefly discussed. The concept of CFD, its relevance to the study in question, and the description of the tool have been provided. Furthermore, specific aspects of CFD in multiphase modeling, especially the VOF method, were also mentioned. The definition of turbulence, the advantages of using RANS-type models, and the presentation of the models used in this thesis were also made. Finally, some works in the literature that inspired the development of the present work were briefly described. The recent nature of the presented works, as well as the conclusions presented in them emphasizing the need for more studies on the subject, indicates that the release of gases in water still requires a lot of investigation. Therefore, the next chapters were prepared as an attempt to make a small contribution to the topic, with the hope that they can serve as support for future research.

Chapter 3

Material and methods

This chapter narrates the steps followed during the development of the methodology proposed in this thesis. The different stages of the work were organized in case studies.

3.1 Case study 1: 3D preliminary study

This part of the study aimed to replicate the experimental results conducted by Engebretsen et al. (1997) using computer simulations. The main details of the CFD simulations are described below.

3.1.1 Geometry and mesh

The geometry consisted of a parallelepiped-shaped tank with 9 m $\times$ 6 m basis and 12 m height filled with 7 m of water. Above the water, a layer of 5 m of air was input. At an elevation of 0.33 m above the tank basis center, just like it was described by Cloete, Olsen, and Skjetne (2009), air leaked through a round opening of 0.34 m diameter. The representation of the geometry is shown in Figure 5.

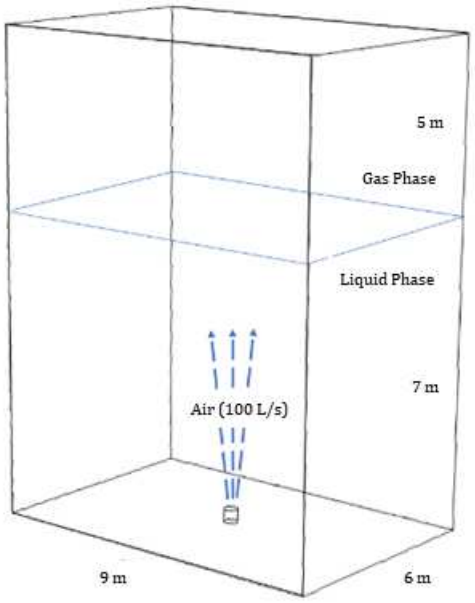

Figure 5: Representation of the geometry used in the 3D preliminary study (Oliveira and Vianna, 2021).

A hexahedral mesh was generated, with refinement concentrated near the gas-liquid interface region and slightly coarser elements in single-phase regions. The smallest mesh elements had edge lengths of 3.7 cm (0.037 m), resulting in a mesh size slightly exceeding 10^6 elements. Figure 6 displays the mesh profile at the center of the tank.

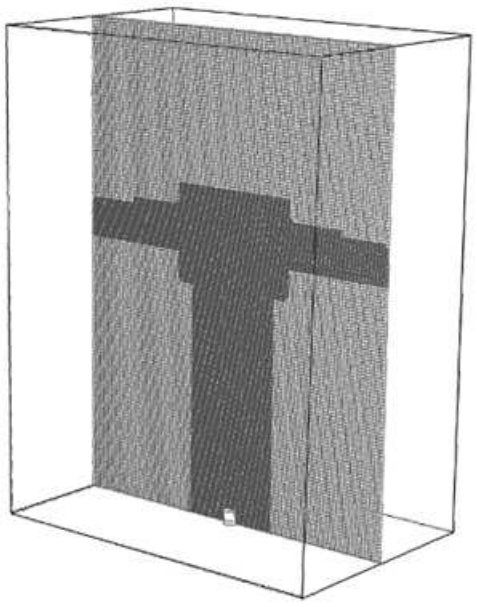

Figure 6: Mesh detail at the center of the tank of the 3D preliminary study (Oliveira and Vianna, 2021).

3.1.2 Simulation setup

The numerical experiment involved the liberation of 100 L/s (0.100 m^3/s) of air from the opening at the center of the tank. The simulation was performed in ANSYS Fluent 19.2. The Eulerian-Eulerian multiphase model Volume of Fluid (VOF) was used instead of the Eulerian-Lagrangian combination of VOF and Discrete Particle Model (DPM) presented by Cloete, Olsen, and Skjetne (2009). The decision to solely utilize VOF was made in order to maintain consistent simulation setup across a wider range of gas flow rates. As previously described, the two fluids involved were air (gas) and water (liquid), input with a constant surface tension of 0.072 N/m between them. The turbulence model applied was the realizable k-ε, which is described as suitable for modeling the turbulence when simulating submerged jets (Sun et al., 2020).

Regarding the numerical methods used, PRESTO! and PISO schemes were selected for pressure discretization and pressure-velocity coupling, respectively. Second-order upwind schemes were chosen for momentum and turbulence equations and the Geo-Reconstruct scheme for volume fraction. The solution was initialized with all variables equal to 0, except for the gas volume fraction, which was patched as 0 below the *xz* 7 m Plane and 1 above it, in order to define the water and air region of the experiment. No compressibility effects were computed. The 8 s simulation with 0.002 s time step size was completed after 48 h using an 8 core computer with 64 GB RAM.

3.1.3 Setup validation

The validation of the proposed setup was made by comparison between the obtained values of gas rising time, initial fountain height (at the rising time) and maximum value of the fountain height in 8 s of simulation with values available in the literature from the corresponding experimental work (Engebretsen et al., 1997).

3.2 Case studies 2 and 3: investigation of the turbulence modeling

The divergence between realistic and simulated data in many studies mentioned in Section 2.5 of the literature review is often attributed to turbulence modeling using RANS models. Therefore, improving the understanding of turbulence phenomena was considered crucial for achieving successful RANS simulations of subsea gas releases. For instance, one potential cause of the observed overestimation of the fountain height was attributed to inappropriate turbulence modeling, leading to excessive concentration of vertical momentum instead of distributing it horizontally. This possibility aroused the investigation into the extent to which modifications to a turbulence model could impact

the behavior of an ascending gas plume underwater.

The success of predicting the fountains height depends on describing the gas ascending behavior along the whole vertical path. Based on this, the experimental study of Fanneløp and Sjøen (1980) was used for validation of the gas ascending velocities during its rising process. The attempt to numerically reproduce their research is below presented.

3.2.1 Geometry and mesh

The tank used by Fanneløp and Sjøen (1980) was filled with 10 m of water and had base dimensions of 260 m $\times$ 10.5 m. At the center of the base of the tank, there was a 0.1 m orifice from where the gas was released. The attempt to reproduce the geometry of the tank with its original width resulted in a coarse mesh with millions of cells, which would make a future simulation with this mesh impractical. To circumvent this problem, a previous simulation was performed, and it was verified that a tank width of 30.0 m would be sufficient to allow the simulation of the desired flow time without significant interference from the edges of the tank in the gas plume formed. Next, it was verified that a 18.0 m height was appropriate to simulate the water and the gas phases in the tank. Then, a tank with 10.5 m $\times$ 30.0 m $\times$ 18.0 m was designed.

The computational 3D domain, represented by the geometry, was divided into four regions for the meshing stage. These divisions were made to reduce the computational cost of the simulations. Figure 7 displays the sectional area of the 3D mesh used. The upper region of Figure 7 is filled initially with air. The lower region is filled with water. Both areas contain a coarse mesh since there was no interest in refining these areas. On the other hand, the mesh in the central and middle regions of the geometry was refined due to the anticipation of gas-liquid interfaces forming within those areas. The resulting mesh was over 5×10^5 elements.

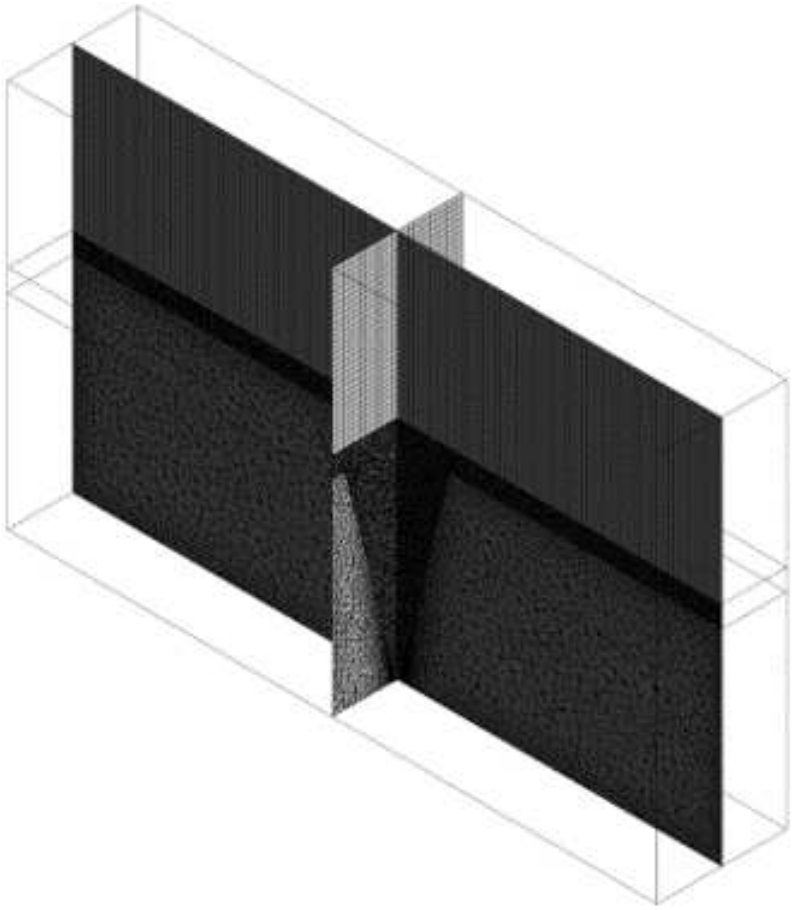

Figure 7: Mesh detail at the center of the tank used for investigation of the turbulence modeling.

3.2.2 Simulation setup

The simulations of the validation and the case studies were run in ANSYS Fluent 20.2 using a setup similar to the one used in case study 1, except for the choice of the turbulence model. Instead of the realizable k-ε, the standard k-ε was selected. This choice allowed the comparison between the obtained results and the data presented by Wu et al. (2017), as well as the data from Fanneløp and Sjøen (1980). Additionally, more information regarding the constants of the standard k-ε model was available in the literature, improving the depth of analysis of the future results.

The considered boundary condition was a velocity inlet which allowed an air flow rate of 0.022 Nm^3/s at the center of the tank base, and a pressure outlet of 0 Pa (gauge) at the top of the open tank. The remaining faces were set as walls. Since Fanneløp and Sjøen (1980) described as small the compressibily effects of their experiments, these effects were not considered in the simulations. The transient simulation, as well as the following ones of this part of the study, ran for 40 s with an adaptive time step optimized for VOF. Using a computer with 128 GB of RAM and 24 cores, each simulation took approximately 60 h to be completed.

3.2.3 Setup validation

The validation of the setup was made by comparison among the velocity profiles at the elevations of 7.75, 6.15, and 2.95 m below the water surface after the 40 s of flow between the results obtained in this study and those from previous works by Fanneløp and Sjøen (1980) and Wu et al. (2017).

3.2.4 Obtaining the normalized velocity profiles

The velocity profiles were obtained in their normalized form. The values were acquired by dividing each velocity value by the experimental central value at the same elevation. The nondimensional distances were calculated as the ratio between the distance from the centerline and the leak diameter. This adjustment was made to increase the visibility of the effects of modifying each constant of the k-ε turbulence model.

3.2.5 Varying the C_μ and $C_{1\varepsilon}$ values

As described in the literature review (Section 2.4), in the k-ε turbulence model equations, different constants assist in describing the model parameters. For this study, the parameters C_μ and $C_{1\varepsilon}$ were altered in case studies 2 and 3, respectively. The modifications were made during the CFD setup aiming at verifying how the underwater velocity profiles, especially at the center of the plume, would behave under these modifications. Table 1 contains the tested values for C_μ and $C_{1\varepsilon}$.

Table 1: Values of C_μ and $C_{1\varepsilon}$ evaluated on the investigation of the turbulence modeling.

Case study	C_μ	$C_{1\varepsilon}$
Default case (validation)	0.09	1.44
2	0.07	1.44
	0.08	1.44
	0.10	1.44
3	0.09	1.20
	0.09	1.25
	0.09	1.30
	0.09	1.50
	0.09	1.25
	0.09	2.00

3.3 Case study 4: validation of a 2D methodology for fast simulation of underwater gas release

During the initial stages of this study, the need to improve the quality of the computational mesh used was observed. Nevertheless, it was recognized that the computational cost of the simulations, particularly for 3D and multiphase investigations, escalates substantially as the number of mesh elements increases. Improving the mesh would mean giving up the possibility of performing a considerable number of simulations in the same period of time. However, as a solution to the difficulty initially encountered, this section proposes a methodology of a setup able of reproducing experimental results of air release in water tanks quickly and with relatively low computational cost.

3.3.1 Geometry and mesh

The geometry used for validating the setup is, once again, based on the experimental work of Engebretsen et al. (1997) and the computational work of Cloete, Olsen, and Skjetne (2009). However, following the intention of reducing the computational cost of the simulations, the numerical experiments were carried out in a 2D domain. The geometry consisted of a tank with dimensions 9 m of base and 12 m of the height of which, from the bottom region, 7 m would be filled with water and the remaining space with the air. The air entrance was designed at the center of the base of the tank. The 0.34 m opening was created at the height of 0.33 m. The resulting geometry was the central cross-section of the geometry shown in Figure 5.

In addition to using a 2D computational domain, another alternative to improve the results and reduce the computational cost of the simulations was the use of adaptive mesh. The original mesh, displayed in Figure 8, contained 10831 cells. Examples of the adapted mesh can be seen in Figure 9. The criteria used for mesh adaptation were the air volumetric fractions: 0.06 was the condition for refinement, and 0.05 was for coarsening. These criteria were evaluated every 10 iterations (dynamic adaptation). The maximum refinement level was 2 and the minimum cell volume was 10^{-8} m^3. With the geometry and meshing correctly reflecting the experimental arrangement of the literature, the case modeling was developed.

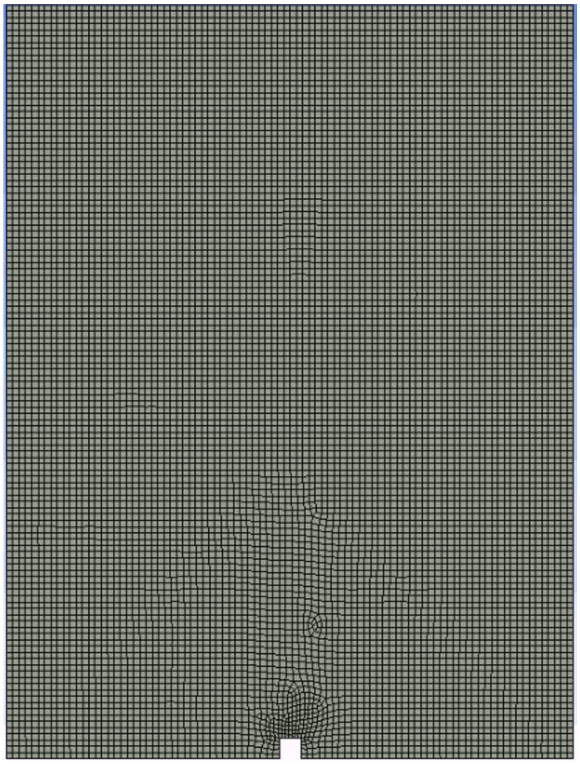

Figure 8: Representation of the initial mesh used in the 2D methodology validation.

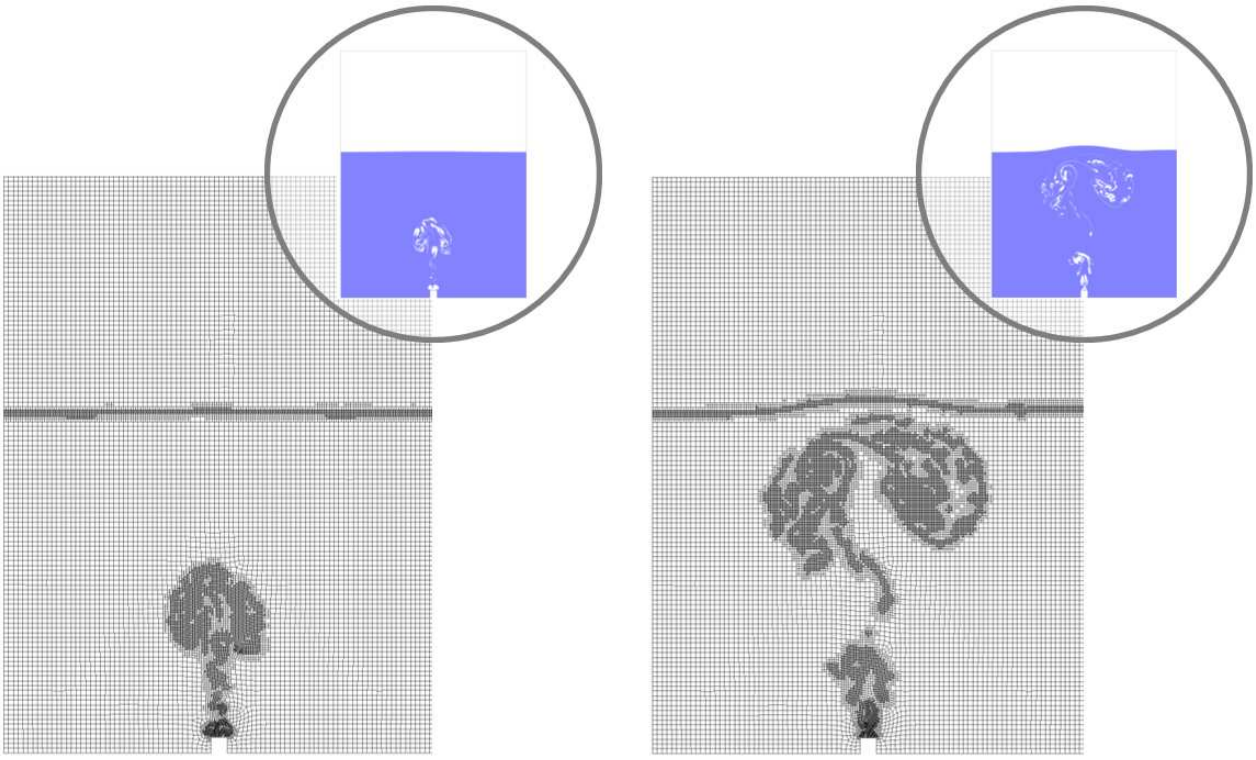

Figure 9: Example of the adapted mesh for two different flow times (Oliveira and Vianna, 2023).

3.3.2 Simulation setup

The setup in ANSYS Fluent followed the steps of case study 1. Once again, instead of using a hybrid DPM and VOF model, only the VOF model was applied. But this time, simulations were run in ANSYS Fluent, version 20.2. The implicit VOF settings were used, along with a constant 0.072 N/m surface tension between air and water. When modeling the turbulence, the realizable k-ε turbulence model was selected, since it had shown good results in the previous 3D study (case study 1) due to its ability to simulate submerged jets.

The boundary conditions were prescribed as inlet velocities of pure air allowing the equivalent 3D flow rates investigated in the experiments of Engebretsen et al. (1997) (0.050, 0.100 and 0.450 m^3/s); pressure outlets of 0 Pa (gauge) with air in the backflow at the top of the open domain; and default wall settings for other boundaries. The reference pressure was the atmospheric (101325 Pa) relative to the interface between water and air in the tank (7 m).

Similar to case study 1, the solution in this case was initialized with all variables set to 0. A patch was applied to define the air volume fraction profile, with a value of 0 below the 7 m line and 1 above it. As well as in the previous cases and in the next ones, the compressibility effects were not taken into account. This choice was made considering the information given by Fanneløp and Sjøen (1980), who observed no significant compressibility effects in water columns up to 10 m. Additionally, the two substances used in the presented work (air and water) have very different densities and the volume of water in the simulations was much greater than the volume of air.

All three simulations were carried out in a transient solver for 20 s with an adaptive time step. The initial time step size was set to 10^{-4} s, with a minimum value of 10^{-5} s and a maximum value of 10^{-1} s. The minimum and maximum step change factors were, respectively, 0.8 and 1.2. The Global Courant Number was limited to 2.

The PISO scheme was selected for pressure-velocity coupling, the PRESTO! scheme for pressure discretization, and the Compressive scheme for volume fraction. Second-order upwind equations were used for continuity, momentum, and turbulence modeling. Each simulation took around 24 h to run on a 64 GB RAM computer, with 8 cores. Among the criteria used to evaluate convergence, a residue value of 10^{-3} was defined for all the variables, although most residuals reached values of around 10^{-5} and 10^{-6} over the iterations in a time step. Furthermore, monitors that checked the closure of the mass balance of air and water in the system were defined.

3.3.3 Setup validation

The observed fountain heights, both initially and at 15 s of flow, as well as the air rising times, were compared with the data of Engebretsen et al. (1997) and Cloete,

Olsen, and Skjetne (2009).

3.4 Defining the boundary conditions of the numerical simulations for the case studies 5 and 6

With the validation of the methodology proposed in case study 4 (Section 3.3), additional simulations were carried out following the steps presented. Simulation data from 36 different flow conditions were acquired, and the results were analyzed in case studies 5 and 6. Each run took approximately 24 h to run on a 128 GB RAM computer, with 24 cores. This section presents the selected flow conditions.

Two new leak sizes with 0.24 m and 0.17 m were chosen to be investigated and, as a consequence, two new geometries and meshes were created. These two new values were adopted because 0.17 m is half of the original leak size (0.34 m) and 0.24 m is the value of the geometric average between the highest and the lowest leak size values. In addition, the new flow rates were selected to keep the values of the initial leak Reynolds numbers similar for the three different leak sizes, and, at the same time respect the order of magnitude of the flow rates for which the methodology was validated. The choice of keeping constant values of Reynolds numbers was made because in subsequent studies it was desired to evaluate the data through dimensional analysis. The Reynolds numbers were calculated considering the air properties constants and equal to 1.225 kg/m^3 for the density and 1.79×10^{-5} Pa.s for the viscosity. The values of the air flow rate varied between 0.006 and 0.150 m^3/s, and the respective velocities were prescribed as inlet boundary conditions. This step followed the same methodology presented in case study 4. The information about the simulations is better expressed in Table 2.

Table 2: Boundary conditions of the 36 simulations evaluated in case studies 5 and 6 (Oliveira and Vianna, 2023).

Case	**Leak size (m)**	**Air flow rate (m^3/s)**	**Velocity inlet (m/s)**	**Leak Reynolds number**
1	0.34	0.013	0.14	3205
2	0.34	0.025	0.28	6409
3	0.34	0.038	0.41	9614
4	0.34	0.050	0.55	12818
5	0.34	0.063	0.69	16023
6	0.34	0.075	0.83	19227
7	0.34	0.088	0.96	22432
8	0.34	0.100	1.10	25637
9	0.34	0.113	1.24	28841
10	0.34	0.125	1.38	32046
11	0.34	0.138	1.51	35250
12	0.34	0.150	1.65	38455
13	0.24	0.009	0.19	3205
14	0.24	0.018	0.39	6409
15	0.24	0.027	0.58	9614
16	0.24	0.035	0.78	12818
17	0.24	0.044	0.97	16023
18	0.24	0.053	1.17	19227
19	0.24	0.062	1.36	22432
20	0.24	0.071	1.56	25637
21	0.24	0.080	1.75	28841
22	0.24	0.088	1.95	32046
23	0.24	0.097	2.14	35250
24	0.24	0.106	2.34	38455
25	0.17	0.006	0.28	3205
26	0.17	0.013	0.55	6409
27	0.17	0.019	0.83	9614
28	0.17	0.025	1.10	12818
29	0.17	0.031	1.38	16023
30	0.17	0.038	1.65	19227
31	0.17	0.044	1.93	22432
32	0.17	0.050	2.20	25637
33	0.17	0.056	2.48	28841
34	0.17	0.063	2.75	32046
35	0.17	0.069	3.03	35250
36	0.17	0.075	3.30	38455

3.5 Case study 5: organizing the data as a function of the Reynolds number

Case study 5 simply contemplated the analysis of the relationship of different plume parameters with the Reynolds number of the leak. Data were obtained through simulations of the cases described in Table 2. The setup followed the methodology guidelines presented in case study 4 (Section 3.3).

3.6 Case study 6: relating the shape of the bubble clusters with their ascending velocity through the liquid phase

When a multiphase simulation is said to be low-cost, in fact, the word "low" is used in relation to the common computational cost of this type of simulation. It is very important to mention that multiphase CFD simulation, despite being more advantageous than other methods used for investigating flow phenomena, will always have a notable computational cost. Therefore, the development of mathematical models that allow calculating, without physical or numerical experiments, flow parameters and obtaining the same information provided by CFD needs to be examined. An initial study aiming at this model development is briefly described in this section.

3.6.1 Dimensional analysis

The rising time of a cluster of bubbles is directly connected to its average rising velocity and the water column height. Another important variable to be considered in the analysis of a rising plume is gravity acceleration since the flow is heavily influenced by gravitational forces.

Naming the bubble cluster characteristic size $r_{bubbles}$, its average velocity $V_{bubbles}$, and the gravity acceleration g, and following the Buckingham Pi Theorem (Pritchard, 2011), it is possible to point the fundamental dimensions L and t. Since there are three parameters and two dimensions, there is one dimensionless group. This group can be mathematically expressed as Equation 35.

$$\Pi = V_{bubbles} r_{bubbles}^{a} g^{b} \tag{35}$$

The exponents a and b in Equation 35 can be equated with the basic dimensions L and t, resulting in a=-1/2 and b=-1/2. Therefore, it is possible to obtain Equation 36.

$$\Pi = \frac{V_{bubbles}}{(r_{bubbles} g)^{1/2}} \tag{36}$$

It is extremely important to note the similarity between the parameter obtained with Equation 36 and the Froude Number ($\frac{V}{(gL)^{1/2}}$), which represents the relationship between inertial and gravitational forces acting. However, while the Froude number uses a variable of length related to the flow field, Equation 36 uses a characteristic length of the bubbles. Hence, Equation 36 is not able to give information regarding the flow being supercritical, critical, or subcritical, whilst the Froude number is. The importance of Equation 36 lacked investigation, which started with an analysis of the relation between the ascending velocity of a single bubble and its characteristic length according to literature.

Other dimensionless numbers were obtained parallel to this analysis. However, among the mathematical relationships obtained through the application of the Buckingham Pi Theorem, Equation 36 showed a great agreement with other parameters of the flow and the plume and was chosen to continue the studies. It is relevant to point out that the proposed dimensionless number associates the inertial and gravitational aspects of the flow with a geometric feature of the plume. In the analysis of multiphase flows, effects related to surface tension between fluids and viscous forces are also very relevant and should be considered. An alternative to circumvent this problem is to include parameters linked to an existing dimensionless number in the proposed one in the future. For example, one can multiply or divide the parameter proposed in Equation 36 by the Weber number, which has the surface tension between the analyzed fluids among its variables. It was decided, although, to keep the consideration of surface tension in the setup of the computational simulations. This consideration allows the results obtained to be associated in the future with other dimensionless numbers, which consider surface tension effects, for example.

3.6.2 Comparing equations

In the literature review (Section 2.2), the equations which govern the rising of a single bubble were presented. However, their applicability in real bubble systems is limited, since most flows occur with a large number of bubbles, and they will not assume the "umbrella" shape in most cases due to the large interactions between them. Hence, assuming the shape factor to be equal to 3/2 in these cases can be an erroneous assumption.

Presumably, there is no clear relationship between the characteristic size of the bubbles in a system and the velocity of these bubbles, as described in the literature review (Section 2.2). But comparing the equations that govern the behavior of a single bubble with Equation 36 obtained by dimensional analysis, it is coherent to propose that the

characteristic size and velocity of bubbles in a complex system is governed by an equation similar to Equation 37, where a parameter α also relates the ascending velocity of the air with its characteristic lenght. In the case of describing the movement of a single bubble, α assumes a constant value of 3/2 acording to the literature (Batchelor, 2000). However, the existence of this variable to describe bubble systems was not verified until this work was carried out. Therefore, it was not possible to be stated whether the variable can be determined and, if so, whether a constant value would be assumed.

$$V_{bubbles} = \frac{1}{\alpha}(gr_{bubbles})^{1/2} \tag{37}$$

It is important to highlight that both Equations 36 and 37 propose a linear relationship between a parameter related to the speed of the gas phase and the product between the gravity acceleration and a characteristic length of the gas phase. This fact aroused the interest in investigating if there was a relationship between the parameters $V_{bubbles}$ and $r_{bubbles}$, which would be governed by a constant α equivalent to the shape factor which guides the flow of a single bubble, such as the presented in Equation 15.

If the proposed relationship is valid, determining the characteristic size of a group of bubbles would be enough to determine the rising velocity and consequent rising time of a portion of gas. This would be extremely helpful for the elaboration of mitigation actions in case of the detection of an underwater gas leak.

3.7 Case study 7: evaluating the proposed models under other flow conditions

This section briefly presents the information necessary for the development of case study 7, which consisted of verifying the applicability of the models developed in case study 6 to other flow conditions.

The validation of the 2D setup proposed in this work included relatively small domains, which allowed the disregard of compressibility and temperature change effects without significantly compromising the analysis. Therefore, the new computational domain for the additional simulations was chosen with similar dimensions in order to guarantee reliability.

A 15 m wide by 15 m height tank was designed. In the center of the tank base, three leak sizes were considered: 0.1 m, 0.2 m, and 0.3 m. The tank was sometimes filled with 5 m of water and sometimes with 10 m of water. According to Fanneløp and Sjøen (1980), in water columns up to 10 m, effects of expansion and temperature change can be considered moderate to small. The flow rates and, consequently, leak velocities were determined based on 5 different values of Reynolds numbers chosen between 4000 and 36000, according to the range of values of case studies 5 and 6. In total, 30 additional

simulations were run. Table 3 includes information about each new case. The inlet velocities were set as inlet boundary conditions in the simulations.

Table 3: Boundary conditions of the additional 30 simulations evaluated in case study 7.

Case	Leak size (m)	Air flow rate (m^3/s)	Velocity inlet (m/s)	Leak Reynolds number	Water depth (m)
37	0.10	0.005	0.58	4000	5
38	0.10	0.014	1.75	12000	5
39	0.10	0.023	2.92	20000	5
40	0.10	0.032	4.09	28000	5
41	0.10	0.041	5.26	36000	5
42	0.20	0.009	0.29	4000	5
43	0.20	0.028	0.88	12000	5
44	0.20	0.046	1.46	20000	5
45	0.20	0.064	2.05	28000	5
46	0.20	0.083	2.63	36000	5
47	0.30	0.014	0.19	4000	5
48	0.30	0.041	0.58	12000	5
49	0.30	0.069	0.97	20000	5
50	0.30	0.096	1.36	28000	5
51	0.30	0.124	1.75	36000	5
52	0.10	0.005	0.58	4000	10
53	0.10	0.014	1.75	12000	10
54	0.10	0.023	2.92	20000	10
55	0.10	0.032	4.09	28000	10
56	0.10	0.041	5.26	36000	10
57	0.20	0.009	0.29	4000	10
58	0.20	0.028	0.88	12000	10
59	0.20	0.046	1.46	20000	10
60	0.20	0.064	2.05	28000	10
61	0.20	0.083	2.63	36000	10
62	0.30	0.014	0.19	4000	10
63	0.30	0.041	0.58	12000	10
64	0.30	0.069	0.97	20000	10
65	0.30	0.096	1.36	28000	10
66	0.30	0.124	1.75	36000	10

The simulations occurred following the validated setup proposed in case study 4 and used for case studies 5 and 6. Each simulation took approximately 24 h to run on

a 24 cores 128 GB RAM computer. After the parameters of the plumes were determined, the value of the shape factor for each water column was calculated. In addition, the expressions for the values of t_{rising} for each water column height were obtained according to the directions followed in case study 6.

3.8 Post-processing: determining the flow parameters

This section presents the methodology applied to determine plume characteristics discussed in this thesis.

3.8.1 Fountain rising times

The rising time of a single bubble was determined by calculating the time that the first amount of gas leaked took to reach the interface water-air. This way, the effects of interaction between bubbles were minimized. When processing the results of the simulations, the value of t_{rising} selected was the instant when a volumetric fraction of air different of 0 was verified in a traced line at the surface between the liquid and gas domain (Oliveira and Vianna, 2023). Figure 10 displays an example of the described procedure for case 18 of Table 2.

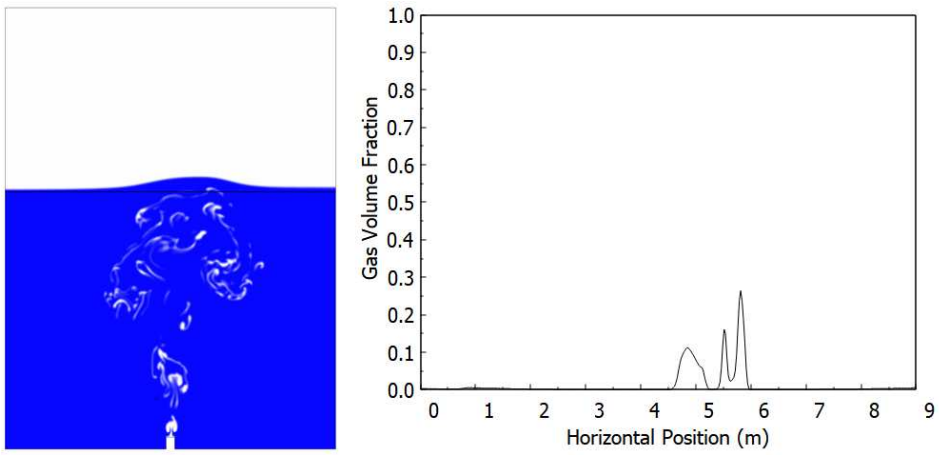

(a) Volume fraction profile in the tank

(b) Volume fraction profile at the surface line

Figure 10: Gas volume fraction at 5.4 s for simulation with leak size of 0.24 m and 0.053 m^3/s of gas flow rate (Oliveira and Vianna, 2023).

3.8.2 Fountain heights

The heights of the fountains, both the initial and after 15 s of flow, were determined by analyzing the volume fraction of water in the vertical line at the center of the domain. For this purpose, the line at the interface between air and water for t=0 s

was used for reference (height=0 m). The height calculated accounted for the maximum point at which it was possible to observe the presence of water (Oliveira and Vianna, 2023).

3.8.3 Average rising velocities of the bubbles

The average velocity of the bubbles was calculated simply by dividing the vertical distance roamed by the first group of bubbles by its rising time.

3.8.4 Plume horizontal dispersion

The horizontal dispersion of the 2D plume equates to the diameter of a 3D plume. This parameter was determined by calculating the largest width of the water fountain formed above the surface water-air (interface line). Furthermore, in order to keep minimizing the interactions between the fluids and the wall during the determination of the parameters, the data were collected at the moment when the plume first touched the surface (rising time).

3.8.5 Average bubble cluster sizes

In all the analyzes, a bubble cluster was defined as a continuous portion of air fully bounded by a region of water in a plume. To reduce the effects of the interactions between the plume, the surface, and the tank walls, the average bubble cluster size accounted for the characteristic of the plume when the first portion of air reached the surface, which is the plume at its rising time. This settlement also makes the presented methodology agree with the other ones used to define the other plume parameters in this work.

The VOF, model chosen when simulating the flows, divides the computational domain into three regions. First, there is the region with the first considered fluid, where the volume fraction is 1. Then, there is the region containing only the other fluid, where the volume fraction of the first fluid is 0. Last, there is the region of the free surface, where a volume fraction is a number between 0 and 1. Since both considered fluids are immiscible, the more refined the mesh, the narrower this third region is (Hirt and Nichols, 1981).

Even with the use of an adaptive mesh for better detailing of the air regions of the plume, there were areas where the gas volume fraction oscillated between 0 and 1. To circumvent these cases, a classification criterion was applied. An iso-surface was created for each plume contour at its rising time. Any region where the volume fraction of air was equal to or greater than 0.5 was classified as the gas phase, otherwise it was assumed as the liquid region (Oliveira and Vianna, 2023).

After the post-precessing criteria were defined, the number of bubble clusters was determined for each plume. In addition, the area of the underwater region that contained gas was calculated. The average area of a bubble cluster was the result of the division of the total gas area for the number of clusters. Then, the clusters were considered round-shaped and theis characteristic size (radius) was obtained. This is an approximation of the regions to circles in order to determine a characteristic size, and not a finding of a circular shape of the bubbles.

Figure 11 displays an example of image treatment for defining the gas and liquid areas for case 16 of Table 2 (Oliveira and Vianna, 2023).

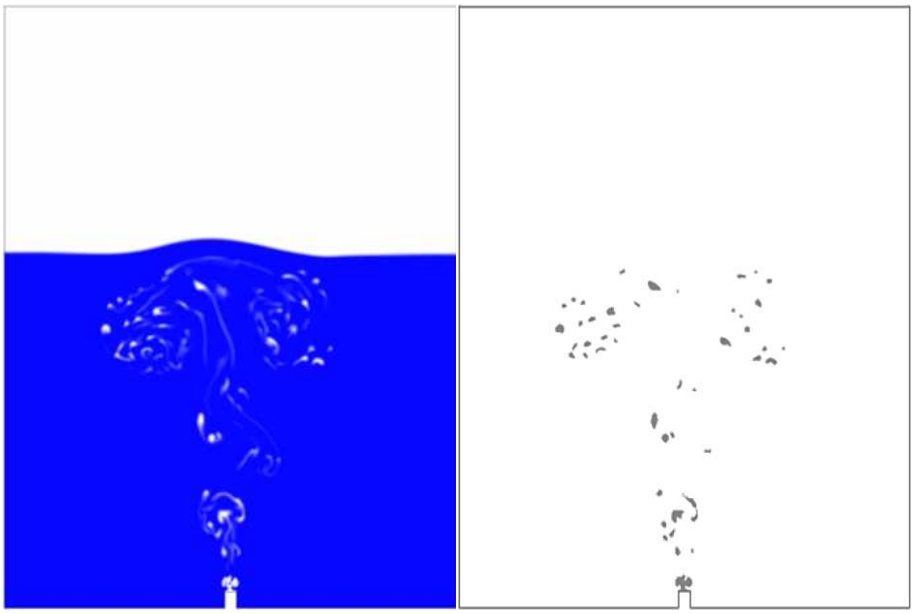

(a) Gas volume fraction profile (b) Isosurface representing the gas phase

Figure 11: Gas volume fraction profile at 6.0 s for simulation with 0.24 m leak size and 0.035 m^3/s of flow rate (case 16) (Oliveira and Vianna, 2023).

The plume presented in Figure 11 has 48 groups of bubbles with a total area of about 0.48 m^2 of air region below the surface. Dividing this area by the number of bubble clusters, we determine the average bubble characteristic size of 0.056 m.

3.9 Chapter conclusion

In this chapter, each section brought a different approach used in the analysis of air releases in water environments, with some being more interconnected than others. Succinctly, the organization of the chapter can be summarized in Figure 12, which properly connects each section presented. Finally, Table 4 brings together the information presented about the computational resources used in each case study, as well as the

average simulation time.

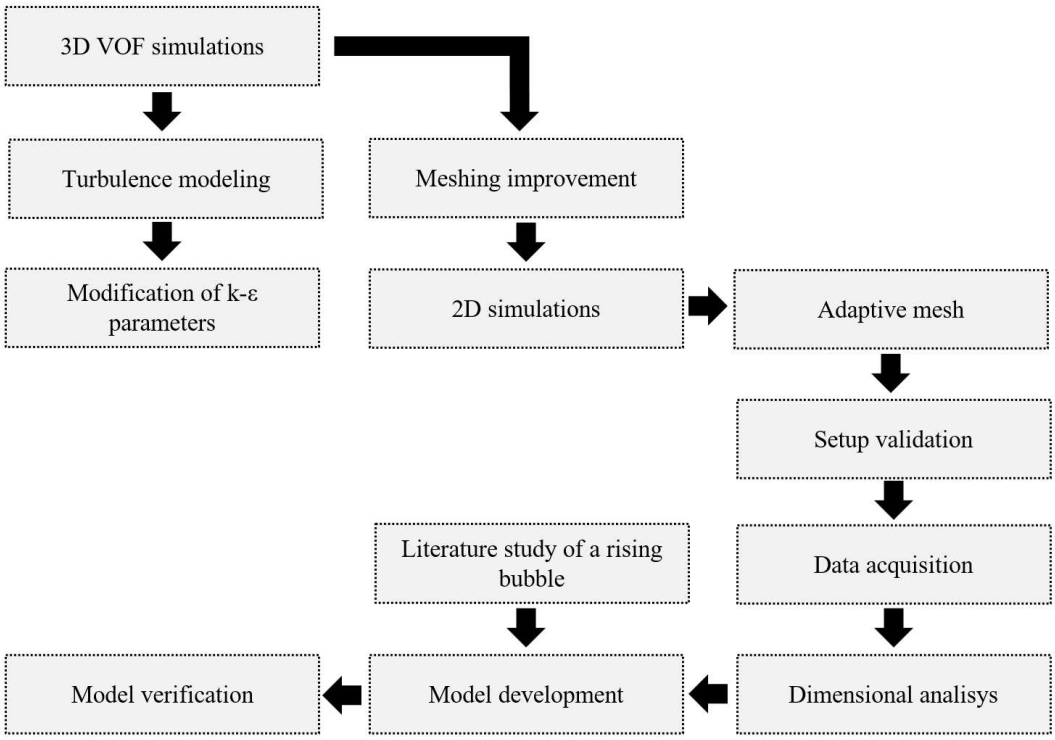

Figure 12: Flowchart with the steps developed in this work.

Table 4: Computational resources and simulation time of each case study.

Case study	**Cores**	**RAM**	**Simulation time (h)**
1	8	64	48
2	24	128	60
3	24	128	60
4	8	64	24
5	24	128	24
7	24	128	24

Next chapter brings the main results obtained in each described stage of the described procedures.

Chapter 4

Results

This chapter presents, section by section, the achievements obtained in each procedure presented (Chapter 3), as well as the relevant discussion for a better interpretation of these results. Partial conclusions of each discussed step are also presented.

4.1 Case study 1: 3D preliminary study

This section presents the main results obtained based on the attempt to numerically reproduce, using a 3D setup as described in Section 3.1, the experimental studies of Engebretsen et al. (1997) concerning the liberation of air in a tank full of water.

4.1.1 Main results

Figure 13 brings the gas volume fraction profiles and Figure 14 the velocity profiles at the center of the geometry for different flow times. It is possible to verify through the volume fraction profile that the plume, while rising vertically, also spreads to the horizontal direction, indicating the momentum transfer between the directions. One may also note that the ascending air is divided into jets due to the recirculation of fluid. This recirculation is also responsible for contributing to creating regions where the gas velocity is lower or higher than the one at the leak. Both observations are possible due to the phenomena of momentum transfer and turbulence, which alters the course of the gas initially directed in the vertical direction.

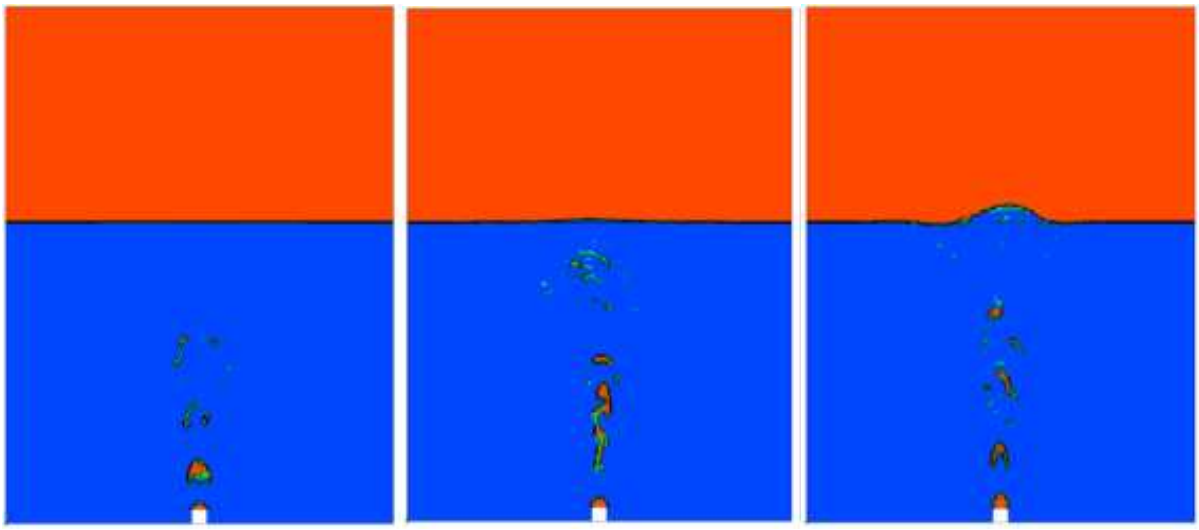

(a) 3.0 s (b) 4.7 s (c) 6.7 s

Figure 13: Gas volume fraction at the center of the geometry at different flow times of the 3D preliminary study (Oliveira and Vianna, 2021).

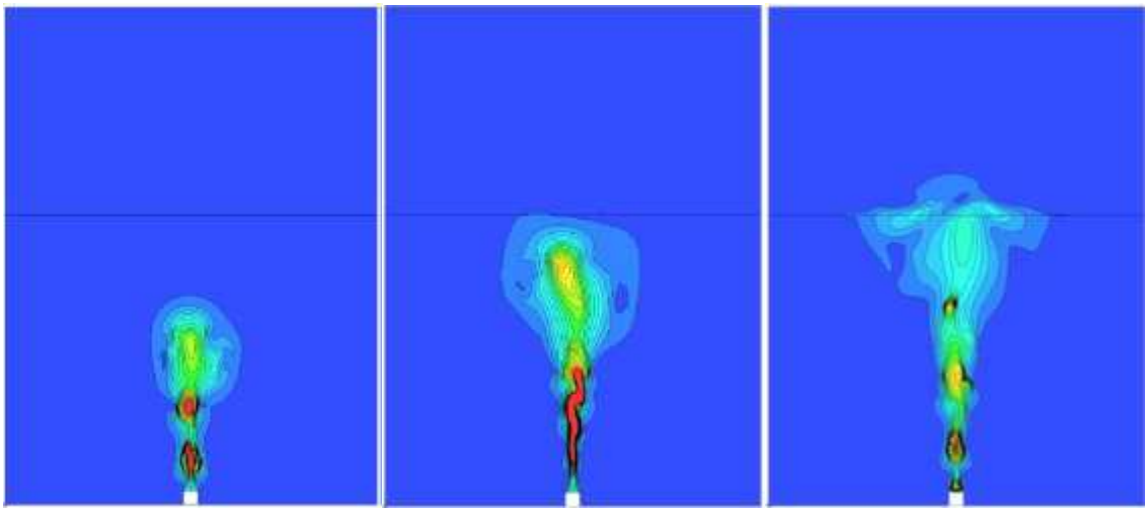

(a) 3.0 s (b) 4.7 s (c) 6.7 s

Figure 14: Gas velocity profile at the center of the geometry at different flow times of the 3D preliminary study (Oliveira and Vianna, 2021).

At 3.0 s of flow, the formation of different jets is observed. At 4.7 s, it is possible to note the moment when the first amount of rising gas reaches the water-air interface. And at 6.7 s, the fountain reaches the height of 0.40 m. While the rising time obtained through the simulations is close to the experimental value of 4.8 s, at 6.7 s, the height of 0.40 m reached by the water fountain diverges from the 0.30 m obtained by Engebretsen et al. (1997). This discrepancy leads to two possible following paths after this study stage: the decision to explore the results obtained using a more refined mesh and/or the ones arising from an improvement in the turbulence modeling. A finer mesh could be capable

of capturing more details about the flow and lead to more accurate results. Regarding the turbulence model, since the chosen model is based on RANS equations, the fluctuations calculated are only average values. When these values are lower than the real fluctuations, vertical momentum is retained at the center of the plume, and there is no distribution of this momentum to the recirculating fluid. As consequence, the velocity at the center line of the plume remains high and the height of the water fountain is overestimated (Wu et al., 2017).

Finally, Figure 15 gives the contour surface of the gas plume at 6.7 s at the 7 m line in *xy* Plane and the 3D plume profile in the tank. The shape of the plume agrees with the one described by Olsen and Skjetne (2016), presenting a region governed by the vertical momentum of the gas and other characterized by the momentum transfer from the center (vertical) to the horizontal, making the plume expand horizontally. The plume at 6.7 s reached an average radius of 2.63 m and an angle of 21° relative to the leak point. There are no experimental data regarding the diameter of the plume, but this value may be underestimated since the calculation of the distribution of vertical to horizontal momentum was not fully successful. Subsequent studies with the correct vertical momentum estimation can be associated with proper horizontal scattering of the plume.

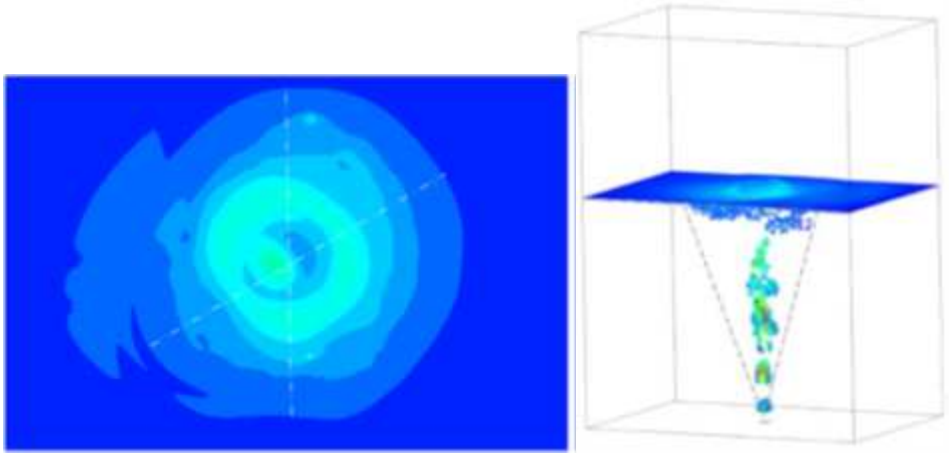

(a) 3.0 s (b) 4.7 s

Figure 15: Contour of the plume at the surface and 3D plume view at 6.7 s of the 3D preliminary study (Oliveira and Vianna, 2021).

4.1.2 Partial conclusions of the section

This preliminary study has shown that the gas plume modeling was acceptable. Until the first amount of gas reaches the surface, the modeling was satisfactorily able to give the right information about the flow. On the other hand, above the surface, there was an excessive prediction of the height of the liquid. These results have pointed to

two directions of study: first to the necessity to improve the turbulence modeling of the simulation, and second to the necessity of improving the mesh of the simulation, especially in regions where the interface between gas and liquid was occurring. The two subsequent studies have been driven to investigate which direction (or both) the thesis should be following.

4.2 Case studies 2 and 3: investigation of the turbulence modeling

This section presents the results of the investigation regarding the modification of the parameters of the standard k-ε in the simulation of air liberation in water according to the methodology presented in Section 3.2.

4.2.1 Plume description

Figures 16 and 17 bring the underwater profiles of volume fraction and velocity, respectively, both obtained for the cross-section region of the tank after 40 s of flow. The standard k-ε model with its default parameters was used (simulation 1 of Table 1).

Figure 16 shows greater intermittence between air bubbles closer to the surface region. This behavior is expected since the air is released exclusively with vertical momentum. Along the path, some amount of momentum is transferred to the horizontal direction or dissipated through the interaction with water and buoyancy effects.

The velocity profile in Figure 17 is very similar to the qualitative description of an underwater gas plume given by Olsen and Skjetne (2016). It is possible to identify the zone of flow establishment, with velocity oscillations, at the beginning of the leak; a zone of established flow, where the gas vaguely disperses horizontally, creating a cone-shaped plume; and the surface zone, where the expansion to the horizontal direction is clearly noted. Besides the qualitative description of the velocity profile, it is also important to note the uniformity in the plume behavior, which is a consequence of the turbulence model. Since k-ε is an averaging model (RANS), it is not capable of capturing the dynamic behavior of the plume.

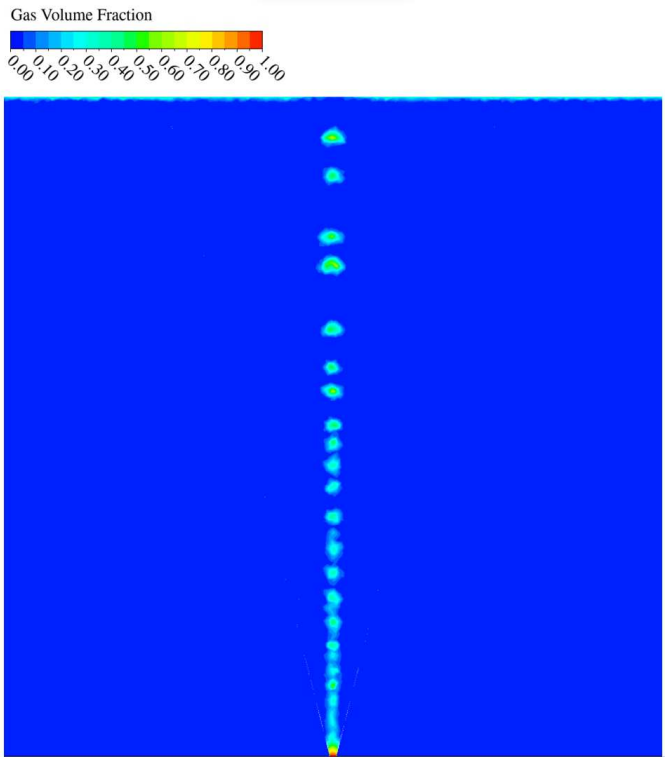

Figure 16: Volume fraction profile at 40 s of flow for the default case of the investigation of the turbulence modeling.

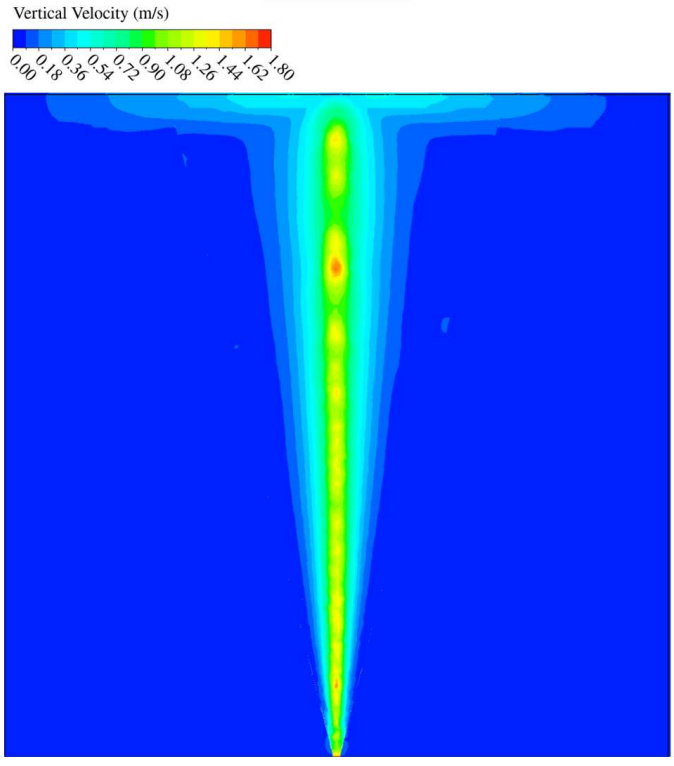

Figure 17: Vertical velocity profile at 40 s of flow for the default case of the investigation of the turbulence modeling.

4.2.2 Case study 2: varying the C_μ values

Figures 18, 19, and 20 present, respectively, the normalized velocity profiles at the depths of 7.75 m, 6.15 m, and 2.95 m below the water surface for the simulations with modified values of C_μ, as well as the experimental data obtained by Fanneløp and Sjøen (1980). The graphic shows that no significant improvement was detected when trying to obtain a better velocity profile by modifying the parameters. Actually, slightly worse results were acquired for C_μ values different than the original value of 0.09. This result is better evidenced in Figure 21, which summarizes the data from the center line of Figures 18, 19, and 20.

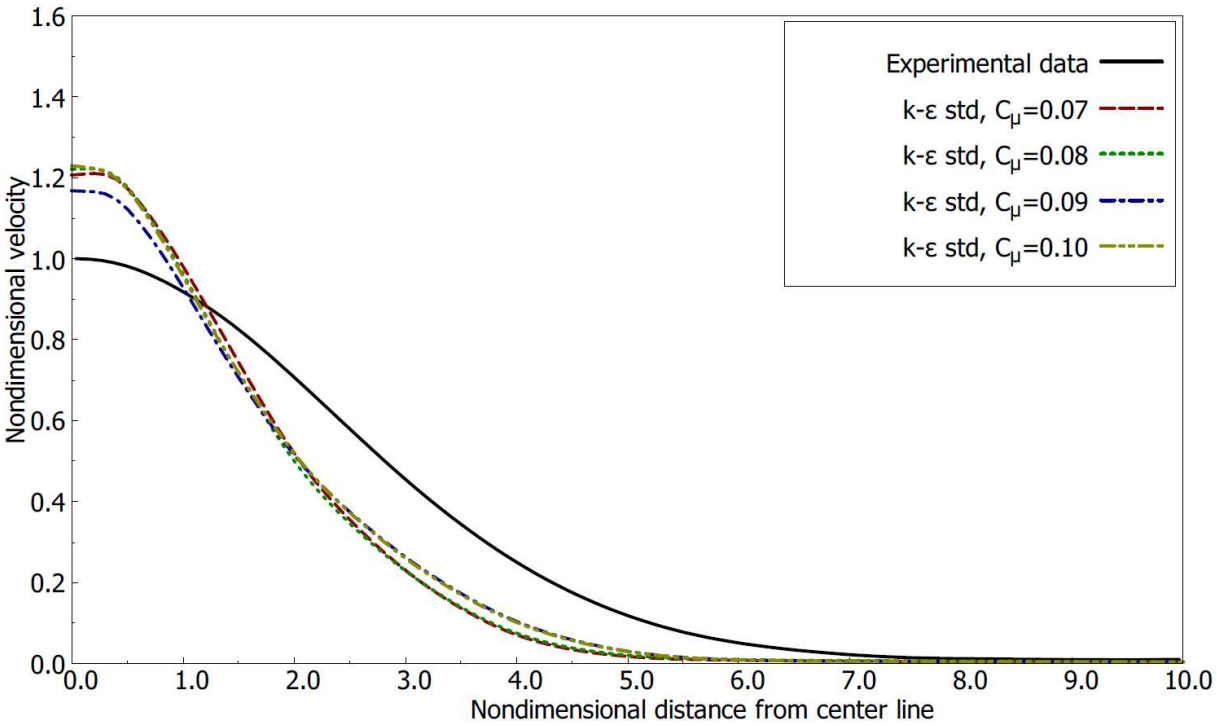

Figure 18: Nondimensional sectional velocity profiles at the elevation of 7.75 m below water surface varying C_μ compared with the experimental data of Fanneløp and Sjøen (1980).

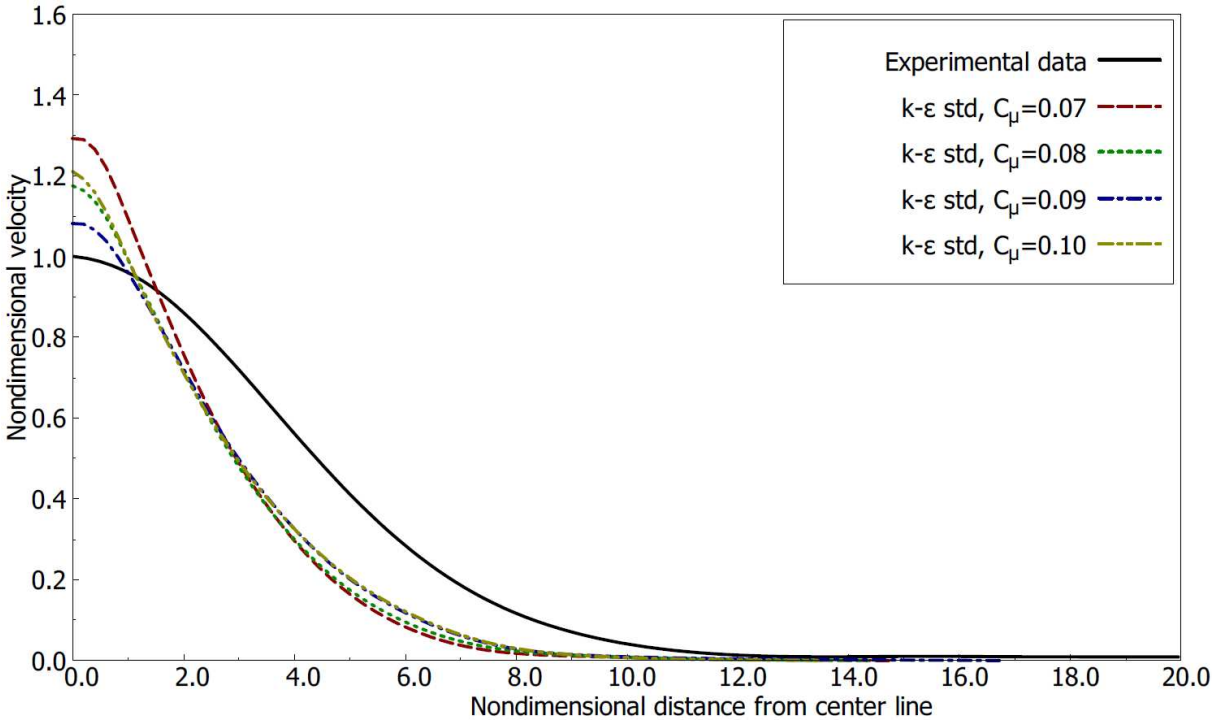

Figure 19: Nondimensional sectional velocity profiles at the elevation of 6.15 m below water surface varying C_μ compared with the experimental data of Fanneløp and Sjøen (1980).

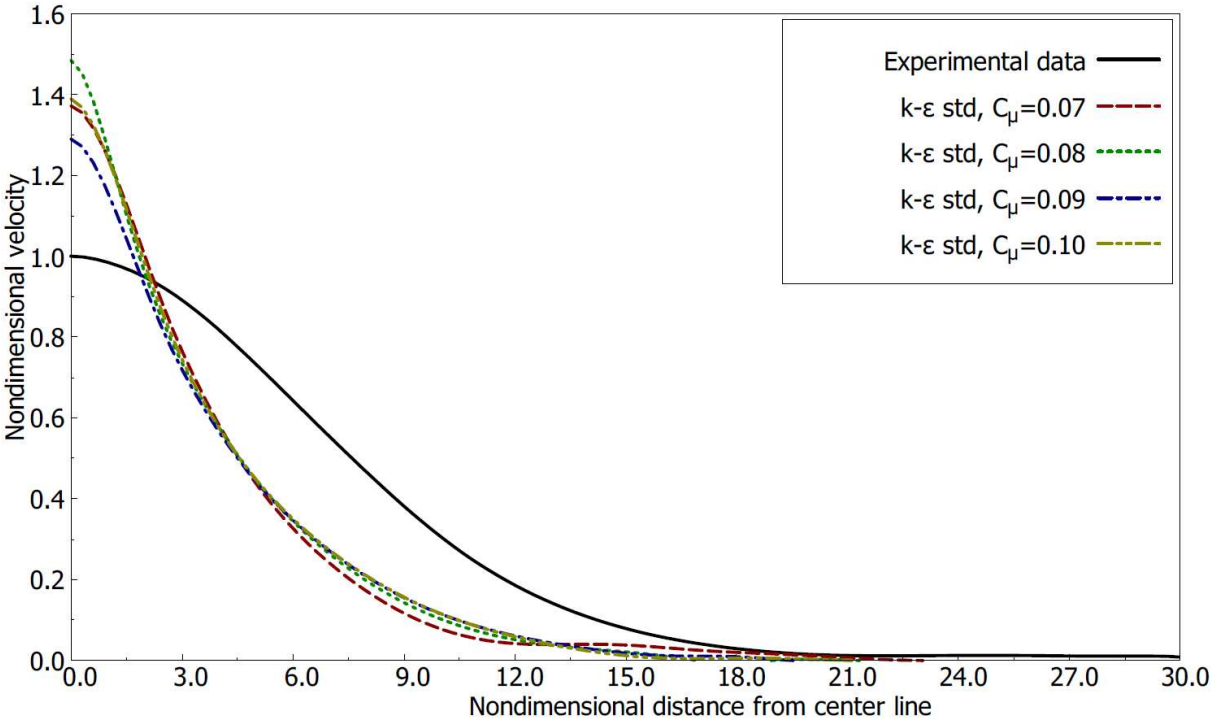

Figure 20: Nondimensional sectional velocity profiles at the elevation of 2.95 m below water surface varying C_μ compared with the experimental data of Fanneløp and Sjøen (1980).

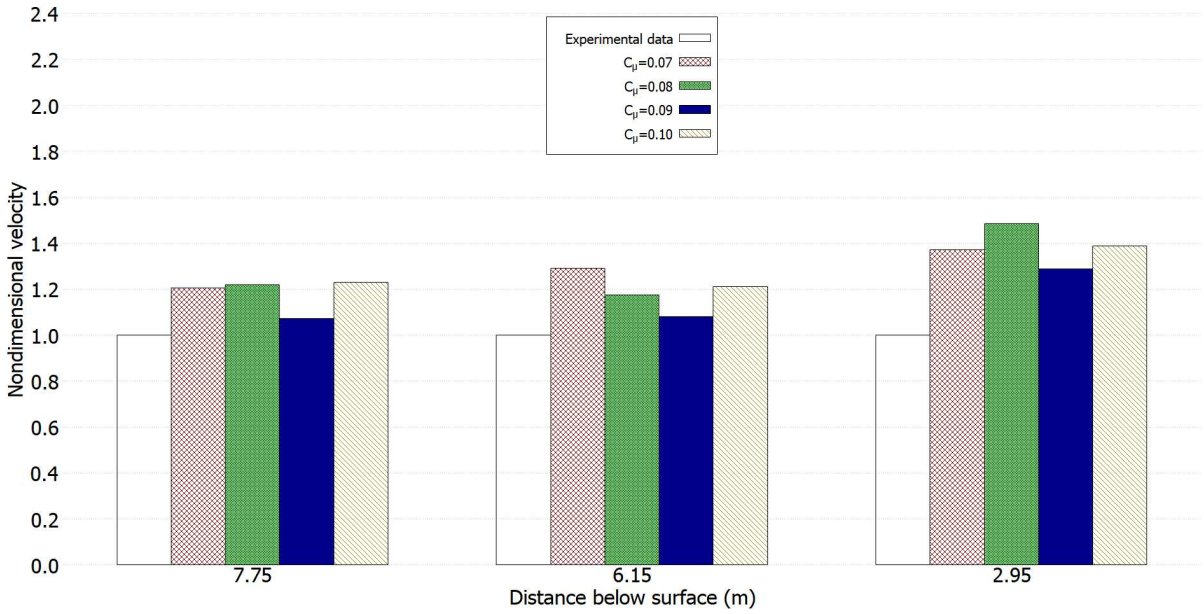

Figure 21: Nondimensional center velocities obtained when varying C_μ.

It is important to observe in Figure 21 that even in the best scenario (C_μ=0.09), the center velocity values presented an error of around 15% for more for the results obtained at 7.75 m and 6.15 m below the surface and 35% for more at 2.95 m below the surface.

While the plume approaches the surface, there is a rise in the rate of the energy cascade. This rise leads to higher turbulent kinetic energy dissipation rates. Then, this greater dissipation influences the transfer of momentum, forcing it to be dispersed in all directions, altering the mean velocities (Cloete, Olsen, and Skjetne, 2009). In addition, despite the errors, the obtained results agree much more with the experimental data than the results available in literature (Wu et al., 2017), which also simulated the same experiment using the standard k-ε model. This happens possibly due to differences in the mesh, and in other settings during the case setup.

4.2.3 Case study 3: varying the $C_{1\varepsilon}$ values

Contrary to what was shown in case study 2, the value of $C_{1\varepsilon}$ of 1.44 is not connected to any empirical equation, and modifying it appeared to be more promising than the first parameter. Similarly to Figures 18, 19, and 20, Figures 22, 23, and 24 present the normalized experimental data and velocity profiles for the simulations with modified values of $C_{1\varepsilon}$.

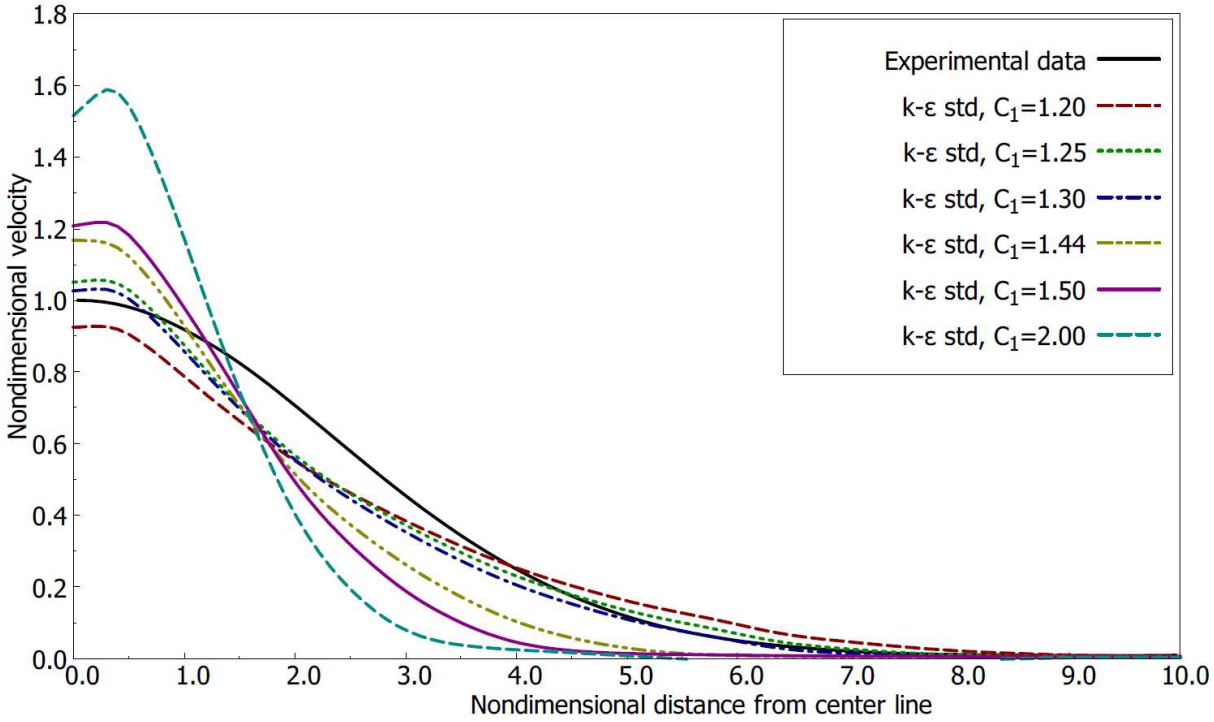

Figure 22: Nondimensional sectional velocity profiles at the elevation 7.75 m below water surface varying $C_{1\varepsilon}$ compared with the experimental data of Fanneløp and Sjøen (1980).

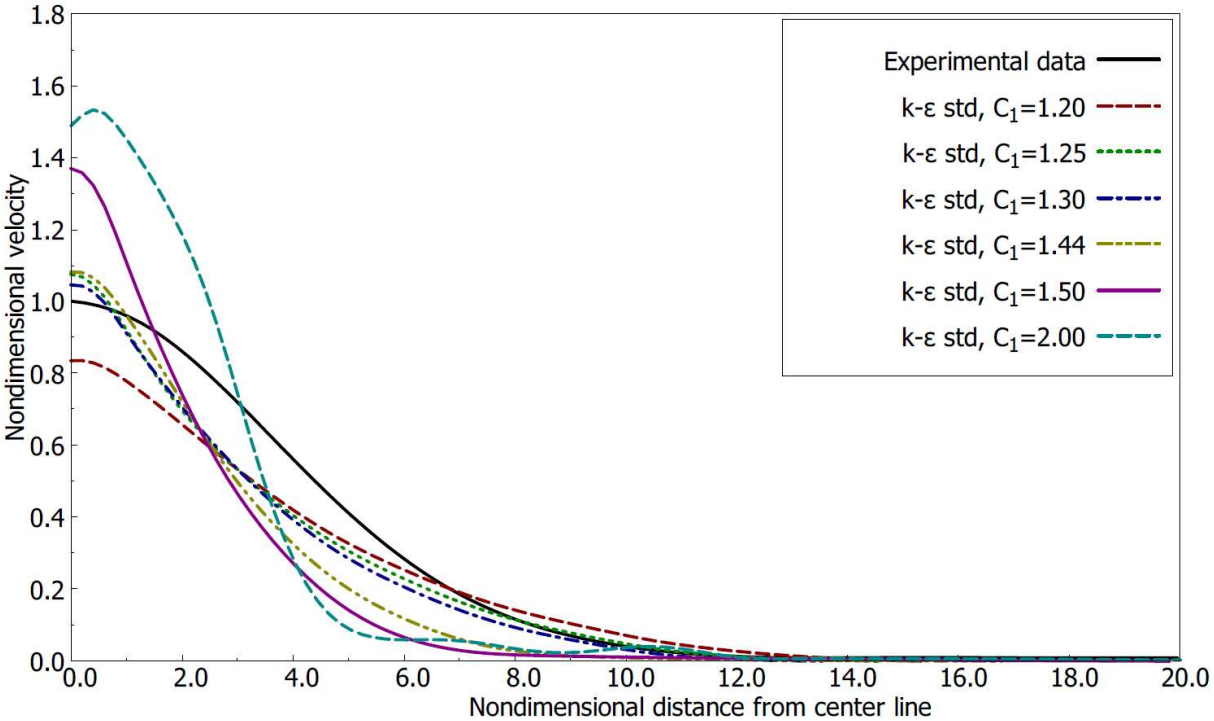

Figure 23: Nondimensional sectional velocity profiles at the elevation 6.15 m below water surface varying $C_{1\varepsilon}$ compared with the experimental data of Fanneløp and Sjøen (1980).

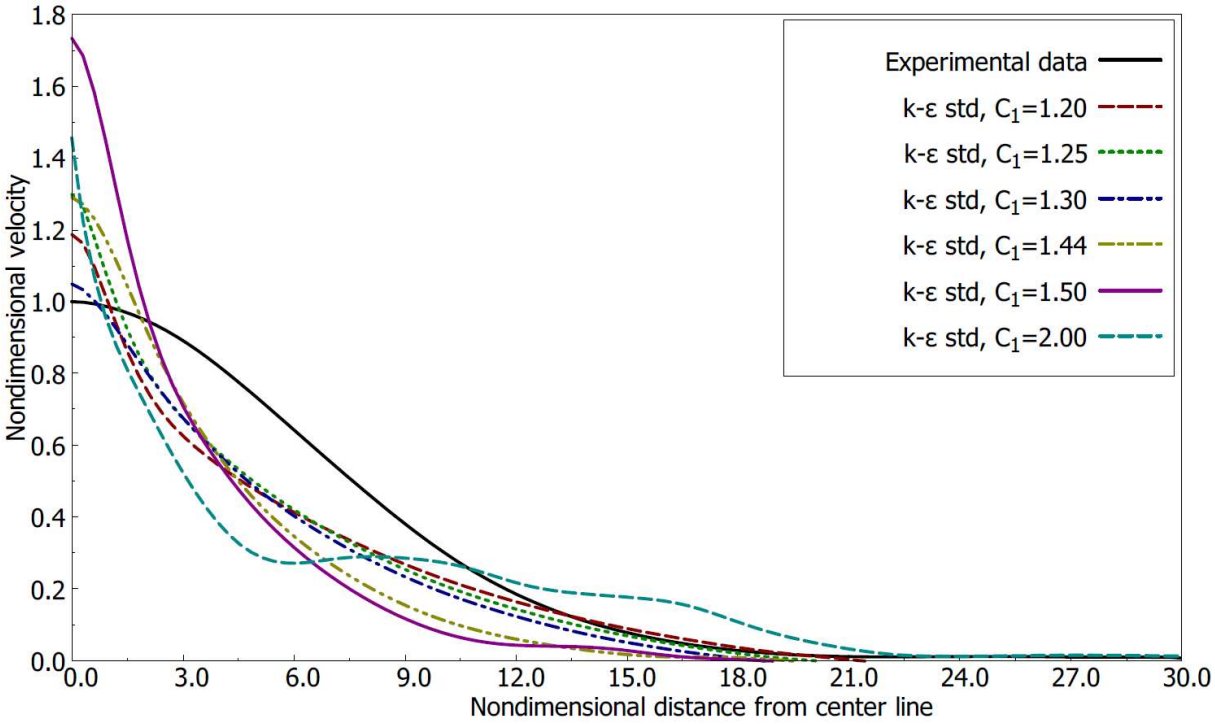

Figure 24: Nondimensional sectional velocity profiles at the elevation 2.95 m below water surface varying $C_{1\varepsilon}$ compared with the experimental data of Fanneløp and Sjøen (1980).

The behavior of the plume varied much more significantly with the modifications $C_{1\varepsilon}$ if compared to the proposed variations of C_μ. For values of $C_{1\varepsilon}$=2.00 in all cases and for $C_{1\varepsilon}$=1.50 at 2.95 m below the surface the results were oscillatory, with the velocity increasing in some points while the nondimensional distance from the center increased. The maximum center velocities calculated also showed a high discrepancy from experimental results. For values of $C_{1\varepsilon}$ lower than 1.44, a better fit to the experimental data was acquired. In special, for $C_{1\varepsilon}$=1.30, the velocity profile at the center line was closer to the experimental data than for the default value for the entire curve for the three elevations. The center velocity improvement is better observed in Figure 25.

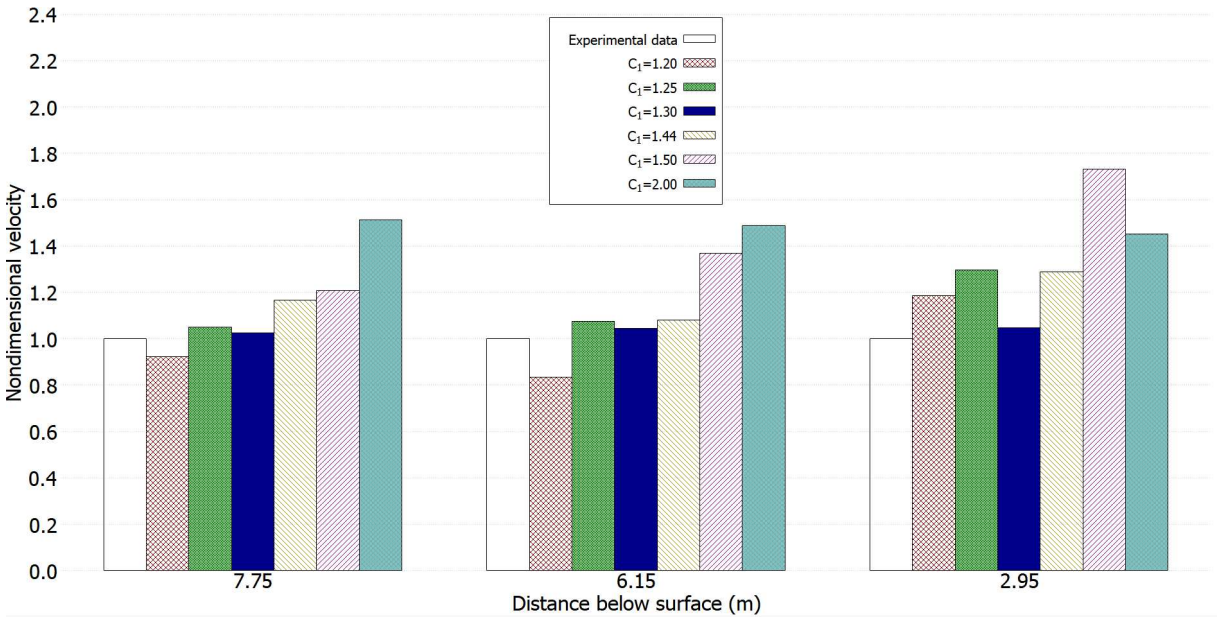

Figure 25: Nondimensional center velocities obtained when varying $C_{1\varepsilon}$.

The correct prediction of the center velocities can be associated with the estimation of the plume width. The RANS equations try to average all the fluctuations in the flow field, and these fluctuations are related to the dissipation of moment gained by the plume. A reduced flow field fluctuation retains the momentum to the core of the gas plume, maintaining a high plume center line velocity, which can also reduce the plume width (Wu et al., 2017). Other works also verified that the standard k-ε underestimates the plume horizontal spreading and retains the momentum to the center of the gas plume (Li, Chen, and Khan, 2019; Olsen, Skjetne, and Johansen, 2017; Xinhong et al., 2018).

The suggestion of $C_{1\varepsilon}$=1.30 resulted in velocities at the center line of the plume closer to experimental data than any other value tested, with an error inferior to 5% for all the three distances below the surface, which is close to the precision of an LES simulation for this parameter (Wu et al., 2017). This result should be considered preliminary, and it should not be assumed that a value of $C_{1\varepsilon}$ should be fixed at 1.3 in future studies. Instead, this parameter requires further investigation and careful examination. The term $C_{1\varepsilon}$ appears in Equation 24 and is associated with the rate of production of ε. Lower values of $C_{1\varepsilon}$, therefore, can be related to a lower dissipation of the turbulent kinetic energy. It is possible that reduced production of ε compensates the low field fluctuations related to the RANS Standard k-ε model, which could lead to overestimated plume centrer velocities and, consequently, underestimated plume widths.

4.2.4 Partial conclusions of the section

In this section, the simulation of an underwater gas release scenario was conducted using varying values of the k-ε turbulence modeling parameters. Future works can also investigate the influence of other parameters of the k-ε model on the behavior of submerged plumes. Another interesting possibility of investigation is trying to express variables of the standard k-ε model as a function of flow parameters instead of trying to define new numeric values for these variables. This would guarantee the wider applicability of the study. However, this part of the thesis was not continued because case study 4, the research developed in parallel to this investigation, has led to more promising results, and was chosen as the basis for the continuation of this study.

4.3 Case study 4: validation of a 2D methodology for fast simulation of underwater gas release

4.3.1 Plume description

The first results obtained were the rising times of the gas bubbles for each flow rate. Figure 26 brings the bubble profile at the rising time for the flow rate of 0.100 m^3/s. Comparing Figure 26 to Figure 13, it is possible to note that the adaptive mesh allowed more detailed visualization of the elevation of the fountain height due to the momentum carried by the ascending air, as well as the recirculating air due to the momentum transfer.

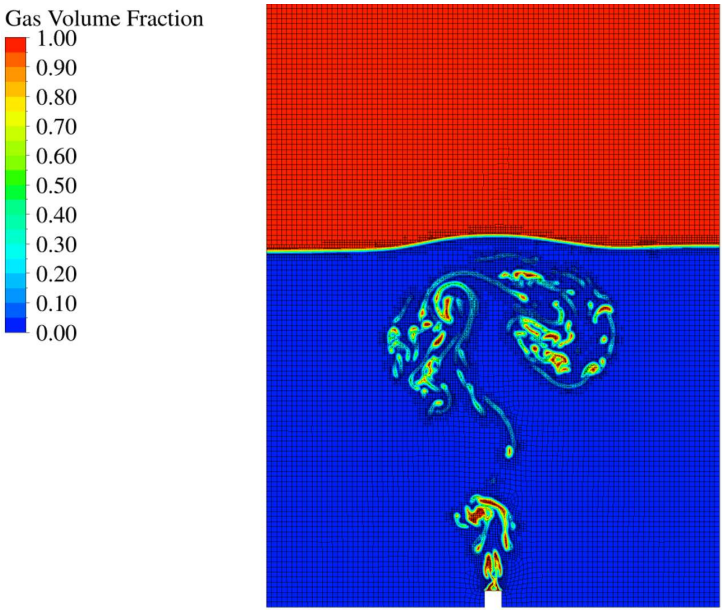

Figure 26: Gas volume fraction at the center of the geometry obtained using the 2D proposed methodology for the flow rate of 0.100 m^3/s.

4.3.2 Setup validation

The obtained rising times of the bubbles for the three evaluated flow rates are presented in Table 5, along with the times obtained by Engebretsen et al. (1997) and Cloete, Olsen, and Skjetne (2009). Table 5 shows that the proposed setup allowed obtaining very accurate rising times if compared to the original experimental data. This similarity between simulated and experimental data can be better visualized through Figure 27.

Table 5: Bubble rising times at flow rates of 0.050, 0.100 and 0.450 m^3/s obtained using the 2D methodology.

	Flow rate (m^3/s)		
Rising time (s)	**0.050**	**0.100**	**0.450**
2D simulation (this work)	6.0	4.8	3.0
Experimental data (Engebretsen et al., 1997)	6.0	4.8	3.1
VOF+DPM simulation (Cloete, Olsen, and Skjetne, 2009)	5.9	5.08	3.16

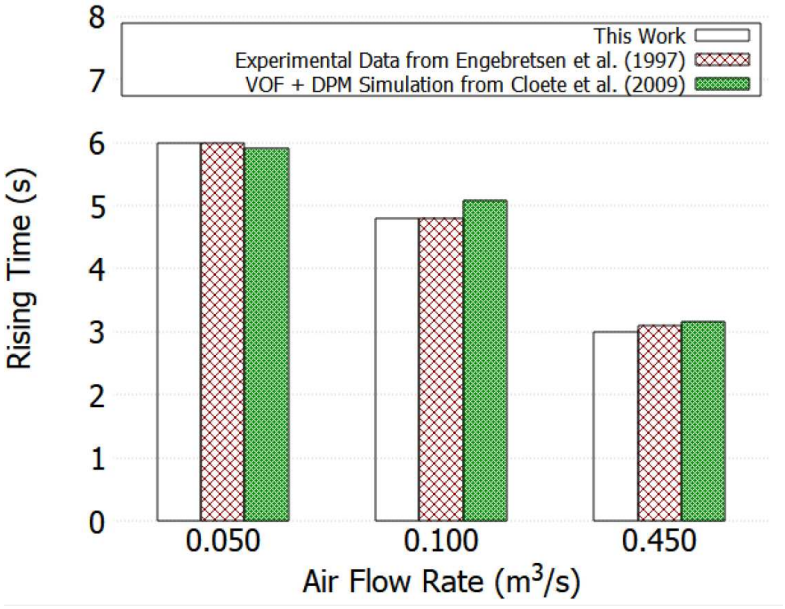

Figure 27: Gas rising times obtained in this work, the corrsponding experimental data, and the values obtained through VOF+DPM simulation (Oliveira and Vianna, 2022).

For the flow rates of 0.050 and 0.100 m^3/s, the error of the simulation of this work achieved 0%, while the error of the simulation using DPM+VOF simulation was 1.6%. For the flow rate of 0.450 m^3/s, the error obtained was 3.3%, while the DPM+VOF simulation in the literature was 5.3%.

Table 6 compares the initial fountain heights (heights at the rising time) of this work, the original experimental data Engebretsen et al. (1997). Since no relevant

elevation was observed for the flow rate of 0.050 m^3/s, the results are shown only for the flow rates of 0.100 and 0.450 m^3/s. Next, the data from Table 6 is summarized in Figure 28.

Table 6: Initial fountain heights obtained for flow rates of 0.100 and 0.450 m^3/s using the 2D methodology.

	Flow rate (m^3/s)	
Fountain height (m)	**0.100**	**0.450**
2D simulation (this work)	0.33	0.69
Experimental data (Engebretsen et al., 1997)	0.30	0.45
VOF+DPM simulation (Cloete, Olsen, and Skjetne, 2009)	0.28	0.81

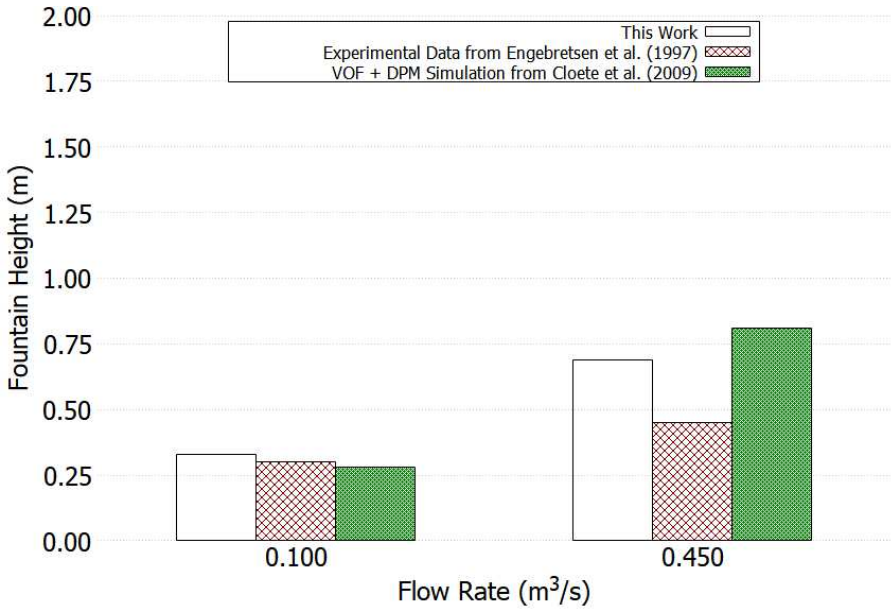

Figure 28: Initial fountain heights obtained in this work, the corresponding experimental data, and the values obtained through VOF+DPM simulation (Oliveira and Vianna, 2022).

The initial fountain height is a water splash which gives no significative information about the flow consequences (Engebretsen et al., 1997). However, it is an important parameter when validating the setup since it is, as well as the gas rising time, related to the distribution of the momentum from vertical to horizontal.

The proposed setup allowed an error of 10% for the flow rate of 0.100 m^3/s and of 53% for the flow rate of 0.450 m^3/s, which are relatively better than the error of 16.7% and 80.0% obtained with the DPM+VOF simulation. This improvement can be attributed to the greater capacity of the Eulerian-Eulerian approaches in describing the flows for a wider range of flow rates, as well as to the more refined mesh used in this study, which is not feasible to be used in 3D simulations. The Eulerian-Lagrangian

simulations, such as the DPM+VOF, assume that the bubbles of the simulation occupy no volume in the computational domain, which also influences how the interactions between the bubbles are calculated.

Finally, the validation of the methodology followed by the comparison between the simulated and the experimental fountain heights at 15 s for the flow rates of 0.100 m^3/s and 0.450 m^3/s, which results are displayed in Table 7 and Figure 29. The corresponding data was not obtained using the DPM+VOF simulation.

Table 7: Fountain heights at 15 s obtained for flow rates of 0.100 and 0.450 m^3/s using the 2D methodology.

	Flow rate (m^3/s)	
Fountain height (m)	**0.100**	**0.450**
2D simulation (this work)	0.69	1.25
Experimental data (Engebretsen et al., 1997)	0.65	1.25

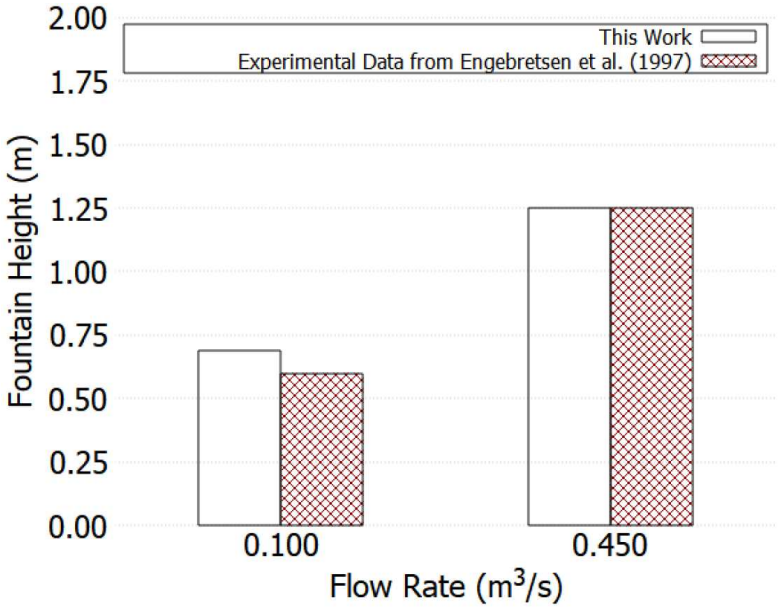

Figure 29: Fountain heights at 15 s obtained in this work, and the corrsponding experimental data (Oliveira and Vianna, 2022).

Once again, the data acquired in this work agreed with the experimental results of Engebretsen et al. (1997), being the height discrepant 6.1% for the flow rate of 0.100 m^3/s and 0% for 0.450 m^3/s.

4.3.3 Partial conclusions of the section

This section presented a legitimate and precise 2D setup capable of satisfactorily predicting the properties of gas plumes in water such as plume rising time, and

fountain heights at different flow times. The accurate prediction of the heights implies indicates that the vertical momentum carried by the plume is well estimated and the horizontal momentum distribution also tends to be correct, indicating that the horizontal spread of the plume obtained with the simulation is a good estimation of the real value. Since the three investigated parameters calculated using the 2D setup were in close agreement with the experimental values, it was considered valid for transient simulations in similar conditions and used for case studies 5, 6, and 7.

4.4 Case study 5: organizing the data as a function of the Reynolds number

This section presents a brief discussion relating the Reynolds numbers of the leaks described in Table 2 and some properties of the resulting plumes.

4.4.1 Gas volume fraction profiles

Figures 30, 31 and 32 present the gas volume fraction profile at the rising times for each plume resulting from the simulations summarized in Table 2. Each simulation combines a gas flow rate with a leak size, resulting in different Reynolds numbers of the leaks.

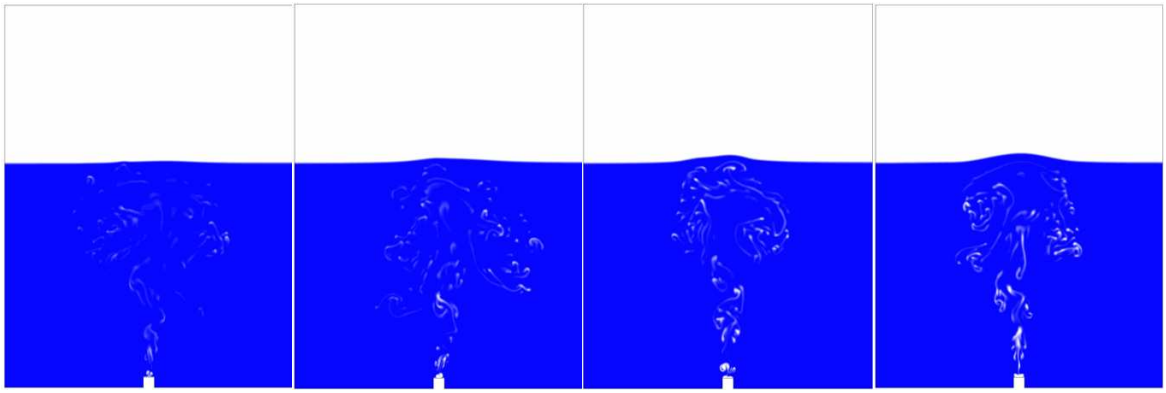

(a) Case 01 (Re=3205) (b) Case 02 (Re=6409) (c) Case 03 (Re=9614) (d) Case 04 (Re=12818)

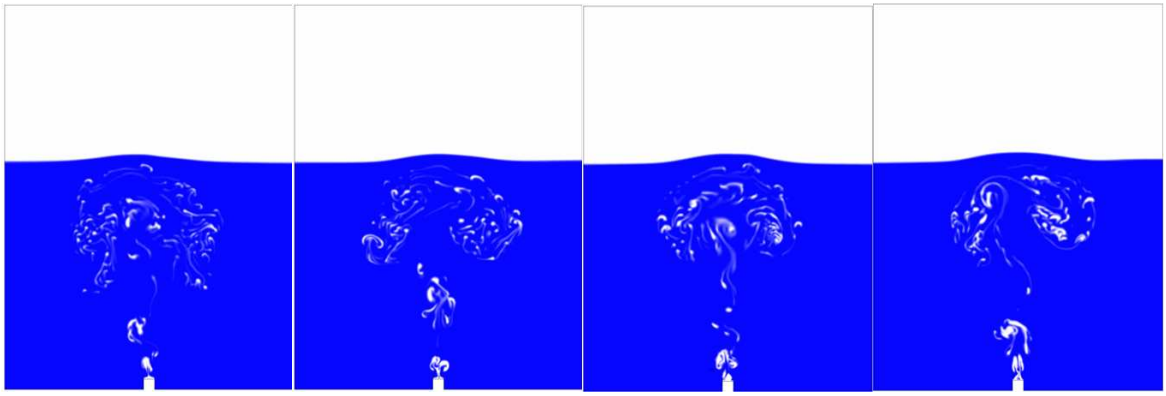

(e) Case 05 (Re=16023) (f) Case 06 (Re=19227) (g) Case 07 (Re=22432) (h) Case 08 (Re=25637)

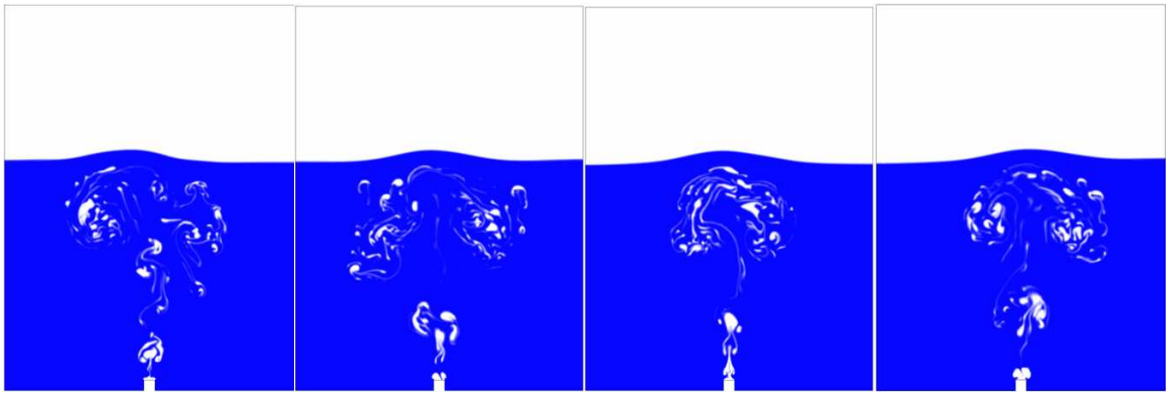

(i) Case 09 (Re=28841) (j) Case 10 (Re=32046) (k) Case 11 (Re=35250) (l) Case 12 (Re=38455)

Figure 30: Plumes at t_{rising} for different Reynolds numbers at the gas discharge obtained for the leak size of 0.34 m (Oliveira and Vianna, 2023).

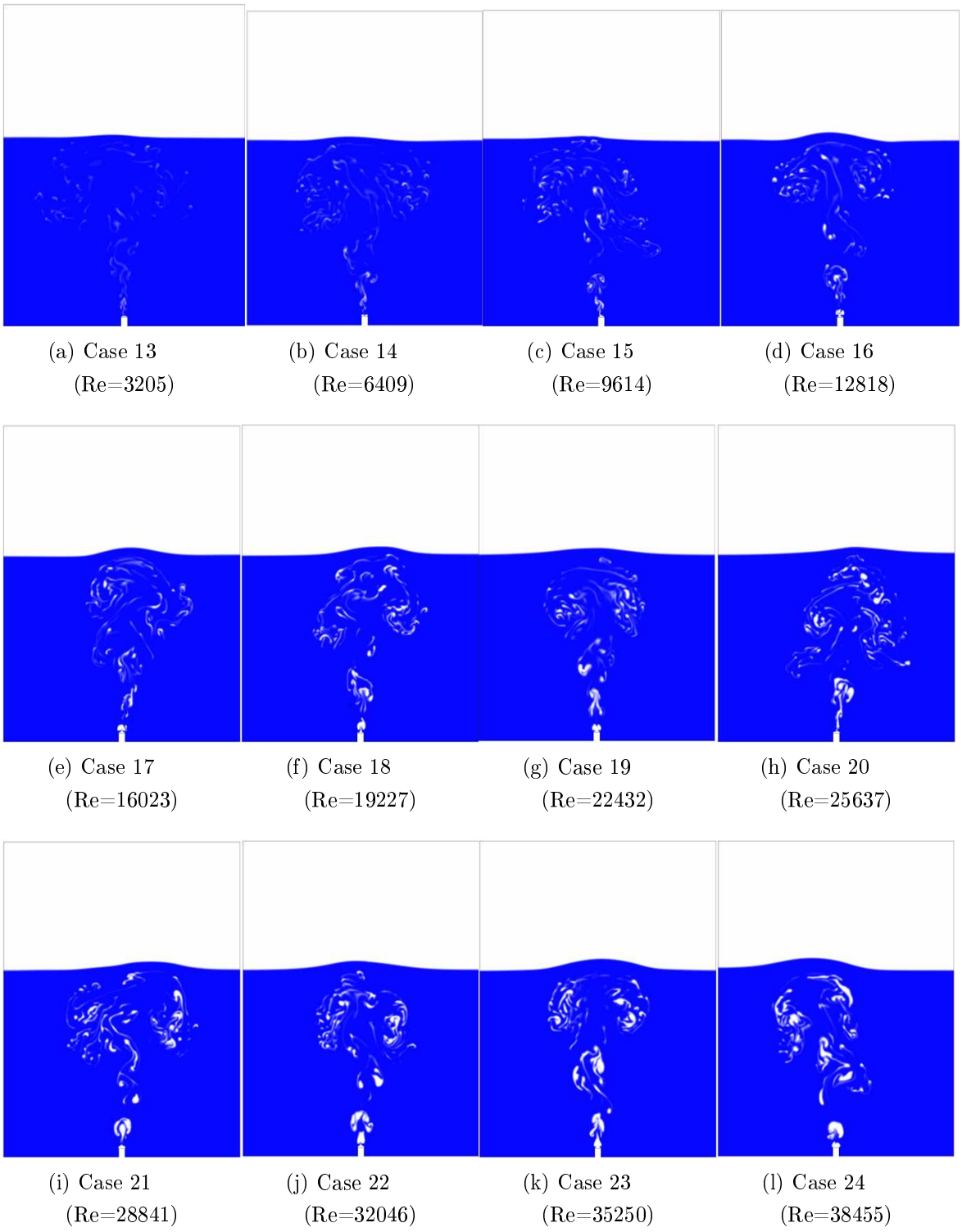

(a) Case 13 (Re=3205) (b) Case 14 (Re=6409) (c) Case 15 (Re=9614) (d) Case 16 (Re=12818)

(e) Case 17 (Re=16023) (f) Case 18 (Re=19227) (g) Case 19 (Re=22432) (h) Case 20 (Re=25637)

(i) Case 21 (Re=28841) (j) Case 22 (Re=32046) (k) Case 23 (Re=35250) (l) Case 24 (Re=38455)

Figure 31: Plumes at t_{rising} for different Reynolds numbers at the gas discharge obtained for the leak size of 0.24 m (Oliveira and Vianna, 2023).

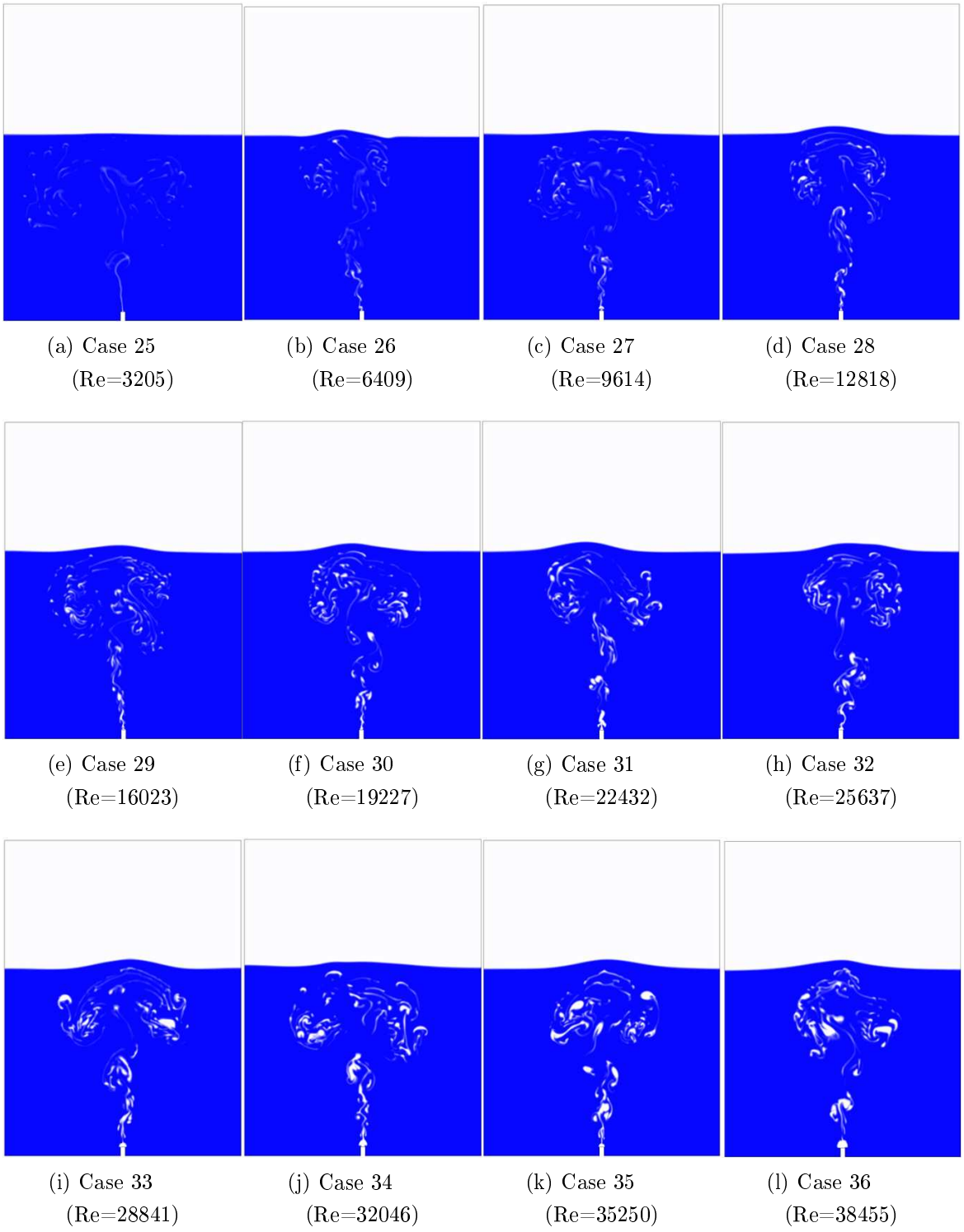

(a) Case 25 (Re=3205) (b) Case 26 (Re=6409) (c) Case 27 (Re=9614) (d) Case 28 (Re=12818)

(e) Case 29 (Re=16023) (f) Case 30 (Re=19227) (g) Case 31 (Re=22432) (h) Case 32 (Re=25637)

(i) Case 33 (Re=28841) (j) Case 34 (Re=32046) (k) Case 35 (Re=35250) (l) Case 36 (Re=38455)

Figure 32: Plumes at t_{rising} for different Reynolds numbers at the gas discharge obtained for the leak size of 0.17 m (Oliveira and Vianna, 2023).

The plumes resulting from the same initial Reynolds numbers have shown similar shapes at their rising times, as it is possible to observe in Figures 30, 31 and 32. This indicates that, for a two-phase system with the same two fluids, the combination of leak size and leak velocity will dictate the behavior of the plume. In all images, the

elevation of the fountain at the surface was observed. As discussed before, the elevation of the fountain is related to the momentum carried by the ascending air. It is also possible to note the gas recirculation which is associated to drag forces between air and water, in addition to turbulence effects and momentum transfer from vertical to horizontal.

A simple visual analysis makes it also possible to verify that plumes resulting from leaks with a greater initial amount of momentum result in fountains with higher heights. It is important to mention that there is a limit fountain height expected to be reached, but this height was not verified in the analyzed conditions. For plumes with very high rising momentum, it is expected that the water at the surface rises to a limit height and then the fountain breaks. On the other hand, the horizontal dispersions of the shown plumes appear very similar for all cases, regardless of the Reynolds number related to the leak. It is not possible to affirm that there is no relationship between the variables, but indeed to attest to the necessity for further investigation of the parameter in future studies.

4.4.2 Gas rising times

The first measured parameters, determined according to the description given in Section 3.8, were the gas rising times. All measurements were computed with an accuracy of $\pm$ 0.2 s. Figure 33 shows the collected rising times organized as a function of the Reynolds number and the leak size.

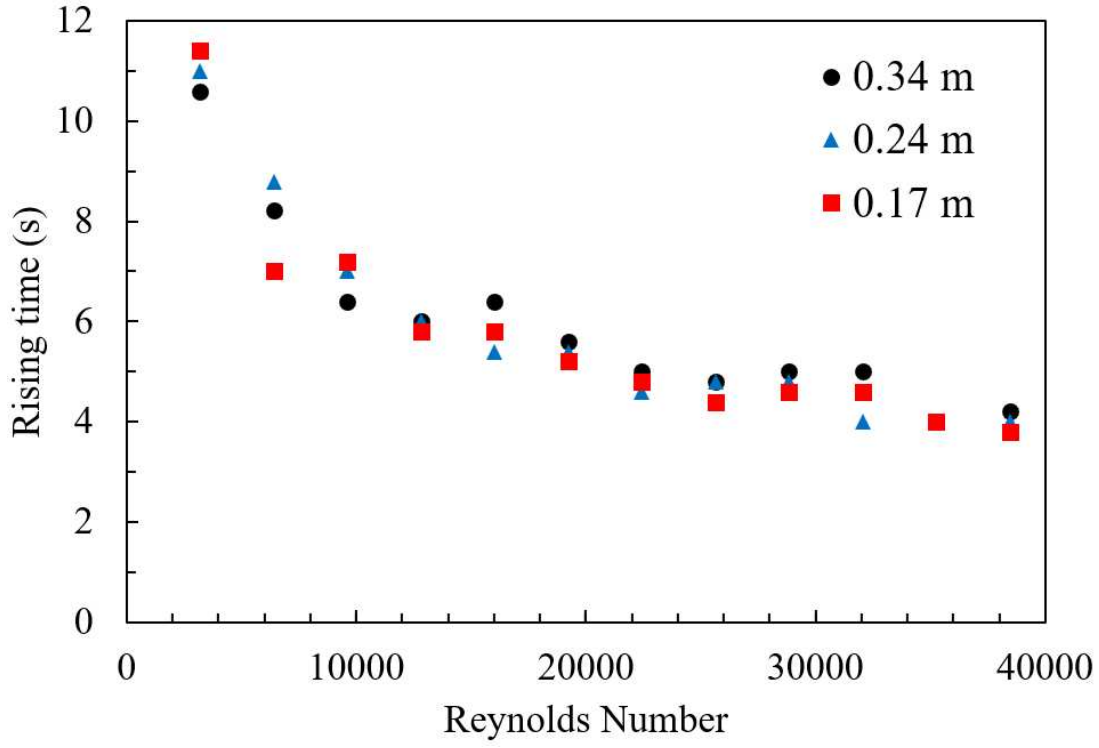

Figure 33: Rising times of the plumes as a function of the Reynolds number of the leak in case study 5 (Oliveira and Vianna, 2022).

Figure 33 indicates that, for the three sets of information, the data follow a logarithmic profile, with lower Reynolds numbers being associated with higher rising times. Higher Reynolds numbers mean higher turbulence effects and lower interaction times between the ascending air and the water. In addition, the rising times are virtually equivalent for the same value of Reynolds, regardless of the flow rate and the leak size. This indicates a strong relationship between the variables and also points to a strong potential for the successful development of mathematical models which relates them.

4.4.3 Initial fountain heights

The initial fountain heights obtained for each of the 36 setups indicated in Table 2 are shown in Figure 34.

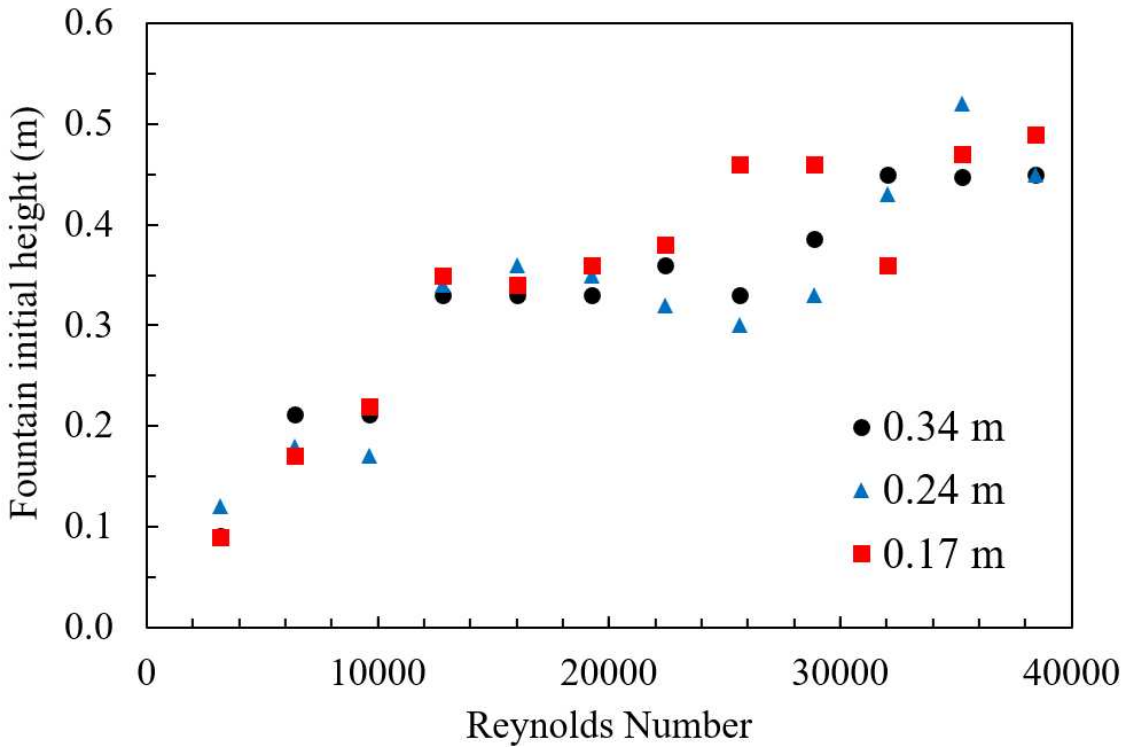

Figure 34: Fountain heights at the rising time as a function of the Reynolds number of the leak in case study 5 (Oliveira and Vianna, 2022).

Figure 34 shows that the initial fountain heights are, such as the rising times, equivalent to the same Reynolds numbers of the leak, irrespective of the leak size. This finding points out that, at least for small water depths, the initial amount of momentum and turbulence of the leaked air is directly connected to the behavior of the air at the surface of the domain. Another important observation is that, for smaller Reynolds numbers of the leak, the fountain heights increase apparently linearly. Then, for two Reynolds intervals, between 10000 and 25000, and between 25000 and 40000, the fountain heights

remain virtually constant. This possibly indicates the effects of interaction between the water moved and the surface air.

4.4.4 Fountain heights at 15 s

The fountain heights were also determined for 15 s of flow. This measurement time was proposed by Engebretsen et al. (1997) and used for the validation of the setup, presented in case study 4. Figure 35 presents the graphic with the collected information.

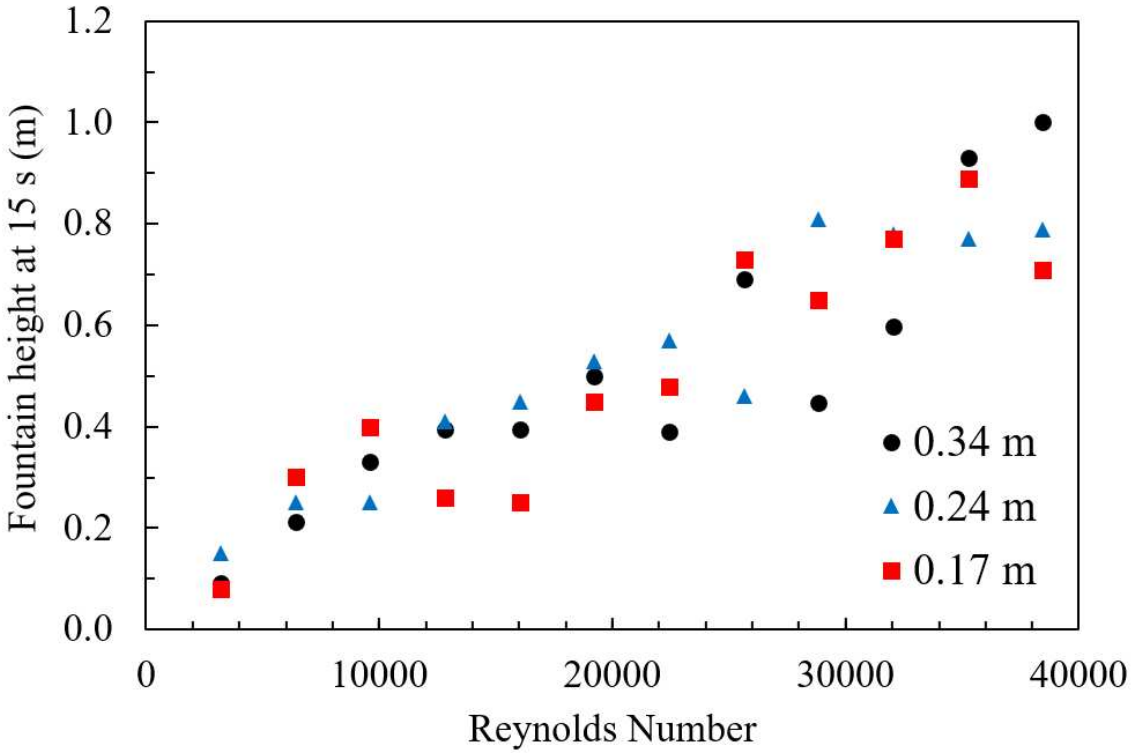

Figure 35: Fountain heights at 15 s of flow as a function of the Reynolds number of the leak for case study 5 (Oliveira and Vianna, 2022).

It is important to mention that some interactions between the plume and the walls were verified, notably for higher flow rates, since more air was leaked. Nevertheless, the fountain heights have shown a great relationship with the Reynolds number of the leak, following the propensity noted in Figures 33 and 34. Figure 35, however, stands out for pointing out a linear relationship, at least within the analyzed range, between Reynolds number and fountain heights, regardless of the leak size. This fact allows inferring that the Reynolds of the leak and the quantity of momentum carried by the air when it reaches the surface are related since both are associated with the vertical momentum of the gas. This verified linearity, however, is limited, since the fountain depends of the effects of surface tension and gravity forces. Above a certain Reynolds value, a threshold font height will be reached. If the value exceeds this critical Reynolds, the moment carried by the rising air can be too high and break the fountain.

The Reynolds number is connected to the turbulence of the flow, which helps to distribute the carried vertical momentum to the horizontal direction. This connects the correct prediction of the vertical behavior of the plume with the horizontal distribution of the fountain.

4.4.5 Fountain horizontal dispersion

The horizontal dispersion was measured at the rising times to minimize interactions between the leaked air and the tank walls. Figure 36 presents the obtained results organized by Reynolds number of the leak and leak size.

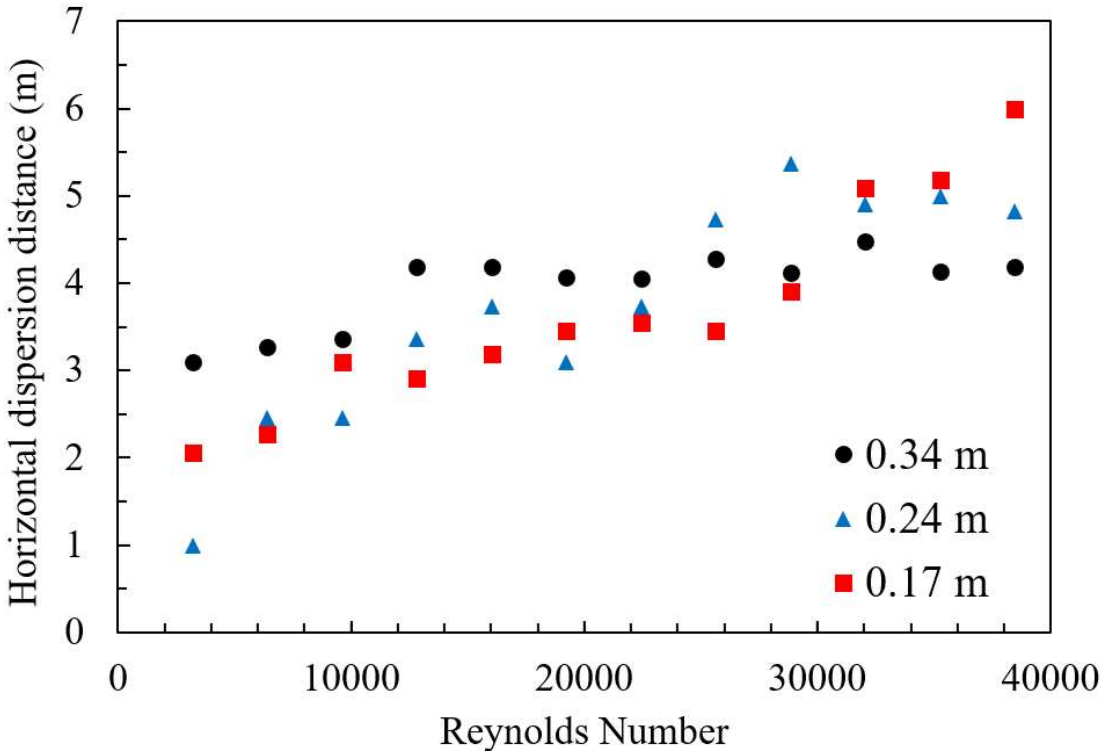

Figure 36: Horizontal dispersion distances for different leak sizes as a function of the Reynolds number of the leak in case study 5 (Oliveira and Vianna, 2022).

For the three sets of points, there is a region where the Reynolds number is directly, and almost linearly directly, related to the horizontal dispersion. However, for the leaks of 0.34 and 0.24 m, there were critical Reynolds numbers, of 12800 and 29000 approximately, from which the values of horizontal spread distance remained practically constant. For the 0.17 m leak size, the critical value was not reached, but it is prudent to affirm that it would be obtained if a wider range of Reynolds numbers was investigated. Taking each leak size individually, since the properties of the fluid do not change, the lower the Reynolds numbers are, the lower the flow rates. Consequently, the longer will be the interaction between the rising air and the water, driven by gravity and surface tension effects that direct the development of the water fountain.

4.4.6 Partial conclusions of the section

This section brought some results obtained when varying the leak size and the flow rate of an amount of air rising in water media.

At least for the considered height of the water column, the air rising times and the resulting fountain heights were directly related to the Reynolds number of the leak, indicating that subsequent studies, especially the ones involving the development of dimensionless numbers could use the Reynolds number to evaluate the new groups. Another important observation is that in the future, with a few simulations varying only the Reynolds of the leak, it will be possible to estimate these variables without the need to study each situation specifically, saving time and computational resources.

On the other hand, the calculated horizontal dispersion distances have not shown a direct relationship with the Reynolds number, being sometimes linear, sometimes constant. The higher the Reynolds, the higher the horizontal dispersion until it reaches a critical value.

4.5 Case study 6: relating the shape of the bubble clusters with their ascending velocity through the liquid phase

This section brings the results of case study 6, which aimed at developing a methodology for estimating the ascending time of a plume submerged in shallow waters using the data obtained from the previous simulations under controlled flow conditions.

4.5.1 Relating the shape of the bubble clusters with their ascending velocity through the liquid phase

Following the directions described in Section 3.8, the average ascending velocities and the average bubble sizes were calculated for all 36 simulations of Table 2. As observed in case study 5, it was possible to relate several plume parameters with the Reynolds numbers of the leaks.

Figure 37 brings the graphic with the average sizes of the bubble clusters as a function of the Reynolds number of the leak. This figure is important because it relates one property of the leak with one property of the resulting plume.

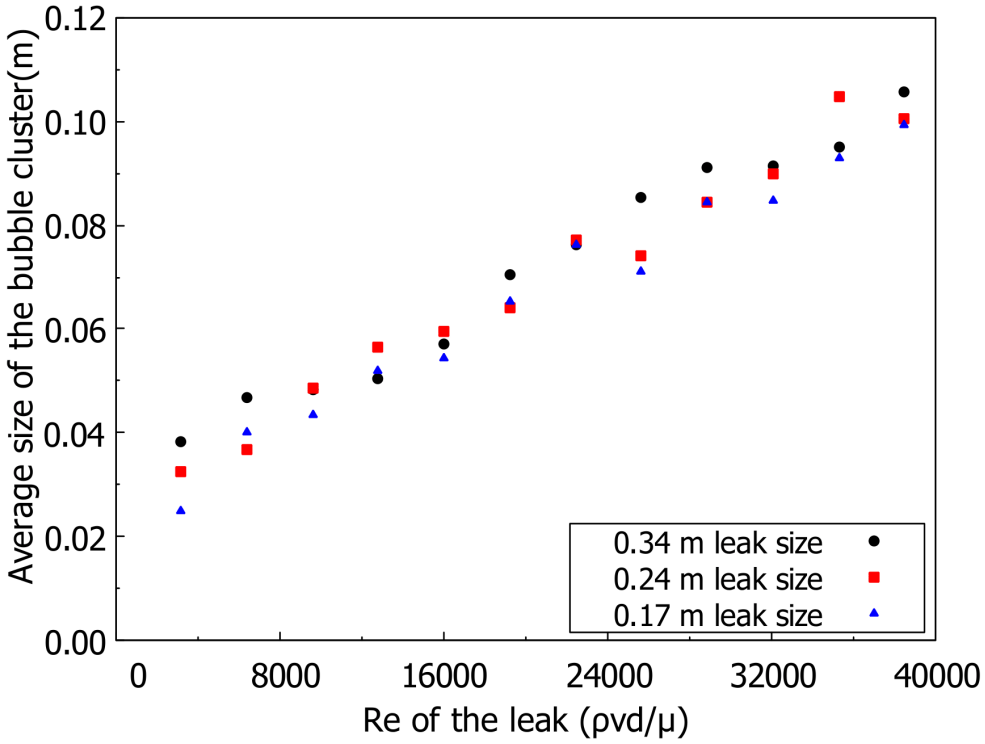

Figure 37: Average size of the bubble clusters as a function of the Reynolds number of the leaks in case study 6 (Oliveira and Vianna, 2023).

It is possible to verify that the average size of the bubble clusters is directly proportional to the Reynolds number since a linear behavior of the data was observed, with R^2=0.96. For the considered range of Reynolds values, if the properties of the leak are known, it is possible to estimate the value of the average size of the bubble clusters.

Continuing with the analysis of the parameters of the plumes, the average rising velocities were calculated. Then, Equation 36 was used to obtain the values of Π, which were organized according to the Reynolds number of the leak in Figure 38.

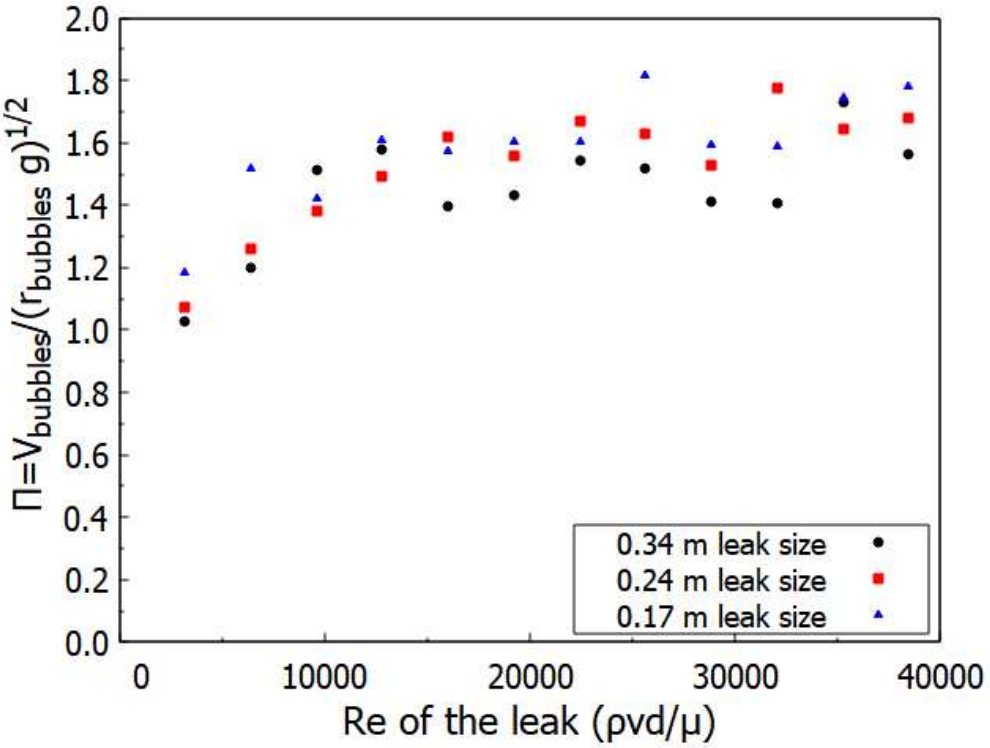

Figure 38: Values of Π as a function of the Reynolds number of the leaks in case study 6 (Oliveira and Vianna, 2023).

The values of Π in Figure 38 were supposed to be independent of the leak size and have a constant value. However, we verify that Π oscillates around a constant value of 1.60 for most points, but for the three lowest Reynolds numbers, the value of Π does not follow this tendency. It was decided to proceed with the proposed mathematical analysis and pay due attention to how these points behave.

4.5.2 Bubble size analysis

Figure 39 evidences the relationship between the variables $V_{bubbles}$ and $r_{bubbles}$, where the first is directly proportional to the square root of the second. It also brings the fit curve obtained.

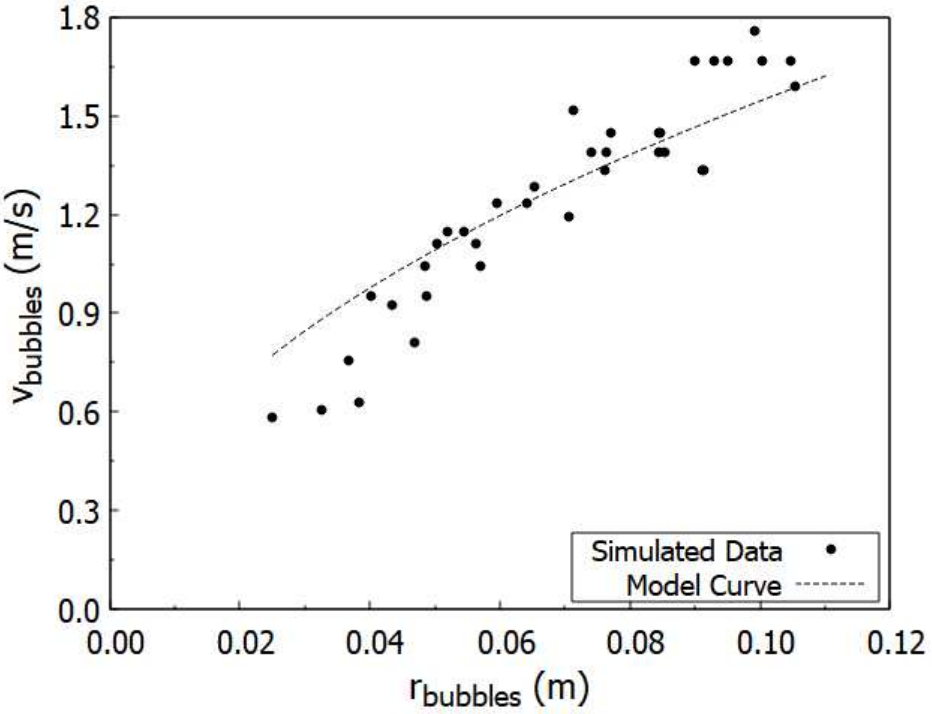

Figure 39: Obtained bubble velocities as a function of the average characteristic size of the buble clusters in case study 6 (Oliveira and Vianna, 2023).

The non-linear fit of Equation 37 resulted in a value for R^2 equal to 0.82. As verified in Figure 38, some discrepant points can be identified. These points correspond to smaller values of $V_{bubbles}$ (lower than 0.75 m/s) and $r_{bubbles}$ (lower than 0.04 m), which are the points related to the lower Reynolds numbers of the leak. One possible explanation for the behavior of the data is that lower Reynolds numbers of the leaks imply higher times for interaction between the air and the water, which results in greater momentum transfer ascending times, and even horizontal dispersion, as verified in Figures 30, 31, 32, and 36, but further investigation is necessary. The calculated α for the fit of Equation 37 to the data resulted in 0.64. Thus, it was possible to obtain Equation 38.

$$V_{bubbles} = \frac{1}{0.64}(g r_{bubbles})^{1/2} \tag{38}$$

4.5.3 Proposing a methodology for estimating the gas ascending time through small columns of liquid

Through Equation 38 it is possible to estimate the value of $V_{bubbles}$ by knowing the average size of the bubble clusters resulting from the leak. However, it means depending on a plume parameter to calculate another. In the attempt to express an equation that relates the rising time of the bubbles with other properties of the plume or the leak, it is possible to replace $V_{bubbles}$ by the ratio between height and rising time, using the definition of the variable presented in Section 3.8. Making the substitution, one can arrive

at Equation 39.

$$t_{rising} = h\alpha(gr_{bubbles})^{-1/2} \tag{39}$$

Where t_{rising} is the rising time, and h is the vertical distance traveled by the gas ascending through the water.

Another expression for t_{rising} can be derived from the empirical observation that the average size of the bubbles and the Reynolds number of the leak varies linearly with each other. In other words, writing $r_{bubbles} = aRe + b$, where a is the slope of the curve and b is the intercept. Replacing the expression in Equation 39, it is possible to express Equation 40.

$$t_{rising} = h\alpha(g(aRe + b))^{-1/2} \tag{40}$$

The only unknown variable that t_{rising} depends on is the Reynolds number of the leak. Thus, by performing the linear adjustment using the points displayed in Figure 37 and substituting the values of the adjustment parameters in Equation 40, it is possible to obtain Equation 41.

$$t_{rising} = 1.366(1.964 \times 10^{-6}Re + 0.028)^{-1/2} \tag{41}$$

Where $1.964{\times}10^{-6}$ and 0.028 are the values of a and b, respectively. The value of R^2 for the adjustment of Equation 41 was 0.64, which indicates a low overall correspondence between predicted and observed points. For this reason, the graph in Figure 40 was designed, which helps to visualize the quality of the fit of Equation 41 to the data.

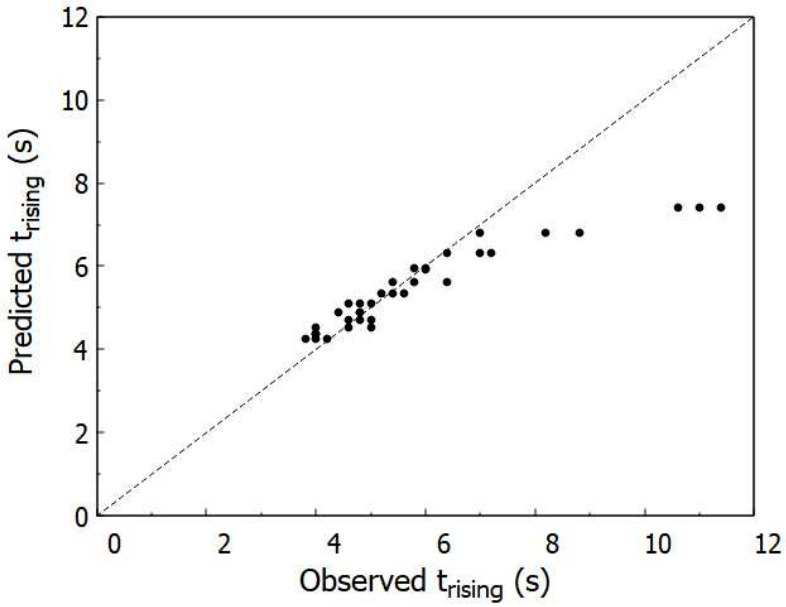

Figure 40: Verification of the model proposed in Equation 41 (Oliveira and Vianna, 2023).

Considering that the precision interval of the experimental measures is ± 0.2 s, the fit of the model to the data is satisfactory, except for the points where the Reynolds numbers are small (higher values of t_{rising}), where the discrepancy between predicted and observed values are very significant. It is possible to affirm that the proposed model is precise for calculating rising times in cases in which the Reynolds number of the leak is greater than 10000.

This inability of the model in describing points related to low Reynolds numbers of the leak may be related to physical effects between water and air, which are intensified because of the higher interaction time between the fluids in cases with low flow rates of air, when the contact time between them is higher. However, without further studies, it is not possible to categorically state the reason behind the poor fit of the model to these points.

4.5.4 Proposing a correction for the model

Based on the behavior of the points, it was defined that the proposed adjustment for calculating the gas rising time would include the term A/Re added in its expression. With this addition, another correction parameter has shown itself necessary to avoid the loss of physical meaning of the remaining mathematical relationship between the parameters. Then, a term equal to B was included by multiplying it by the part of the expression corresponding to Equation 40. Equation 42 presents the new model.

$$t_{rising} = \frac{A}{Re} + Bh\alpha(g(aRe + b))^{-1/2} \tag{42}$$

Note that the ratio between A and Re will assume higher values for lower values of Reynolds numbers, acting like a correction factor. The values of the parameters α, a and b remain the same values from the previous model, shown in Equation 41 since they were determined through a physical analysis. The calculated values for A and B were 14868 and 0.85 respectively. The obtained expression for the rising time of the gas becomes Equation 43.

$$t_{rising} = \frac{14868}{Re} + 1.159(1.964 \times 10^{-6}Re + 0.028)^{-1/2} \tag{43}$$

The value o R^2 for this expression is 0.97, which is much greater than the value of 0.64 from the previous model. This improvement indicates that the addition of the correction factors in the mathematical model was successful. The physical meaning of the values of A and B needs to be investigated in future studies.

Figure 41 compares predicted and observed data obtained through Equation 43.

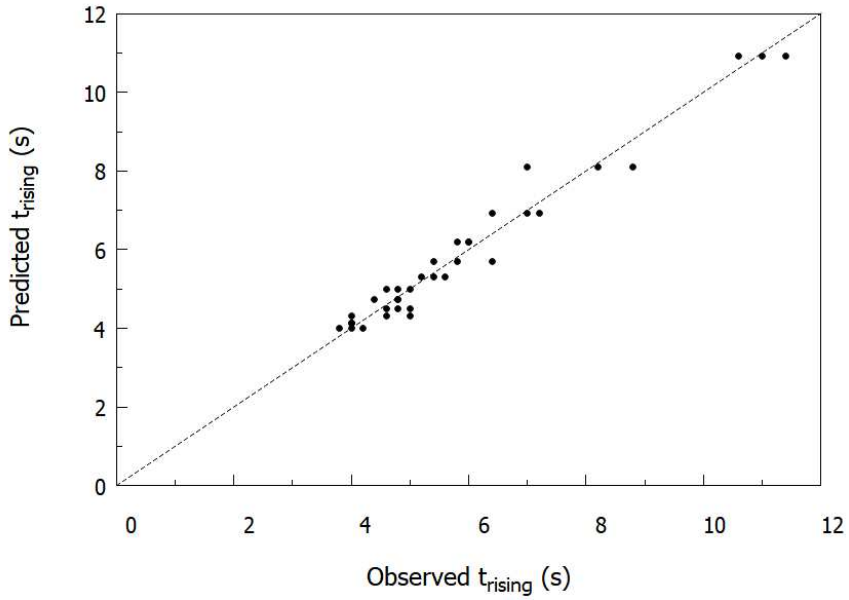

Figure 41: Verification of the model proposed in Equation 43.

Note in Figure 41 that the points were well described within the entire range of Reynolds values analyzed, which proves the good fit of the model to the data. It is very important, however, to recognize the possible applicability limitations of the proposed model. The model can be applied to scenarios of shallow waters, where the effects of compressibility of the gas and its temperature change are less significant. Even so, after all the methodology developed had disregarded the effects of air compressibility along the pressure change in the flow, it was noted that having included these effects in the simulations could have allowed even more accurate results to be achieved. In addition, if another gas than air, such as CO_2 or CH_4, is considered, shallow waters will render the solubility and reaction effects of these gases unimportant, which does not happen in deeper water. It is also necessary to assume that the water is stable and there are no effects of water currents. Lastly, it is necessary to assume that the gas volumetric flow underwater is constant, which is coherent since the leak rate is very low.

4.5.5 Partial conclusions of the section

This section presented a sequence of steps for analyzing the data obtained with the 2D simulations in order to develop a precise mathematical model capable of estimating the gas ascending time in an underwater gas release. After verifying that the behavior of the plume is directly related to the Reynolds number of the leak, the empirical correlation variables were substituted in the expression obtained through the dimensional analysis. With the obtained model, future data can be estimated without the need for new simulations. This finding can be of great relevance in future studies aiming at predicting parameters of real accidents involving subsea gas leaks.

4.6 Case study 7: evaluating the proposed models under other flow conditions

This section presents the results of the proposed verification of the methodology presented in this thesis to obtain a mathematical model for calculating the rising time of air bubbles submerged in water under different flow conditions.

4.6.1 Analyzing the resulting plumes

The gas volume fraction profiles obtained for each simulation of case study 7 are presented in Figures 42, 43 and 44. The images were obtained at the calculated rising time of each case. The information of the simulations is summarized in Table 3.

As can be verified in Figures 42, 43, and 44, and also in Figures 30, 31, and 32, plumes with the same Reynolds number of the leak have a similar shape. This information points again to the conclusion that the characteristics of the leak and the behavior of the resulting plume are related.

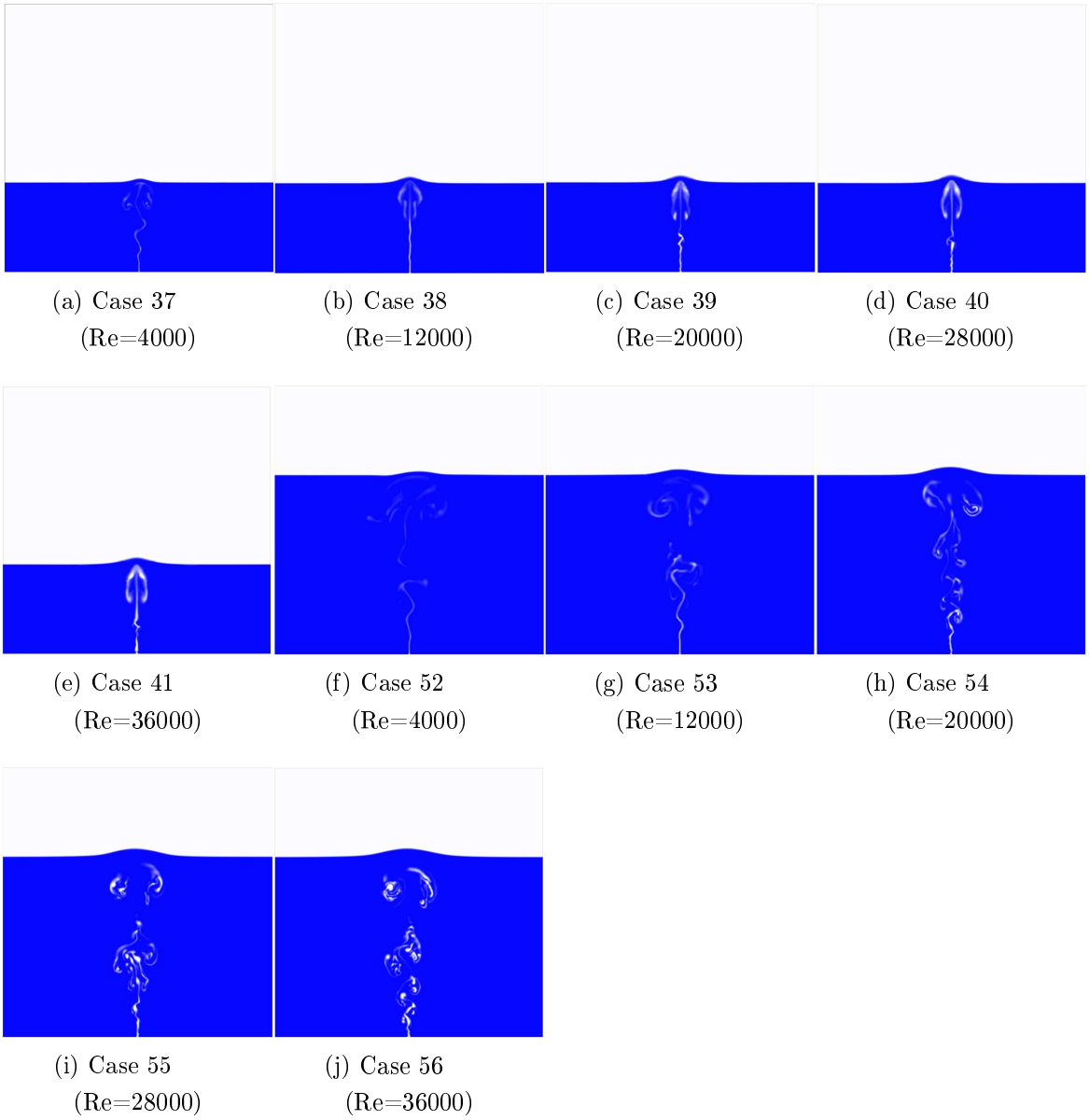

(a) Case 37 (Re=4000) (b) Case 38 (Re=12000) (c) Case 39 (Re=20000) (d) Case 40 (Re=28000)

(e) Case 41 (Re=36000) (f) Case 52 (Re=4000) (g) Case 53 (Re=12000) (h) Case 54 (Re=20000)

(i) Case 55 (Re=28000) (j) Case 56 (Re=36000)

Figure 42: Plumes at t_{rising} for different Reynolds numbers at the gas discharge obtained for the leak size of 0.10 m in case study 7.

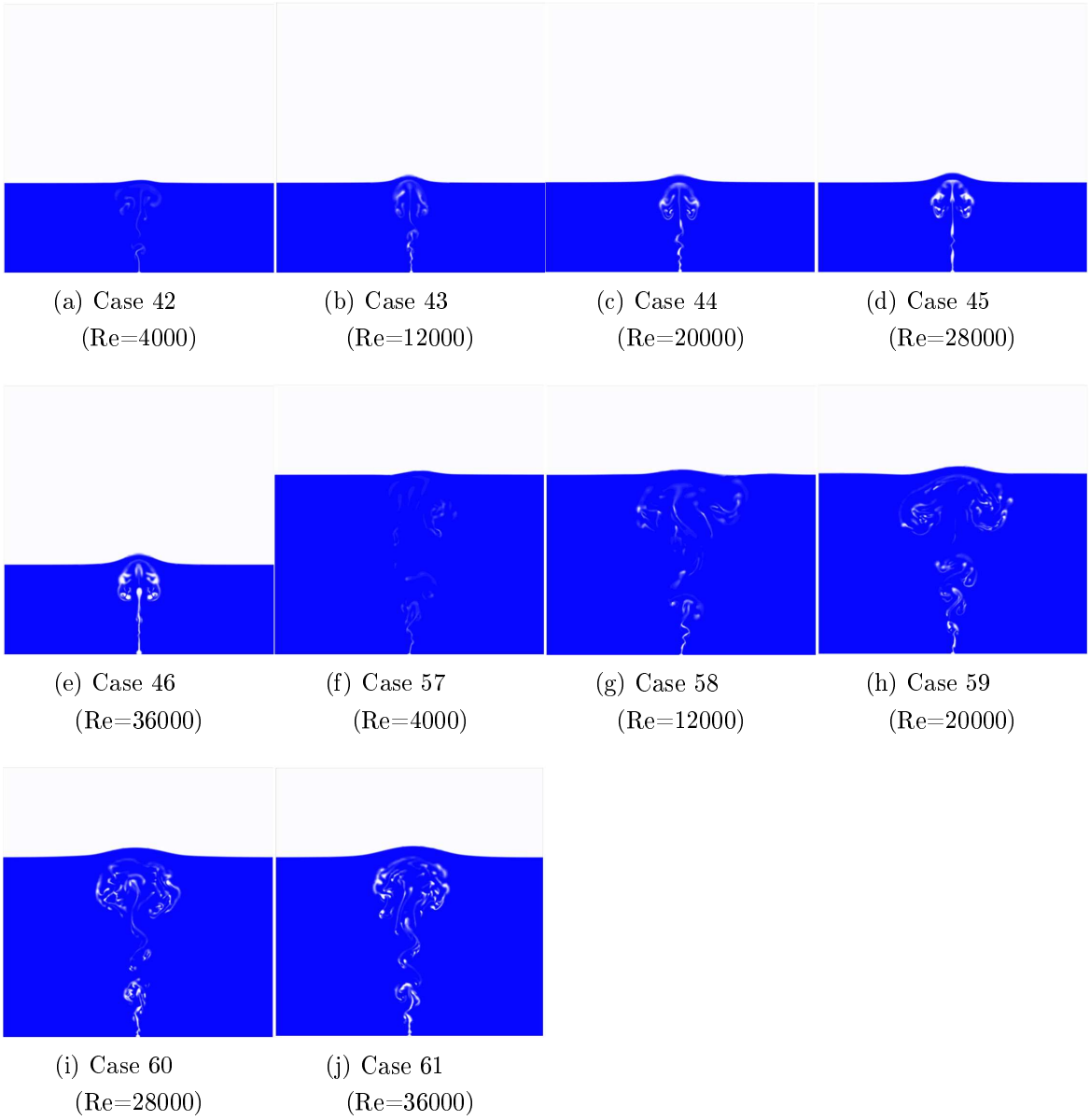

(a) Case 42 (Re=4000) (b) Case 43 (Re=12000) (c) Case 44 (Re=20000) (d) Case 45 (Re=28000)

(e) Case 46 (Re=36000) (f) Case 57 (Re=4000) (g) Case 58 (Re=12000) (h) Case 59 (Re=20000)

(i) Case 60 (Re=28000) (j) Case 61 (Re=36000)

Figure 43: Plumes at t_{rising} for different Reynolds numbers at the gas discharge obtained for the leak size of 0.20 m in case study 7.

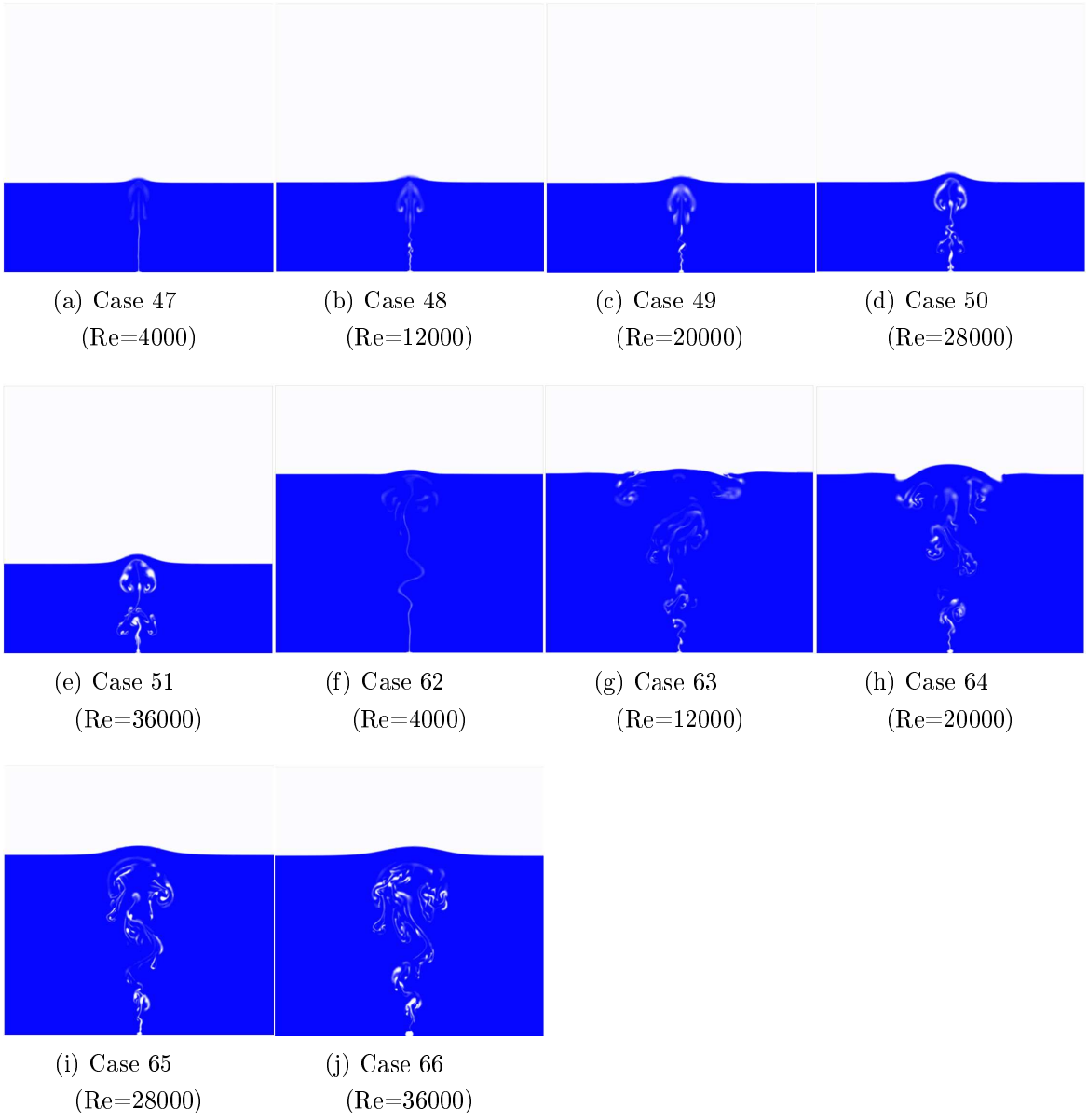

(a) Case 47 (Re=4000) (b) Case 48 (Re=12000) (c) Case 49 (Re=20000) (d) Case 50 (Re=28000)

(e) Case 51 (Re=36000) (f) Case 62 (Re=4000) (g) Case 63 (Re=12000) (h) Case 64 (Re=20000)

(i) Case 65 (Re=28000) (j) Case 66 (Re=36000)

Figure 44: Plumes at t_{rising} for different Reynolds numbers at the gas discharge obtained for the leak size of 0.30 m in case study 7.

4.6.2 Obtaining the mathematical models

Following the same steps of case study 6, the rising times of the plumes were obtained according to the methodology proposed in Section 3.8, and the parameters α, a and b were calculated. The value of α, the shape factor of which relates bubble characteristic size and the air average ascending velocity, was determined for both sets of cases (37 to 51, and 52 to 66) according to the water depth. For the depth of 5 m, α=0.67, and for the depth of 10 m, α=0.56. Compared with the value of α=0.64 calculated in case study 6, it is possible to notice that smaller values of α are obtained for larger values of the water column. However, without further studies, the behavior of α according to the

properties of the domain can not be estabilished. An expression similar to Equation 42 was obtained for depth of 5 m an another for the depth of and 10 m. Equations 44 and 45 show the obtained models. They were developed in a range of Reynolds numbers between 4000 and 36000, which includes all the data obtained.

$$t_{rising} = \frac{8168}{Re} + 0.905(2.514 \times 10^{-6} Re + 0.081)^{-1/2} \tag{44}$$

$$t_{rising} = \frac{14465}{Re} + 1.580(1.376 \times 10^{-6} Re + 0.058)^{-1/2} \tag{45}$$

The values for A and B were 8168 and 0.84, respectively, for the adjustment for the depth of 5 m (Equation 44) and 14465 and 0.81, respectively, for the adjustment for the depth of 10 m (Equation 45). Comparing these values with the values from case study 6 (Equation 43), it is possible to form some initial hypotheses about the value of the parameters, and these need to be further verified in future analyses. Firstly, somehow the parameter A is related to the linearity between $r_{bubbles}$ and the Reynolds number of the leak, since more linear relationships are associated with higher values of A, and the model without this parameter is not efficient in describing points associated with low Reynolds numbers, which are linked to low values of $r_{bubbles}$. Another hypothesis is that the value of parameter B could be predetermined or within a specific range, as the parameter value in the three analyzed cases fluctuated between 0.81 and 0.85. These values, considering the margin of error, may even be mathematically equivalent.

Once again, the above expressions relate a parameter of the flow with a parameter of the leak. The values of R^2 for both the adjustments were 0.85 for Equation 44 and 0.81 for Equation 45. As occurred in case study 6, without the correction factors A and B proposed in Equation 42 the calculated points referring to higher rising times ($Re < 12000$) differ significantly from the observed values. The R^2 of the adjustment of Equation 40 to the data is 0.40 for the cases in which the water depth is 5 m and 0.38 when it is 10 m. This indicates again that the model presented in Equation 40, which is equivalent to the Equation 42 without the correction parameters A and B, was not able to capture some interaction effects between air and water, especially when the contact time between them is longer.

To visually verify the good adjustment of Equations 44 and 45 to the data, Figures 45 and 46 were built.

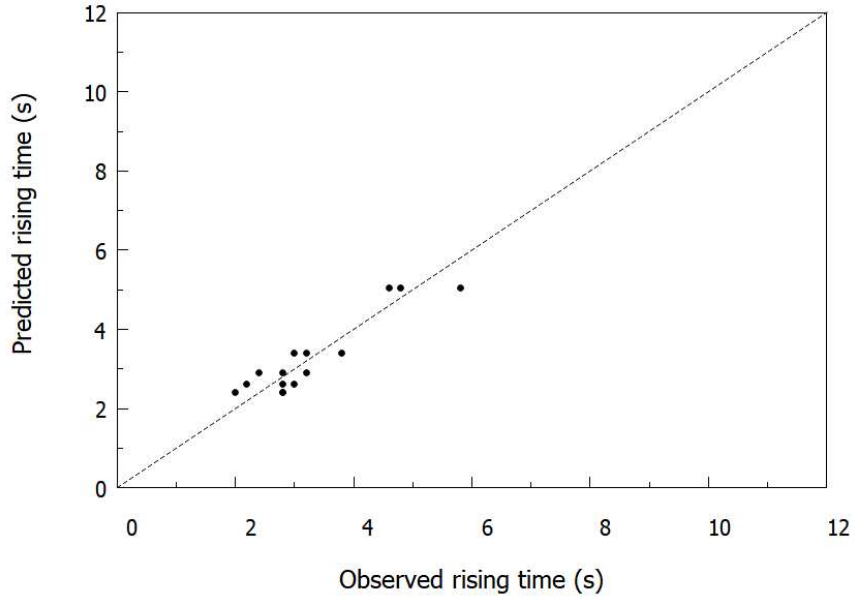

Figure 45: Verification of the model proposed in Equation 44.

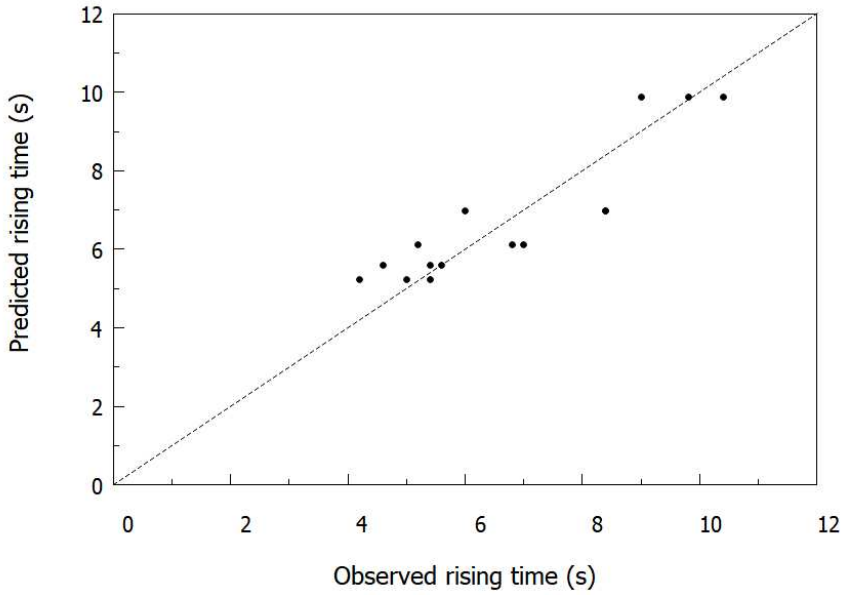

Figure 46: Verification of the model proposed in Equation 45.

Visually, it is verified that the proposed model which associates the gas rising time to the Reynolds number of the leak is satisfactory under similar conditions to which the model validation was carried out.

4.6.3 Partial conclusions of the section

This section of results was able to prove the viability of applying the procedure proposed in this thesis to find the relationship between a parameter of the leak with a parameter of the resulting plume in an underwater gas release. It is important to reinforce,

once again, that the physical limitations of the applicability of the numerical setup must be respected and that extrapolations of this analysis to different flow conditions require experimental validation and deeper mathematical analysis. At the end of the analyses, it was noted that the consideration of compressibility effects would allow for obtaining even more accurate results, although the reliability of the study was not compromised due to the neglect of air compressibility.

4.7 Chapter conclusion

This chapter presented the results achieved in this study, as well as the analysis of the obtained information. Case study 1 pointed out the necessity to investigate turbulence modeling and its improvement, as well as the improvements of the meshing used for the simulations. Case studies 2 and 3 indicated that modifying the parameters of the k-ε model also implies changing the description of the behavior of the plume, with some improvements verified in the central ascending velocity of the gas, but still with no further benefits in describing the full plume. Case study 4 allowed the validation of a simple and relatively fast methodology for obtaining data regarding the release of gas in a liquid medium using adaptive mesh. When there was was a need to choose the direction in which the study would follow, it was decided to continue the investigation based on the results obtained in case study 4. Case study 5 consisted of data acquisition and analysis of the plume parameters and how they were qualitatively related to the Reynolds number of the leak. Case study 6 resulted in a methodology to obtain a mathematical expression capable of predicting the rising time of the gas based on the properties of the leak. Finally, case study 7 verified the applicability of the proposed methodology for small water depths. All the results, especially the ones from case studies 6 and 7, contributed to the understanding of the phenomenon of underwater gas release.

Chapter 5

Conclusions and sugestions

This chapter summarizes the most relevant conclusions of this thesis, as well as some proposed suggestions for future works related to this research. Finally, the list of scientific production derived from this work is also available, containing only the works already accepted for publication or published in national and international conferences and journals.

5.1 Main findings

The understanding of accidental subsea gas releases is still a subject that needs further investigation. This happens because the acquisition of knowledge in this area is still at an early stage, and the phenomenon is very complex and influenced by several variables, sometimes difficult to account for. Among the tools available for studying this theme, the CFD presents advantages over other methods, since it allows the obtaining of reliable data in a relatively cheaper, safer, and faster way. However, in order to be considered reliable, the CFD needs to be carefully validated before being used, and the experimental data for validation of CFD in more complex scenarios are still very scarce.

This work contains the steps for the development and validation of a 2D methodology for the simulation of underwater air release for small water depths. The setup was precise in predicting some properties of gas plumes, such as their rising time and their fountain heights at different moments of the flow. In order to make this statement, the setup proposed in this work was validated against a set of experimental data widely established in the literature. The accurate prediction of the properties of the plumes in their central region suggests that the selected turbulence model, realizable k-ε, successfully facilitated the appropriate distribution of momentum across the flow region, despite still exhibiting limitations inherent to a typical RANS model.

After the proposed setup was validated, a set of data from 36 simulations under 12 different Reynolds numbers of the leak was collected. This data was analyzed and, after using the Buckingham Pi Theorem, a shape factor α of 0.64 was proposed. This α related

the ascending velocity of the plume with the characteristic size of the resultant bubble clusters. Another relevant contribution was a the proposition of a mathematical model which relates the Reynolds number of the leak with the gas ascending time. Initially, the expression $t_{rising} = 1.364(1.969 \times 10^{-6} Re + 0.028)^{-1/2}$ was obtained for the data. However, the expression was adjusted to better describe the value of the points at low Reynolds numbers of the leak. The new expression was $t_{rising} = \frac{14868}{Re} + 1.159(1.964 \times 10^{-6} Re + 0.028)^{-1/2}$. It is important to mention that the physical meaning of the new parameters added to the model still needs to be investigated.

The methodology proposed was also applied to model the data obtained for water depths of 5 m and 10 m. The calculated shape factors and the obtained equations were: α =0.67 and $t_{rising} = \frac{8168}{Re} + 0.905(2.514 \times 10^{-6} Re + 0.081)^{-1/2}$ for the water depth of 5 m and α =0.56 and $t_{rising} = \frac{14465}{Re} + 1.580(1.376 \times 10^{-6} Re + 0.058)^{-1/2}$ for the depth of 10 m. The correspondence between obtained and observed data was very high, however, it is necessary to establish that the model can only be said to be effective under the conditions in which it was developed.

Besides the methodology developed to calculate the gas rising time and the determination of the shape factor of the bubble groups, which were the major contributions of this work, other investigations related to the release of air in water were also carried out. Another important finding was the understanding of how plume parameters such as initial fountain heights and fountain heights after some time of flow behave. Additionally, the information of how the horizontal dispersion of the fountain varies with the Reynolds number of the leak was also discussed. All the observed relationships lead to the hypothesis that the interaction between gas and liquid phases is extended for lower flow rates, which results in greater values of rising times, fountain heights, and horizontal dispersions.

As the main conclusion, it can be stated that the methodology presented is effective under the conditions in which it was tested and that the model presented is valid for small heights of water depths and in the range of Reynolds number values in which it was developed. Although there are limitations in this study, it can be said that it may in the future serve as a basis for other studies that wish to investigate phenomena related to subsea gas releases, as well as an auxiliary on the understanding of the physics involved in two-phase flows.

5.2 Future work

The findings of this study are a preliminary, but still very relevant, contribution to the field of study of submerged gas plumes. It is important to mention, however, that the applicability of the developed work is still restricted to systems with dimensions of the same order of magnitude.

The depth used for validation, as well as the additional ones used for data acquisition, were small. This circumstance, along with the fact that the volume of water in the part of the domain where all the analyzes occurred was much higher than that of air, whose density is also much lower than that of water under the evaluated conditions, made the influence of gas compressibility and temperature change being neglected. The consideration made throughout the work slightly reduced the computational cost of the simulations. However, during the final analysis of the results, it was found that the accuracy of the data obtained may have been slightly affected by this choice. It is very important, therefore, to point out that this compressibility should be considered in future studies, regardless of the size of the water column used.

Furthermore, since the air was considered as the gas phase, this work developed a model which works well for two immiscible fluids. New validation is necessary to develop a model which considers mass transfer between phases, in cases where the gases are CH_4 and CO_2, for example. This information will depend on the water depth, and the salinity of the liquid phase, among other parameters.

Lastly, two other conditions of the flow assumed for the validation need to be accounted for: the initial immobility of water, with no presence of water currents, since the experiments were performed in a tank; and second, the content of the flow rate, with no presence of intermittence on the value of the Reynolds of the leak.

Considering the still-existing literature gap, future studies must include the validation and development of CFD setups able to simulate submerged plumes formed at great depths, accounting, therefore, for the effects of gas compressibility, temperature change, and the presence of water currents. Additionally, the mass transfer between gas and water should be considered if other gases than air, such as CH_4 and CO_2, were used in these simulations.

However, it is important to mention again that the experimental data for validating the above-suggested simulation conditions are very scarce, and additional experimental work needs to be developed in parallel with these CFD studies.

Thus, another important suggestion for future studies is to carry out more experimental studies of gas leaks in tanks of liquids. Even if the dimensions of this tank are limited, it would be possible to collect information for validation of simulations involving issues of gas solubility, salinity, temperature, compressibility, and other deficiencies already mentioned.

Regarding the proposed mathematical modeling, it is interesting that, in the future, the developed dimensionless parameters try to consider more flow variables, in particular, surface tension effects. This will enable the analysis conducted for one pair of fluids to be applicable to another pair.

With the advancement of computational power, future studies may also consider more sophisticated turbulence accounting, such as the Reynolds Stress Model (RSM), which is still a RANS approach, LES, or DNS. Although the computational cost increases significantly, these approaches will be able to calculate more precisely the momentum distribution along the plume. These changes would also provide more reliable results of the plume properties

Overall, this study, despite its limitations, was able to contribute to the research area of multiphase flows, and, with the advances in experimental studies and the technology available for the simulations, the contributions tend to become even more significant.

5.3 Scientific production

Up to the time of publication of this thesis, the following scientific works have been developed:

- "A new methodology to estimate the gas ascending time from underwater gas releases", 2023, published in *Journal of Loss Prevention in the Process Industries*;
- "Evaluating the Influence of the Leak Reynolds Numbers on the Behavior of Underwater Gas Plumes: a CFD Study", 2022, presented at the *10th International Conference on Safety & Enviroment in Process & Power Industry* (CISAP), and published in *Chemical Engineering Transactions*;
- "Validação de metodologia para simulação rápida de liberação de gás em tanque de líquido", 2022, presented and published in the conference proceedings of the *III Brazilian Congress of Computational Fluid Dynamics* (CBCFD);
- "Avaliação da Pluma Resultante de Liberação de Gás em Tanque de Líquido Utilizando Modelo VOF e Abordagem RANS", 2021, presented and published in the conference proceedings of the *23th Brazilian Congress on Chemical Engineering* (COBEQ);
- "Analysis of the Behavior of Subsea Gas Plume Resulting from a Two-Phase Flow Using Computational Fluid Dynamics", 2021, presented and published in the conference proceedings of the *2021 Congress of the Brazilian Association of Risk Analysis, Process Safety and Reliability* (ABRISCO);
- "Accidental subsea releases: Characterisation of flammable gas plumes", 2021, presented in the *2021 Mary Kay O'Connor Process Safety Symposium.*

References

ANSYS Fluent. *ANSYS Fluent Theory Guide*. Release 19. ANSYS, Inc., 2019.

Bai, Yong and Qiang Bai. *Subsea Engineering Handbook*. Elsevier Inc., 2010.

Balachandar, S. and John K. Eaton. "Turbulent Dispersed Multiphase Flow". *Annual Review of Fluid Mechanics* 42.1 (2010): 111–133.

Batchelor, George K. *An Introduction to Fluid Dynamics*. Cambridge University Press, 2000. 615.

Bjerketvedt, Dag, Jan Roar Bakke, and Kees Van Wingerden. "Gas explosion handbook". *Journal of Hazardous Materials* 52.1 (1997): 1–150.

Brennen, Christopher Earls. *Fundamentals of multiphase flow*. Cambridge University Press, 2005. 345.

Cassano, Katia, et al. "High-pressure gas release from subsea pipelines: Multiphase modelling and CFD simulation for consequences analysis in risk assessment". *Journal of Loss Prevention in the Process Industries* 81 (2023): 104962.

Çengel, Yunus A. and John M. Cimbala. *Fluid mechanics: fundamentals and applications*. McGraw-Hill Higher Education, 2006. 956.

Chaouat, Bruno. "The State of the Art of Hybrid RANS/LES Modeling for the Simulation of Turbulent Flows". *Flow Turbulence Combust* 99 (2017): 279–327.

Cloete, Schalk, Jan Erik Olsen, and Paal Skjetne. "CFD modeling of plume and free surface behavior resulting from a sub-sea gas release". *Applied Ocean Research* 31.3 (2009): 220–225.

CNN Brasil. "Vazamentos no gasoduto Nord Stream são possivelmente sabotagem, dizem líderes europeus". 2022. <`https://www.cnnbrasil.com.br/internacional/vazamentos-no-gasoduto-nord-stram-sao-possivelmente-sabotagem-dizem-lideres-europeus/?amp`>.

Cordes, Erik E., et al. "Environmental impacts of the deep-water oil and gas industry: A review to guide management strategies". *Frontiers in Environmental Science* 4.SEP (2016).

Crowe, Clayton T., et al. *Multiphase flows with droplets and particles*. 2nd ed. CRC Press, 2011. 509.

CSB. "Drilling Rig Explosion and Fire at the Macondo Well". 2016. 24.

Energy Global News. "October 1985: Shallow Gas Blow Out on the West Vanguard". 2021 09/03/2021 <http://www.energyglobalnews.com/october-1985-shallow-gas-blow-out-on-the-west-vanguard/>.

Energy Voice. "How Ocean Odyssey was almost the UK's second Piper Alpha - News for the Oil and Gas Sector". 2021 09/03/2021 <https://www.energyvoice.com/oilandgas/43727/ocean-odyssey-almost-uks-second-piper-alpha/>.

Engebretsen, T., et al. "Surface flow and gas dispersion from a subsea release of natural gas". *Proceedings of the International Offshore and Polar Engineering Conference* 1 (1997): 566–573.

Fanneløp, Torstein K. and Karl Sjøen. "Hydrodynamics of Underwater Blowouts". *18th Aerospace Sciences Meeting*. 1980. 45.

Flowe, Anita, Ashok Kumar, and Sunil Ojha. "Choosing and using commercial CFD packages for modeling contaminant dispersion". *Environmental Progress* 20.2 (2001): J07–J12.

Fobes Mexico. "Pemex enfrenta incendio en su activo petrolero más importante". July 2021 07/07/2021 <https://www.forbes.com.mx/pemex-enfrenta-incendio-en-su-activo-petrolero-mas-importante/>.

Folha de São Paulo. "Vazamento em oleoduto causa incêndio na superfície do mar no Golfo do México". July 2021 07/07/2021 <https://www1.folha.uol.com.br/mundo/2021/07/vazamento-em-oleoduto-causa-incendio-na-superficie-do-mar-no-golfo-do-mexico-veja-video.shtml?utm%7B%5C_%7Dsource=whatsapp%7B%5C&%7Dutm%7B%5C_%7Dmedium=social%7B%5C&%7Dutm%7B%5C_%7Dcampaign=compwa>.

Friedl, Markus Josef and Torstein K. Fanneløp. "Bubble plumes and their interaction with the water surface". *Applied Ocean Research* 22.2 (2000): 119–128.

G1 - France Presse. "Quarto vazamento é detectado no gasoduto Nord Stream no Mar Báltico". 2022. <https://g1.globo.com/mundo/noticia/2022/09/29/quarto-vazamento-e-detectado-no-gasoduto-nord-stream-no-mar-baltico.ghtml>.

Geng, Zhiyuan, et al. "Experimental and numerical study on gas release and dispersion from underwater soil". *Process Safety and Environmental Protection* 149 (2021): 11–21.

Hirsch, Charles. *Numerical Computation of Internal and External Flows: Fundamentals of Computational Fluid Dynamics*. 2nd ed. Butterworth-Heinemann, 2007. 656.

Hirt, C. W. and B. D. Nichols. "Volume of Fluid (VOF) Method for the Dynamics of Free Boundaries". *Journal of Computational Physics* 39 (1981): 201–225.

IEA. "World energy balances 2020: Overview". *Statistics Report*. Paris, 2020. 703.

Ismail, Zubaidah, et al. "Evaluating accidents in the offshore drilling of petroleum: Regional picture and reducing impact". *Measurement* 51.1 (2014): 18–33.

Launder, Brian E. and Dudley Brian Spalding. "The numerical computation of turbulent flows". *Computer Methods in Applied Mechanics and Engineering* 3.2 (1974): 269–289.

Li, Xinhong, Guoming Chen, and Faisal Khan. "Analysis of underwater gas release and dispersion behavior to assess subsea safety risk". *Journal of Hazardous Materials* 367 (2019): 676–685.

Li, Xinhong, Ziyue Han, et al. "Underwater gas release modeling and verification analysis". *Process Safety and Environmental Protection* 137 (2020): 8–14.

Li, Xinhong and Jingwen Wang. "Modelling underwater dispersion of gas released from seabed soil considering current and wave". *Process Safety and Environmental Protection* 171.December 2022 (2023): 260–271.

Michaelides, Efstathios, Clayton T. Crowe, and John D. Schwarzkopf. *Multiphase Flow Handbook*. 2nd ed. CRC Press, 2016. 1394.

Moaveni, Saeed. *Finite element analysis: theory and application with ANSYS*. 3rd ed. Pearson Prentice Hall, 2008. 861.

Mokhatab, Saeid and William Poe. *Handbook of Natural Gas Transmission and Processing*. 4th. Gulf Professional Publishing, 2012. 862.

Moukalled, Fadl Hassan, Luca Mangani, and Marwan Darwish. *The finite volume method in computational fluid dynamics: an advanced introduction with OpenFOAM® and Matlab®*. Springer, 2016. 791.

Offshore. "Lightning storm ignited gas leak in Gulf of Mexico, says Pemex". July 2021 07/07/2021 <https://www.offshore-mag.com/regional-reports/latin-america/article/14206288/lightning-storm-ignited-gas-leak-in-gulf-of-mexico-says-pemex?utm%7B%5C_%7Dsource=OFF+Daily%7B%5C&%7Dutm%7B%5C_%7Dmedium=email%7B%5C&%7Dutm%7B%5C_%7Dcampaign=CPS210706115%7B%5C&%7Do%7B%5C_%7Deid=0541H9950723I1E%7B%5C&%7Drdx.ident%7B%5C%7D5Bpull%7B%5C%7D5D=omeda%7B%5C%7D7C05>.

Oliveira, Maria Fernanda and Sávio Souza Venâncio Vianna. "A new methodology to estimate the gas ascending time from underwater gas releases". *Journal of Loss Prevention in the Process Industries* 82 (2023).

——."Avaliação da pluma resultante de liberação de gás em tanque de líquido utilizando modelo VOF e abordagem RANS". *23° Congresso Brasileiro de Engenharia Química*. Gramado - RS, 2021. 1–4.

——."Evaluating the Influence of the Leak Reynolds Numbers on the Behavior of Underwater Gas Plumes: a CFD Study". *Chemical Engineering Transactions* 91.May (2022): 559–564.

Olsen, Jan Erik and Paal Skjene. "Summarizing an Eulerian-Lagrangian model for subsea gas release and comparing release of CO2 with CH4". *Applied Mathematical Modelling* 79 (2020): 672–684.

Olsen, Jan Erik and Paal Skjetne. "Current understanding of subsea gas release: A review". *The Canadian Journal of Chemical Engineering* 94.2 (2016): 209–219.

——."Modelling of underwater bubble plumes and gas dissolution with an Eulerian-Lagrangian CFD model". *Applied Ocean Research* 59 (2016): 193–200.

Olsen, Jan Erik, Paal Skjetne, and Stein Tore Johansen. "VLES turbulence model for an Eulerian–Lagrangian modeling concept for bubble plumes". *Applied Mathematical Modelling* 44 (2017): 61–71.

ONGC. "Fire Case Study Off Shore - Santa Fe Al Baz, Nigeria". 2014: 1. <http://fireconsultancy.co.uk/wp-content/uploads/2017/01/fcs-os-santa-fe-al-baz-nigeria.pdf>.

Pan, Qing Qing, et al. "CFD study of surface flow and gas dispersion from a subsea gas release". *International Conference on Offshore Mechanics and Arctic Engineering - OMAE*. American Society of Mechanical Engineers (ASME), 2014. 1–6.

Patankar, Suhas V. *Numerical heat transfer and fluid flow*. Taylor & Francis, 1980. 214.

Pritchard, Philip J. *Fox and McDonald's Introduction to Fluid Mechanics*. 8th ed. John Wiley & Sons, 2011. 877.

Riddick, Stuart N., et al. "Methane emissions from oil and gas platforms in the North Sea". *Atmospheric Chemistry and Physics* 19.15 (2019): 9787–9796.

Robert H. Perry, Don W. Green. *Perry's Chemical Engineers' Platinum Edition*. 7th ed. McGraw-Hill, 1999.

Shoham, Ovadia. *Mechanistic modeling of gas-liquid two-phase flow in pipes*. Society of Petroleum Engineers, 2006. 396.

Sokolichin, Alexander A., et al. "Dynamic numerical simulation of gas-liquid two-phase flows Euler/Euler versus Euler/Lagrange". *Chemical Engineering Science* 52.4 (1997): 611–626.

Souza, José Francisco Almeida de, et al. "Uma revisão sobre a turbulência e sua modelagem". *Revista Brasileira de Geofísica* 29.1 (2011): 21–41.

Sun, Yuan, et al. "Investigation on underwater gas leakage and dispersion behaviors based on coupled Eulerian-Lagrangian CFD model". *Process Safety and Environmental Protection* 136 (2020): 268–279.

The Guardian. "Revealed: 1,000 super-emitting methane leaks risk triggering climate tipping points". 2023. <https://www.theguardian.com/environment/2023/mar/06/revealed-1000-super-emitting-methane-leaks-risk-triggering-climate-tipping-points>.

Versteeg, Henk Kaarle and Weeratunge Malalasekera. *An introduction to computational fluid dynamics: the finite volume method*. Pearson Education Limited, 2007. 503.

Vinnem, Jan-Erik. *Offshore Risk Assessment: Principles, Modelling and Applications of QRA Studies*. Springer London, 2007.

Wallis, Graham B. *One-dimensional two-phase flow*. McGraw-Hill, 1969. 408.

Wu, Kejia, et al. "Modelling subsea gas releases and resulting gas plumes using Computational Fluid Dynamics". *Journal of Loss Prevention in the Process Industries* 49 (2017): 411–417.

Xinhong, Li, et al. "Simulation and assessment of underwater gas release and dispersion from subsea gas pipelines leak". *Process Safety and Environmental Protection* 119 (2018): 46–57.

Yeoh, Guan Heng and Jiyuan Tu. *Computational techniques for multi-phase flows: basics and applications*. Butterworth-Heinemann, 2010. 643.